STATUS OF THESIS

Title of thesis	Synthesis and Characterization of Zeolite Beta Supported Fe and Ni Catalysts for Steam Gasification of Palm Kernel Shell for Hydrogen Production

I SITI EDA ELIANA BINTI MISI

hereby allow my thesis to be placed at the Information Resource Center (IRC) of Universiti Teknologi PETRONAS (UTP) with the following conditions:

1. The thesis becomes the property of UTP
2. The IRC of UTP may make copies of the thesis for academic purposes only.
3. This thesis is classified as

☐ Confidential

☑ Non-confidential

If this thesis is confidential, please state the reason:

_____
_____
_____

The contents of the thesis will remain confidential for _____ years.

Remarks on disclosure:

_____
_____
_____

Endorsed by

_____ _____

Signature of Author | Signature of Supervisor

Permanent address:
Lot 3120, Taman Amina
Jalan Merdeka
93050 Kuching , Sarawak

Name of Supervisor
Assoc. Prof. Dr. Anita Ramli

Date : _____ Date : _____

UNIVERSITI TEKNOLOGI PETRONAS

SYNTHESIS AND CHARACTERIZATION OF ZEOLITE BETA SUPPORTED Fe AND Ni CATALYSTS FOR STEAM GASIFICATION OF PALM KERNEL SHELL FOR HYDROGEN PRODUCTION

by

SITI EDA ELIANA BINTI MISI

The undersigned certify that they have read, and recommend to the Postgraduate Studies Programme for acceptance this thesis for the fulfilment of the requirements for the degree stated.

Signature: _____

Main Supervisor: Assoc. Prof. Dr. Anita Ramli

Signature: _____

Co-Supervisor: Assoc. Prof. Dr. Suzana Yusup

Signature: _____

Head of Department: Assoc. Prof. Dr. Shuhaimi Mahadzir

Date: _____

SYNTHESIS AND CHARACTERIZATION OF ZEOLITE BETA SUPPORTED Fe AND Ni CATALYSTS FOR STEAM GASIFICATION OF PALM KERNEL SHELL FOR HYDROGEN PRODUCTION

by

SITI EDA ELIANA BINTI MISI

A Thesis

Submitted to the Postgraduate Studies Programme

as a Requirement for the Degree of

MASTER OF SCIENCE

DEPARTMENT OF CHEMICAL ENGINEERING

UNIVERSITI TEKNOLOGI PETRONAS

BANDAR SERI ISKANDAR,

PERAK

SEPTEMBER 2011

DECLARATION OF THESIS

Title of thesis	Synthesis and Characterization of Zeolite Beta Supported Fe and Ni Catalysts for Steam Gasification of Palm Kernel Shell for Hydrogen Production

I SITI EDA ELIANA BINTI MISI

hereby declare that the thesis is based on my original work except for quotations and citations which have been duly acknowledged. I also declare that it has not been previously or concurrently submitted for any other degree at UTP or other institutions.

Witnessed by

Signature of Author	Signature of Supervisor
Permanent address: Lot 3120, Taman Amina Jalan Merdeka 93050 Kuching , Sarawak	Name of Supervisor Assoc. Prof. Dr. Anita Ramli
Date :	Date :

ACKNOWLEDGEMENTS

Alhamdulillah. “In the name of Allah the most gracious the most merciful”. Praise to Allah for blessing me with health and the opportunity to gain precious knowledge and experience to complete this project successfully.

First and foremost, I wish to express my sincere and deep appreciation to my kind supervisor, AP Dr. Anita Ramli for her constant assistance and guidance supervising this project. Her willingness to share extra time doing some experiments and revising all my paper work as well as this thesis will always be appreciated. Her moral support and sacrifices will always be in my memory. Special thanks to co-supervisor, AP Dr. Suzana Yusup for her assistance and guidance on this project.

I would like to thank my parents, Misi b. Ahim and Sapiah bt Hj Alin and also my siblings for their constant support and patience. Their love, prayers and care have given me a big motivation to finish this research succesfully. I am also grateful for the support from my husband, Mushrizuwan b. Mustaffa throughout my study. His sacrifices, patience and understanding will never be forgotten.

My thanks also go to Universiti Teknologi PETRONAS for providing the financial support for the project and to the Biohydrogen Team for their co-operation and enjoyable working experience. Not forgetting the lab technicians from the Chemical and Mechanical Department for their help in running the characterization testing. I would also like to express my sincere gratitude to Prof Hengyong Xu and his research team for their kind assistance in performing the catalytic tests at Dalian Institute Chemical Physics (DICP), China.

My sincere appreciation also extends to all my friends at UTP especially Mas Fatihah bt. Mohammad for her willingness to share insightful ideas and willing to help whenever a problem arises. Thanks also to Noor Diana bt. Abdul

Majid, Ruzanna bt Ibrahim, Nurhidayah bt. Mohammad, Nurul Huda bt. Zailani, Nurul Huda bt. Yunus, Nurul Shahida bt. Mohd Zi, Sharifah Shahidah bt. Abdullah, Athirah bt. Mohd. Tamidi and Mustakimah bt. Mohamed for their support and friendship over the last three years. I wish them all future success.

ABSTRACT

Production of hydrogen gas (H_2) from biomass gasification usually comes with several problems such as the existence of unacceptable level of tars and also ineffectiveness of the catalysts' performance due to coke deposition. In order to eliminate most of the inconvenience encountered, new types of catalysts have been developed. In this study, monometallic Fe and Ni supported on zeolite beta (BEA) have been prepared by incipient wetness impregnation method. Fe and Ni based bimetallic catalysts supported on BEA were also prepared using two different approach; sequential impregnation and co-impregnation method. The BEA support was impregnated with the solution containing the required amount of metal salts for 4 hours, dried at 120 ^{o}C for 16 hours and later calcined at temperatures between 500-700 ^{o}C for 16 hours. These catalysts were structurally characterized using BET, XRD, FESEM-EDX and TPR. A screening process was performed at temperatures between 600 – 900 ^{o}C in a fixed-bed quartz micro-reactor in the absence of a catalyst to determine the optimum temperature for the steam gasification of palm kernel shell (PKS) to H_2. The gases produced were analyzed using two on-line gas chromatographs; to analyze sulphur compound in the product gases and to determine the composition of H_2, CH_4, CO and CO_2. The catalysts were then tested for their ability to produce H_2 in the steam gasification of PKS in a fixed-bed quartz micro-reactor with an on-line gas chromatograph at 700 ^{o}C. BET analysis shows that the isotherms plots of the prepared catalysts are type IV which is mesoporous materials. Moreover, the Fe-Ni/BEA catalysts possess lower surface area, higher pore volume and larger pore diameter as compared to other prepared catalysts. Calcination temperature is found to contribute to the crystallization of the prepared catalysts where high crystallization of Fe and Ni was observed in Fe-Ni/BEA (700) catalyst with the formation of NiO and $NiFe_2O_4$ phase. The TPR profiles of the bimetallic catalysts show the combination of nickel and iron phases' reduction which attributed to weak interaction with support (NiO and Fe_2O_3 phase) and strong interaction with the support ($NiAl_2O_4$ and $FeAl_2O_4$). From the screening process, the optimum

temperature for steam gasification of PKS is 700 ºC. This is because maximum of H_2 evolvement was achieved at 700 ºC without existence of H_2S. The differences in the physicochemical properties of the catalysts affect the catalytic performance whereby it exhibit the PKS to undergo either steam reforming for higher in H_2 evolvement or facilitates the oxidation of CO to produce more CO_2. In terms of monometallic, both Ni/BEA (500) and Fe/BEA (600) catalysts show the highest concentration of H_2 evolved where Ni/BEA (500) catalyst has higher reducibility and surface area while Fe/BEA (600) has larger pore diameter. For bimetallic catalysts, the highest concentration of H_2 evolvement in the steam gasification of PKS achieved in the presence of FeNi/BEA (700) and NiFe/BEA (500). At a suitable calcination temperature, FeNi/BEA able to enhances the water gas shift reaction while NiFe/BEA facilitates the steam methane reforming. However, in co-impregnation catalyst, both Fe and Ni promote the active site of the catalyst to increase the crystallization of $NiFe_2O_4$ and exhibit the steam methane reforming as well as water gas shift reaction. Fe-Ni/BEA (700) shows the highest composition of H_2 gas evolved with 76.32 vol% H_2, 18.72 vol% CO_2, 4.96 vol% CO and the absence of CH_4. The outlet gas composition also shows that the steam gasification of PKS in the presence of Fe-Ni/BEA (700) has a potential to replace the commercial methane reforming for H_2 production. Therefore, it can be concluded that various parameters in catalyst preparation resulted in deviation in the catalyst properties and interaction between the active metals with support as well as the catalytic activity.

ABSTRAK

Penghasilan gas hidrogen (H_2) daripada penggasan hampas biasanya mendatangkan beberapa masalah seperti kehadiran tar yang tidak diingini dan juga prestasi mangkin yang kurang cekap kerana pengenapan jelaga. Untuk menghalang masalah yang terjadi, mangkin baru telah dihasilkan. Dalam kajian ini, monologam Fe dan Ni berpenyokong zeolite beta (BEA) telah disediakan dengan menggunakan kaedah pengisitepuan pembasahan permulaan. Mangkin dwilogam Fe dan Ni berpenyokong BEA juga telah disediakan dengan menggunakan dua kaedah; pengisitepuan berterusan dan pengisitepuan serentak. Mangkin berpenyokong BEA telah diisitepukan dengan larutan yang mengandungi garam logam yang diperlukan selama 4 jam, dikeringkan pada suhu 120 ^oC selama 16 jam dan kemudian dikalsinkan pada suhu di antara 500-700 ^oC selama 16 jam. Struktur mangkin tersebut telah dianalisa dengan menggunakan kaedah BET, XRD, FESEM-EDX dan TPR. Proces penyaringan telah dijalankan pada suhu di antara 600 – 900 ^oC dalam reaktor mikro padatan tetap tanpa kehadiran mangkin untuk mengenal pasti suhu optimum penggasan berstim isirung kelapa sawit (PKS) kepada H_2. Gas yang telah dihasilkan telah dianalisisa dengan menggunakan dua kromatograf gas; untuk analisa komposisi sulfur di dalam produk gas dan untuk mengenalpasti komposisi H_2, CH_4, CO and CO_2. Kebolehan mangkin untuk menghasilkan H_2 dalam penggasan berstim PKS kemudiannya telah dikaji dalam reaktor mikro padatan tetap yang disambungkan dengan kromatograf gas, pada suhu 700 ^oC. Analisa menggunakan teknik BET menunjukkan plot isoterma terhadap mangkin yang disediakan adalah jenis IV iaitu berliang-rongga sederhana. Selain itu, mangkin Fe-Ni/BEA menghasilkan luas permukaan yang kecil, isipadu rongga yang tinggi dan diameter rongga yang besar berbanding dengan mangkin yang lain. Suhu pengkalsinan didapati menyumbang kepada kristalisasi mangkin yang dihasilkan di mana mangkin Fe-Ni/BEA (700) menghasilkan kristalisasi yang tinggi melalui pembentukan fasa NiO dan $NiFe_2O_4$. Butiran TPR terhadap mangkin dwilogam menunjukkan penggabungan penurunan fasa Fe dan Ni iaitu tindak balas yang

lemah dengan penyokong (fasa NiO dan Fe_2O_3) dan tindak balas yang kuat dengan penyokong ($NiAl_2O_4$ and $FeAl_2O_4$). Daripada proses penyaringan, suhu optimum untuk penggasan berstim PKS adalah 700 ºC. Ini kerana perubahan maksimum H_2 telah dicapai pada 700 ºC tanpa kehadiran H_2S. Perbezaan dalam sifat fizikal kimia mangkin memberi kesan kepada prestasi mangkin di mana ia menggalakkan PKS samada untuk melalui pembentukan semula stim untuk meningkatkan perubahan H_2 atau membantu pengoksidaan CO untuk menghasilkan lebih banyak CO_2. Bagi monologam, kedua- dua mangkin Ni/BEA (500) dan Fe/BEA (600) menunjukkan kepekatan H_2 yang paling tinggi di mana mangkin Ni/BEA (500) mempunyai penurunan dan luas permukaan yang tinggi manakala Fe/BEA (600) mempunyai diameter rongga yang besar. Untuk mangkin dwilogam pula, perubahan kepekatan H_2 yang paling tinggi dalam penggasan berstim PKS tercapai dengan kehadiran FeNi/BEA (700) dan NiFe/BEA (500). Pada suhu pengkalsinan yang sesuai, FeNi/BEA berpotensi untuk menambah tindak balas berganjak gas air manakala NiFe/BEA menggalak pembentukan semula stim mathana. Walau bagaimanapun, bagi mangkin pengisitepuan serentak, kedua-dua Fe dan Ni berupaya mengaktifkan mangkin untuk menghasilkan kristalisasi $NiFe_2O_4$ yang tinggi dan menggalakkan pembentukan semula stim methana dan tindak balas berganjak gas air. Fe-Ni/BEA (700) menghasilkan komposisi H_2 yang paling tinggi iaitu 76.32 % H_2, 18.72 % CO_2, 4.96 % CO dan tanpa kehadiran CH_4. Komposis gas yang dihasilkan menunjukkan penggasan berstim PKS dengan kehadiran Fe-Ni/BEA (700) berpotensi untuk menggantikan pembentukan komersil methana untuk penghasilan H_2. Oleh itu, ini boleh dirumuskan bahawa pelbagai parameter dalam penyediaan mangkin menyebabkan perbezaan dalam sifat mangkin dan tindak balas di antara logam aktif dengan penyokong dan juga aktiviti pemangkinan.

TABLE OF CONTENTS

LIST OF TABLES

LIST OF FIGURES

ABBREVIATIONS

Al_2O_3	Aluminium Oxide
BEA	Zeolite Beta
BET	Brunauer-Emmett-Teller
BJH	Barrett-Joyner-Halenda
Btu	British Thermal Unit
^oC	Degree Celsius
CDM	Clean Development Mechanism
CeO_2	Cerium(IV) oxide
CH_4	Methane
cm^3/min	Cubic Metre Per Minute
Co	cobalt
CO	Carbon Monoxide
CO_2	Carbon Dioxide
COS	Carbonyl Sulphide
C_2H_4	Ethene
C_2H_6	Ethane
DICP	Dalian Institute Of Chemical Physics
EDX	Energy Dispersive X-Ray
EIA	Energy Information Administration
EFB	Empty Fruit Bunches
Eq	Equation
Fe	Iron
FeO	Iron Oxide
Fe_2O_3	Iron (II) Oxide
Fe_3O_4	Iron (III) Oxide
FESEM	Field Emission Scanning Electron Microscopy

FELDA	Federal Land Development Authority
FFB	Fresh Fruit Bunch
g	Gram
H_2	Hydrogen
H_2O	Water
H_2S	Hydrogen Sulphide
ICDD	International Centre Diffraction Data
IUPAC	International Union of Pure and Applied Chemistry
JCPDS	Joint Committee On Powder Diffraction Standards
K	Kelvin
K_2CO_3	Potassium Carbonate
kV	Kilo Volt
$LaFeO_3$	Lanthanum Hydroxyl
$LaNi_{0.3}Fe_{0.7}O_3$	Tri-Metallic Perovskite Catalysts
MPOB	Malaysian Palm Oil Board
Mg	Magnesium
$mgmin^{-1}$	Milligram Per Minute
$MgCO_3.CaCO_3$	Dolomite or magnesium ore
$(Mg,Fe)_2SiO_4$)	olivine or magnesium aluminosilicate
MgO	Magnesium Oxide
Min	Minute
$mlmin^{-1}$	Millilitre Per Minute
Mm	Millimetre
Mpa	Mega Pascal
MW	Mega Watt
Na_2CO_3	Sodium Carbonate
N_2	Nitrogen
NGO	Non-Government Organization
Ni	Nickel
$NiFe_2O_4$	Trevorite
Nm	Nanometre
NiO	Nickel Oxide
PKS	Palm Kernel Shell

ppm	Part Per Million
Pt	Platinum
Rh	Rhodium
RM	Ringgit Malaysia
Ru	Ruthenium
SiO_2	Silicon Dioxide
SREP	Small Renewable Energy Programme
SO_2	Sulphur Dioxide
TCD	Thermal Conductivity Detector
TNB	Tenaga Nasional Berhad
TPR	Temperature Programmed Reduction
US	United State
Vol	Volume
WGS	Water Gas Shift
wt. %.	Weight Percentage
XRD	X-Ray Diffraction
%	Percent
$^0Cmin^{-1}$	Degree Celsius Per Minute
µm	Micrometer

CHAPTER ONE

INTRODUCTION

1.1 Background of Research

The consumption of energy over the years relied heavily on fossil fuels have resulted in significant crisis towards depletion of energy resources and environmental problems. The energy produced from fossil fuel releases various harmful pollutants such as greenhouse gases (GHG) and toxic gases: CO_2, CH_4, SO_2, NO_x and other pollutants [1-2]. The overall national energy demand increased at an average rate of 6.3% annually from 2006 to 2010 in Ninth Malaysia Plan (2006-2010), with the industrial sector consuming 38.8% of total energy demand [3] and the statistic is expected to increase in the Tenth Malaysia Plan (2011-2016). Therefore, it is crucial to develop suitable alternative energy that would gradually substitute the declining fossil fuel production which is technically feasible, economically competitive, environmentally acceptable and readily available [4].

With scientific and engineering advancements, biomass can be viewed as a key economically viable component to a renewable energy economy. This is due to the fact that, biomass is a renewable resource that could be sustainably developed in the future and appears to have significant economic potential than high price and scarcity of fossil fuels. In addition, biomass also appears to have formidably positive environmental properties resulting in no net releases of carbon dioxide and very low sulphur content [5-6].

Due to biomass unique potential, its gasification to synthesis gas and hydrogen is an environmentally attractive method for energy production. The hydrogen production derived from biomass is super clean and has many advantages such as able to solve some of the negative effects of using hydrocarbon fuels. This is because bio-hydrogen is non-toxic, non-poisonous and clean without producing any pollution. It helps to reduce the emission of greenhouse gases and other emissions, thus mitigating the global warming [2, 7]. Furthermore, producing hydrogen through biomass gasification is carbon-neutral economy where biomass resources consume CO_2 in the atmosphere as part of their natural growth process [2].

The gasification of biomass is known to produce hydrogen rich gas, CO, CO_2, CH_4 and various light hydrocarbons [8-12] which can be potentially used either as a gaseous fuel for power generation or as a feedstock for clean transportation fuel. Certainly hydrogen is three times lighter than gasoline or diesel fuel per unit of mass for the same energy which formulate it higher in performance. Hydrogen is also crucially important as a chemical feedstock in chemical process such as petrochemical, methanol, dimethyl ether, Fisher-Tropsch oils and as an energy carrier in clean sustainable energy systems [13-15]. With the advantages of hydrogen production, the development of industry sector can be facilitated and thus provides higher income to the world as well as creating new jobs to the society [2]. Furthermore, it could also help farmers earn extra income from their crops as farmers will be able to supply their biomass for hydrogen energy production [14].

There are several biomass solid wastes available in Malaysia such as oil palm wastes, rubber wood wastes, timber wastes and rice husks. However, biomass from oil palm plantations would be the best candidate for utilization as sources for hydrogen production due to the fact that Malaysia is the world's leading producer and exporter of palm oil. In 2005, oil palm industry was producing the largest amount of oil palm biomass with 85.5% out of more than 70 million tonnes of biomass in Malaysia and this amount increases every year [16]. The palm oil industry generates large volume of biomass from the oil extraction process such as empty fruit bunches (EFBs), mesocarp fiber, palm kernel shell (PKS), fronds and trunks [17-18].

Instead of biomass, hydrogen can also be produced from steam reforming of naphtha or methane, natural gas, residual oil, petroleum coke and coal or from primary energy sources such as wind, solar, geothermal and nuclear as well as hydropower through electrolysis. However, at present hydrogen is extensively produced from fossil fuels by the steam reforming of methane followed by partial oxidation of natural gas and coal gasification. Instead of reacting methane with steam as in the reforming reaction, a fraction of methane is also reacted with oxygen first to produce CO and H_2. On the other hand, coal is reacted with oxygen and steam at high pressure and temperature to produce a gas mixture consisting mainly of H_2, CO and CO_2 [19-21].

Research and developments projects have also been carried out to investigate the production of hydrogen from biological path through photobiological of water and algae, anaerobic digestion as well as fermentative microorganisms of biomass. However, due to the environmental effects and limitation of all processes, the gasification of biomass is considered the most valuable process in enhancing the hydrogen production which applies green technology concept [21-23]. Moreover, the hydrogen production through gasification of biomass also cannot be depleted, thus sustainable for the long term [2]. Therefore, from the above perspective, hydrogen is expected to become one major source of energy in the future [1].

1.2 Problem Statements

The production of hydrogen from gasification of biomass as an alternative fuel for transportation, power generation and chemical feedstock is the principal part of the effort to meet the goal of a biomass-based technology. The development on this process started over century ago and has sustained into the present. However, this effort is allied with a number of problems [13] whereby hydrogen economy requires a cost-effective and highly efficient process in hydrogen production.

Biomass gasification also produces several undesirable amounts of ash particle, volatile alkali metals, char and tar [24]. The formation of tar and char is the most

severe problems because the components are very harmful and could limit the hydrogen production. Moreover, the continual build up of tar present in producing gas can cause blockage and damage to the equipment which can reduce the efficiency of the gasification system [12, 25]. Tar can be defined as a complex mixture of acids, aldehydes, ketones, alcohol, phenol and aromatic hydrocarbons [24] while char is a solid carbonaceous material.

The nature of the tar produced is principally affected by the type of biomass, gasification process, gasifying agent and the operating conditions. Air gasification produces a low viscosity and low reactivity tar, while steam gasification produces a liquid tar with a low molecular weight. In addition, high temperature gasification produces tar with low oxygen content, consisting mostly of hydrocarbons [11].

Several procedures have been taken to mitigate the problems including utilization of catalytic cracking or thermal cracking to some extent by emphasizing on the production of hydrogen and hydrogen-rich gas. Catalytic cracking takes place at 800–900 ºC while thermal cracking at 900-1100 ºC. Compared to catalytic cracking, thermal cracking requires additional energy to heat up the gas as gasification is usually in the range 800-900 ºC. Therefore, catalytic cracking is preferred since it can increase the overall efficiency of the biomass conversion process by 10% [11, 25].

The use of catalysts in the biomass gasification is not only to accelerate reaction rate and lower the reaction temperature but also to eliminate tar in the product thus, adjusting the composition of the product gas [26]. As the raw gas passes over the catalyst, the hydrocarbons or tar may be reformed on the catalyst surface with steam to produce additional carbon monoxide and hydrogen. The reaction can be represented in the Eq. 1.1 [25].

$$C_nH_m + nH_2O \Leftrightarrow nCO + (n + m/2)H_2 \qquad \text{[Eq. 1.1]}$$

Nonetheless, in most cases, catalyst deactivation can be one of the critical problems in limiting the catalyst activity. There are five major mechanisms which

contributed to the loss of activity of the catalyst which are poisoning, fouling, thermal degradation, vapour-solid or solid-solid reaction and mechanical failure. However, most researchers are having problems with catalyst fouling due to deposition of carbon or coke onto the catalyst surface. Coke is a solid carbon (char or tar) and typically consists of polymerised heavy hydrocarbon [27-28].

There are three distinct groups of catalyst that have been extensively investigated in the biomass gasification; non-metallic oxides such as dolomite and olivine, alkali metals and supported metal oxides [25-26]. For non-metallic oxides, dolomite and olivine are widely investigated since they are inexpensive, abundant and can significantly reduce the tar content in the product from a gasifier. However, the main limitation in using dolomite is that it is easily friable which causes it to disintegrate into fines particles and therefore affect the stable operation of the fluidized bed gasifier [8].

A few alkali metal catalysts also have been studied such as potassium carbonate (K_2CO_3) and sodium carbonate (Na_2CO_3). It was noted that the activity of alkali carbonate catalyst presented some operational problems during the gasification because of particle agglomeration. However, K_2CO_3 supported on alumina (Al_2O_3) was found to have significant activity and more resistant to carbon deposition although it was not as active as nickel catalyst [25, 29].

The application of metal based catalysts such as nickel (Ni), Cobalt (Co), Iron (Fe), Ruthenium (Ru) and Platinum (Pt) in biomass gasification is an effective method of reducing tar content. Among these catalysts, supported Rhodium (Rh) catalyst showed the best performance in steam gasification whereby catalyst having with Rh loading of 1.2×10^{-4}/g-cat can convert 98-99% of the carbon in biomass to products at 873K [13]. However, for economic reason, Ni and Fe based catalysts are still the preferred choice due to their wide availability and cheapness [8, 10, 24-25, 30]. Moreover, Ni and Fe based catalysts allow for methane reforming and water gas shift activity during the gasification process provide adjustment of the H_2/CO ratio in the product gas [31-32].

Nevertheless, the activity of the Ni based catalyst is sensitive to Ni loading and Ni dispersion [25]. The reaction is frequently accompanied by coke formation and sintering of Ni metal particles, leading to catalyst deactivation. This may be due to metallic particles that tend to migrate and form larger aggregates, reducing the dispersion of catalyst and consequently the catalyst activity [33].

Some studies have demonstrated that the nickel sintering could be limited when nickel oxide has strong interaction with some support [34] or promoter [32] and have well defined structure like perovskite [33]. Dolomite and olivine which contains Fe helps stabilize Ni in the support and gives an important effect on precursor reducibility as well as catalytic properties [8]. Some studies also verified that the addition of metallic noble metals as promoter may help to improve the metallic dispersion, decrease sintering and enhance the thermal stability [32].

Commercially available iron metal catalysts are also active in hydrocarbon reforming and diminish the tar content in the gas mixture. According to Nordgreen *et al.* [10], when metallic Fe is utilised as tar-depleting catalyst in the gasification of biomass, the product gas has significantly lower tar content. Almost 100% tar was broken down during the catalytic reaction at operating temperature of approximately 900 ºC. The capacity of Fe to diminish the tar content in the product gas has been demonstrated to be in the range of the capability of dolomite.

However, catalysts with highly dispersed metals or Fe on supports are more preferred in the industrial process compared to metal catalysts in the form of powders or screens. This is because the metal catalysts are very expensive and in addition, it has about the same catalytic activity with the metal exposed on the surface of the support in the metal supported catalysts [35]. In the case of iron supported catalyst, surface area of the iron oxide catalyst played an important role in the catalytic tar decomposition. It was found that the addition of Al_2O_3 to iron oxide is one method for the improvement of the surface area without deactivation [24].

In order to eliminate most of the inconveniences encountered with the present catalysts in the biomass gasification processes, zeolite beta (BEA) supported

monometallic and bimetallic Fe and Ni catalysts have been developed. A second metal component is introduced to form a bimetallic catalyst system with the intention of improving the anti-coking property of the catalyst.

1.3 Objectives of Research

In this study, monometallic and bimetallic structures such as FeNi and NiFe in which the Fe and Ni are compatible elements with different sequence as a second metal have been proposed. The strong interaction between Fe and Ni elements used in the bimetallic structure is proposed to have the capability to limit the sintering of the active species as well as carbon build-up.

Zeolite Beta (BEA) has been selected as support because of their molecular sieve properties as well as shape selective characteristic and excellent acid support [36]. Compared to amorphous support and due to higher density of acidic sites present in the BEA, BEA would be able to improve the selectivity of the production, increase the reaction activity and able to act as additional resistance to sulphur poisoning [37]. Therefore, combination of Fe and Ni active metals with BEA as support is expected to mitigate the problems faced with current gasification catalysts.

The main objectives of this study are:

i. To develop Zeolite Beta supported monometallic and bimetallic catalysts with Fe and Ni.

ii. To characterize the physicochemical properties of the prepared catalyst using N_2 adsorption-desorption to determine the total surface area, volume and pore distribution, Powder X-Ray Diffraction (XRD) for crystalline phase and crystallite size identifications, Field Emission Scanning Electron Microscopy with Energy Dispersive X-ray spectroscopy (FESEM-EDX) to study the morphology and elemental analysis of the catalysts and Temperature Programmed Reduction (TPR) to determine the reducibility of metal present on the catalyst surface as well as to investigate interaction between metal.

iii. To determine the catalytic activity of the BEA supported Fe and Ni catalysts in the steam gasification of PKS for H_2 production.

1.4 Scope of Research

Several phases are involved in completing the study. The first phase is catalyst preparation where BEA was impregnated with Ni and Fe using incipient wetness impregnation method. Various parameters in catalyst preparation have been varied to determine the differences in the catalysts properties and interaction between the active metals and support leading to the catalyst activity.

i. Metal loading

The catalysts were prepared with different Ni and Fe metal loading. 5%Ni or 5%Fe are referred as monometallic catalysts while 5%Fe5%Ni or 5%Ni5%Fe are referred as bimetallic catalysts.

ii. Impregnation method

The bimetallic catalyst preparation can be divided into two methods which is sequential impregnation (SI) and co-impregnation (CI) method. Sequential impregnation means the Ni and Fe metals will be impregnated one after another via 2 step impregnation processes while co-impregnation means the Ni and Fe metals will be impregnated together in a single step impregnation process.

iii. Calcination temperatures

As a final process, the catalysts prepared were calcined at 500, 600 and 700ºC. Different calcination temperatures will give a significant effect on the carbon decomposition and crystallization of the catalysts.

The next phase is catalyst characterization to determine the structural properties of the catalysts prepared. The synthesized catalysts were characterized by typical characterization methods such as Brunauer-Emmett-Teller (BET) to determine the total surface area, volume and pore distribution, Powder X-Ray Diffraction (XRD)

for crystalline phase and crystallite size identifications, Field Emission Scanning Electron Microscopy with Energy Dispersive X-ray spectroscopy (FESEM-EDX) to study the morphology and composition of the catalysts and Temperature Programmed Reduction (TPR) to determine the reducibility of metal present on the catalyst surface as well as to investigate interaction between metals.

All the prepared catalysts were then tested in the steam gasification of PKS to determine the catalysts' performance. This study only focused on the gas compositions produced from the steam gasification process. The prepared catalyst which was able to exhibit higher in concentration of hydrogen gas was selected as the best catalyst.

1.5 Thesis Outline

This dissertation consists of five chapters and the details were stated below:

i. Chapter 1 is the introduction of the study where it includes background of research, definition of the problem, brief history leading to the problem, scope and outline of the thesis.

ii. Chapter 2 is the literature review section. It consists of critical evaluation, discussions of what has been done along the line of the problem, certain findings, theory, the issues and challenges faced by other researchers, as well as the summary of the general body of knowledge.

iii. Chapter 3 is the methodology section or method of investigation. This section discussed the general framework of the problem being addressed. It also discussed the comprehensive research methods such as experimental procedure, characterizations, instrumentations and equipments being used in the study.

iv. Chapter 4 is the analysis of data and discussion of results. This chapter includes detailed description of the findings and results obtained, followed by discussions, analysis and interpretations of the data.

v. Chapter 5 is the final section of the thesis which concludes and summarises the study, results and findings. Recommendations and suggestions for future work have also been stated in order to improve and extend the current work to other related areas.

The sufficient information and findings from this thesis can be used as a future reference for the catalyst development especially regarding biomass gasification application in order to produce high yield of hydrogen gas.

CHAPTER TWO

LITERATURE REVIEW

2.1 Renewable Energy

The rapid decrease in fossil energy resources and the accumulation of carbon dioxide and other greenhouse gases in the atmosphere are thought to give a major impact on mother earth, mainly on the global climate and economy. Due to these concerns, there is a growing trend towards employing modern technologies in the development of renewable energy sources. Renewable energy has contributed about 8.064 Quadrillion Btu from 75.031 Quadrillion Btu of the total energy produced globally in 2010 and this statistic is estimated to increase in the year 2012. Figure 2.1 shows the world percentage share of energy resource reported by U.S Department of Energy [38] while the potential renewable energy resource in Malaysia is tabulated in Table 2.1 [39].

The main renewable energy sources can be classified as biomass, hydropower, geothermal, wind and solar energies. When compared to conventional energy such as natural gas, petroleum and coal, renewable energy is cleaner and produces lower or negligible levels of greenhouse gases and other pollutants. Renewable energy is also inexhaustible energy where the energy sources can be replenished in a short period and occur naturally in the environment [9]. Therefore, the sustainability of renewable energy can be considered to be a prime fuel for future energy in meeting energy needs, economical factor and environmental sustainability.

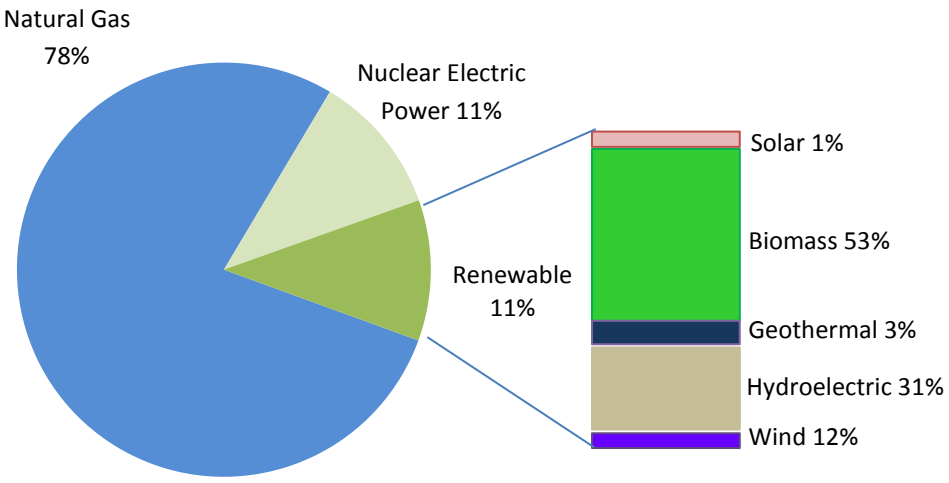

Figure 2.1: Percentage share of energy resource [38]

It has been estimated that the volume of biomass that can be modestly obtained is not affecting any other agriculture crops or forest usage. This is because biomass availability is considered as residue from agriculture, forest, mill or municipal solid waste. Biomass energy consumption stood at 3,596 trillion Btu or 53 percent of the global renewable energy market in 2007 [38] and it was also expected to increase in the year 2011. Indeed, Malaysia generated 18 million of biomass energy per year of the local renewable energy production [39].

Table 2.1 Renewable energy resource potential in Malaysia [39]

Renewable energy resource	Energy value (RM million per year)
Forest residues	11,984
Oil palm biomass	6,379
Solar thermal	3,023
Mill residues	836
Hydro	506
Solar PV	378
Municipal waste	190
Rice husk	77
Landfill gas	4
Total	18, 000

Apart from that, the Malaysian government has identified oil palm biomass as the biggest resource that can be easily generated, thus having the greatest potential for bringing renewable energy into the mainstream energy supply [40]. Therefore, due to biomass spread and worldwide availability, biomass energy potential is addressed to be the most promising among the renewable energy sources.

Even though the renewable energy production is still minimal, with the high attention and proactive efforts from all agencies such as the government and NGOs will certainly guarantee renewable energy has a promising future. In Malaysia, there was a significant attempt towards the utilization of renewable energy in power generation under Small Renewable Energy Programme (SREP) [1, 16]. Industry such as oil palm mills were encouraged to develop integrated plant by using biomass for power generation [18]. In 2008, Tenaga National Berhad (TNB), the largest power company in Malaysia signed an agreement with Federal Land Development Authority (FELDA) and Japan's J-Power to develop a biomass power plant in Jengka, Pahang. This project uses EFB as fuel source to generate electricity with 10MW capacity and is expected to be completed by the end of 2010 [16]. Apart from that, in Ninth Malaysia Plan (RMK 9), Clean Development Mechanism (CDM) under the Kyoto Protocol have been utilised to provide support for the implementation of Small Renewable Energy Programme (SREP). As a result, a few biomass steam and power plant were built in Sabah and Lumut to accomplish the energy demand in Malaysia [3].

Furthermore, the production of biodiesel as an alternative source of biofuel has also received major interests. Biodiesel produced through oil palm possessed similar properties to petroleum diesel and can be used directly as fuels in diesel engines with little or no modification [41-42] This was achieved with the construction of 2 biodiesel plants by Malaysian Palm Oil Board with projected capacity of 60,000 metric tons of production in Pulau Indah Klang, Selangor and Pasir Gudang, Johor [17].

2.2 Biomass

In general, biomass can be defined as an organic material that has stored sunlight in the form of chemical energy [9]. Biomass is available on a renewable basis, either through natural processes or it can be made available as by-product of human activities such as wood waste or organic waste from agricultural processes as well as municipal solid waste and industrial waste [5].

Biomass also has the unique advantage where it can provide solid, liquid and gaseous fuels energy through thermochemical and biological routes. The energy that is being utilized does not contribute to environmental pollution due to negligible amounts of sulphur and nitrogen in biomass [23]. Therefore, biomass is known as a clean energy and formidably positive environmental as compared to conventional fossil fuels. Moreover, McKendry [5] has suggested that the use of biomass could help address many concerns facing our world such as reducing the impact of energy production and global environment.

On top of that, all biomass is one part of the carbon cycle. The energy derived from biomass released CO_2 into the atmosphere and naturally recycles the CO_2 by converting into biological matter via photosynthesis. This CO_2 cycle will not only help biomass energy limiting the greenhouse effect but also help to achieve the CO_2 emission targets established by the international agreements, such the Kyoto protocols [5].

Major organic components of biomass materials can be classified as 40-50 wt.% cellulose, 20-40 wt.% hemicellulose and 10-25 wt.% lignin on a dry basis. Cellulose is a glucose polymer which constitutes to approximately 50% of the cell wall material. The empirical formula for cellulose is $(C_6\ (H_2O_5))_n$ where it is very long polymer of glucose units without any branches, strong and resistant to hydrolysis. Meanwhile, hemicellulose is a mixture of polysaccharides, composed almost entirely of sugars such as glucose, manose, xylose and arabinose. Molecular formula for hemicelluloses is $(C_5\ (H_2O_4))_n$. In contrast to cellulose, hemicelluloses consist of branched polysaccharide that bind tightly and is easily hydrolyzed by a dilute acid or base. Lignin is a complex structure and established by three carbon chain attached to

rings of six carbon atoms called phenyl-propane [1, 5]. The chemical structure of cellulose, hemicelluloses and lignin are shown in Figures 2.2, 2.3 and 2.4, respectively.

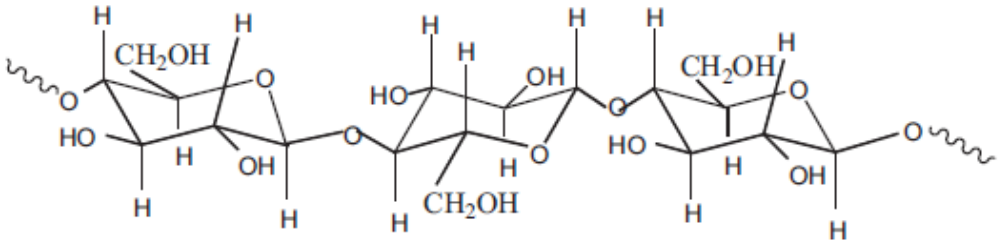

Figure 2.2 The chemical structure of cellulose [43]

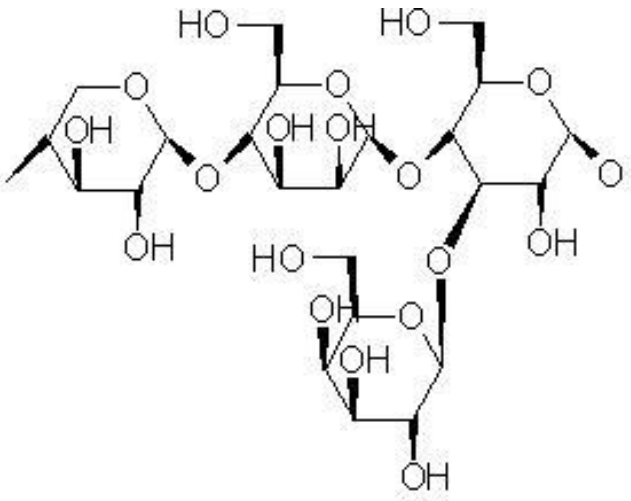

Figure 2.3 The chemical structure of xylose, a type of hemicellulose [43]

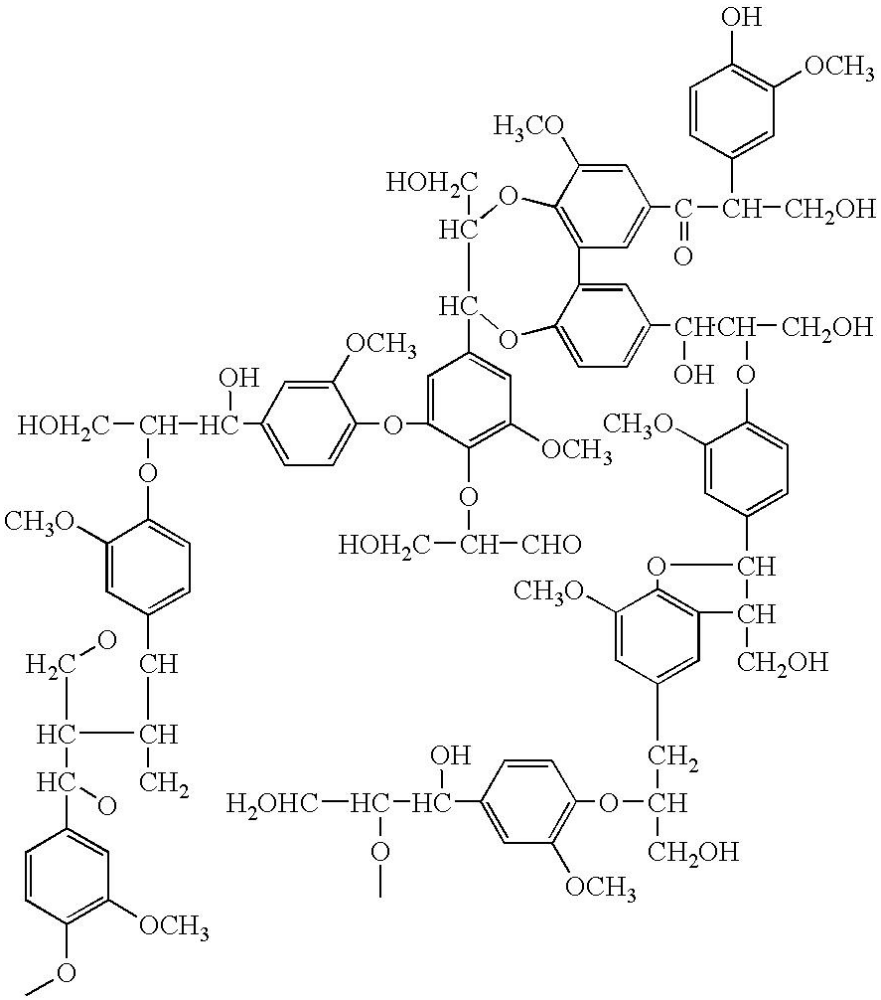

Figure 2.4 The chemical structure of lignin [43]

The pyrolysis of hemicelluloses and cellulose occurred quickly, where the degradation of hemicelluloses occurred at 220-315 °C and cellulose happened at 315-400 °C. Lignin is more difficult to decompose due to degradation of lignin occurred at a range of 150 to 900 °C. However, according to Yang *et al.* [44] hemicelluloses, cellulose and lignin promote different gases during the pyrolysis. The overall gas composition produced from pyrolysis of hemicelluloses, cellulose and lignin is tabulated in Table 2.2. The data was calculated by integrating the gas produced from 200-900 ºC.

Hemicelluloses produced higher CO_2 while cellulose enhanced the CO production. Higher formation of H_2 and CH_4 was observed in the degradation of lignin. This happened due to different chemical structure of biomass whereby hemicelluloses has higher carboxyl (C=O) content, while cellulose higher in

carbonyl (C-O-C) and carboxyl (C=O) group. As compared to hemicelluloses and cellulose, lignin has higher content of aromatic ring and methoxyl (O-CH_3) functional group and actively degraded at above 600 ºC which resulted in higher activity.

Table 2.2 Yield of gas produced from pyrolysis of biomass [44]

Sample	Gas product yield (milli mol/g-biomass)					
	H_2	CO	CH_4	CO_2	C_2H_4	C_2H_6
Hemicellulose	8.75	5.37	1.57	9.72	0.05	0.37
Cellulose	5.48	9.91	1.84	6.58	0.08	0.17
Lignin	20.84	8.46	3.98	7.81	0.03	0.42

2.2.1 Availability of Oil Palm Biomass

Palm oil industry is an important component of the national economy, especially the agricultural sector. Oil palms in Malaysia are a species of the *Elaeis guineensis* group which originated from West Africa. Generally, each oil palm tree produces 12-20 fresh fruit bunches per year with more than 1000 fruits per bunch. Each fruit consists of a hard kernel inside a shell which is surrounded by the mesocarp (Figure 2.5). The oil palm produces two kinds of oil crude namely, palm oil from mesocarp and palm kernel oil from the kernel [18].

Figure 2.5 Palm fruits [18]

Malaysian palm oil industry has grown tremendously over the last 4 decades and since then, it has maintained its position as the world's leading country in the production of palm oil. The amount of residues generated also shows a corresponding increase with the growth of palm oil production in Malaysia. One hectare of oil palm plantation can produce about 50–70 tonnes of biomass residues. In 2005, the oil palm industry produced the largest amount of biomass in Malaysia with 85.5% out of more than 70 million tonnes as shown in Figure 2.6. Therefore, its production is estimated to increased in the year 2011. Other types of biomass also generated in Malaysia are from the wood and sugarcane industry, municipal solid waste, rice husks from agriculture and others [16].

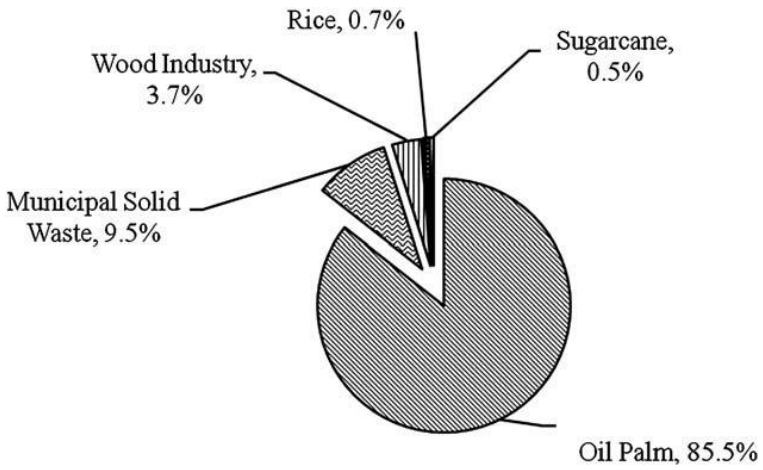

Figure 2.6 Biomass produced from different industry in Malaysia [16]

Figure 2.7 shows the biomass produced from oil palm industry. There are empty fruit bunches (EFBs), fiber, palm kernel shell, fronds and trunks. According to Warbeck [18], an average content of the fresh fruit bunch (FFB) can produced about 25% oil, 5.5% kernel, 6% shell, 12% fibre, and 25% empty fruit bunch (EFB) while the balance is moisture. The availability of oil palm biomass generated annually is tabulated in Table 2.3. Yearly, a hectare of plantation can generate about 4.42 tons of EFB, 2.71 tons of mesocarp fibers, 1.10 tons of palm kernel shells, 2.52 tons of palm kernel trunks and 10.88 tons of fronds [7].

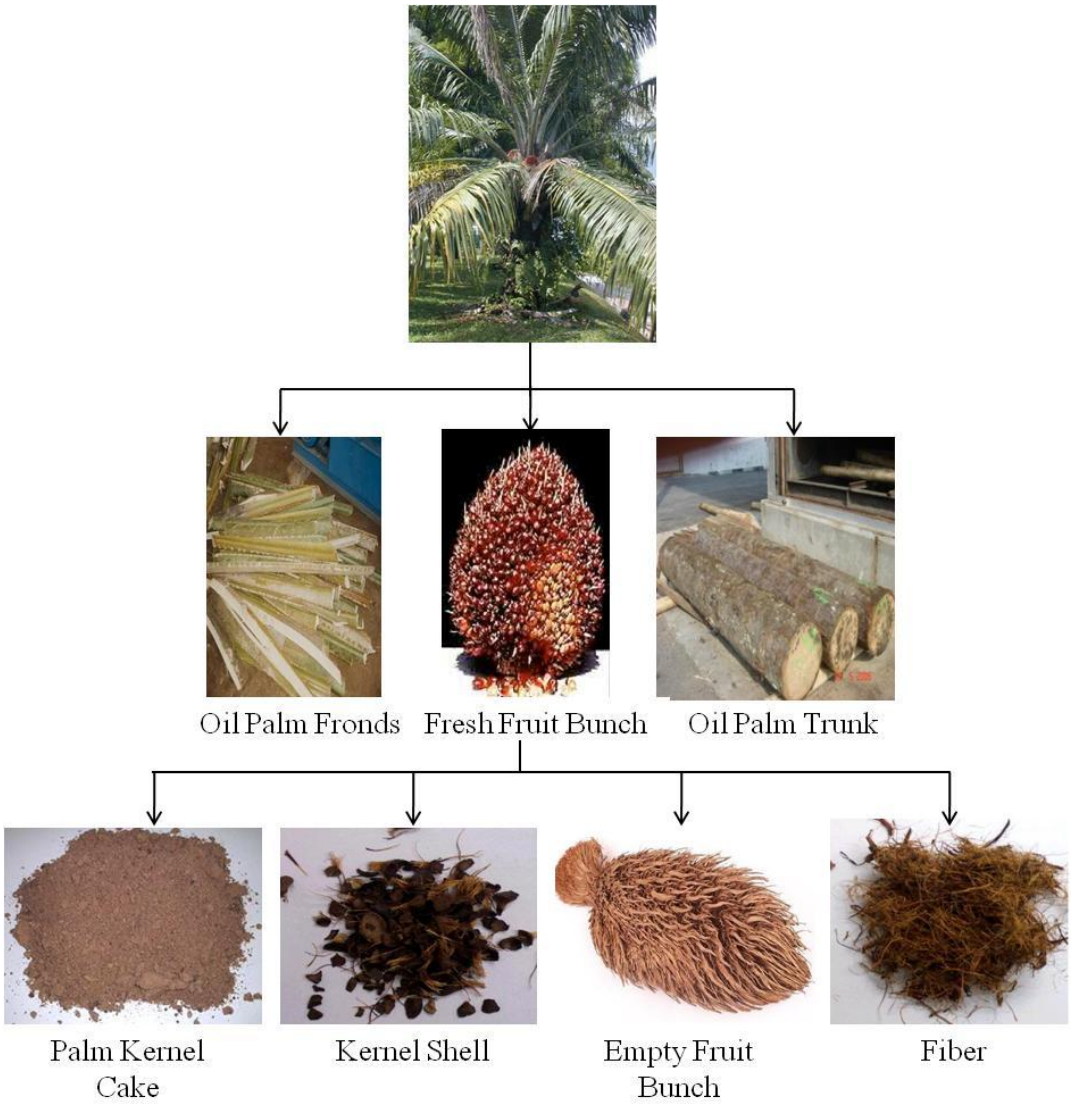

Figure 2. 7 Biomass produced from oil palm industry [17]

Table 2. 3 Oil palm biomass generation [45]

Biomass component	Quantity available (million tonnes)
Empty fruit brunches	4.42
Mesocarp Fiber	2.71
Palm Kernel Shell	1.10
Fronds	10.88
trunks	2.52
Total	21.63

Figure 2.8 shows that 184.6 million tons of oil palm biomass was produced globally and the amount increases exponentially each year [7]. Due to the huge amount of biomass generated annually, Malaysia has the potential to utilize the biomass efficiently and effectively to other value added products.

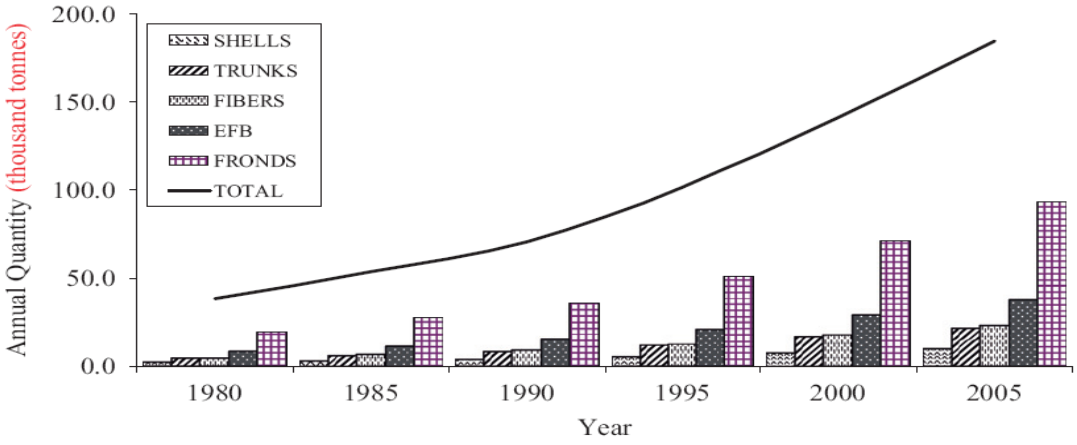

Figure 2.8 World annual oil palm biomass generation [7]

Currently, the shell and fibres are the main sources of energy in palm oil mills where they are burnt in boilers to produce heat and electricity for the milling process. Although other initiatives have started to find use of oil palm biomass, the conversion process is still not enough to fully utilize the biomass. This is because the quantity of oil palm biomass generated is very large hence some of it was discarded and burnt causing air pollution and green house gases. Therefore, more research and development need to be focused to identify the potentials of this oil palm biomass to grow as 'zero waste' concepts [18, 46].

2.2.2 Current Biomass Conversion Technologies

There are several main routes or technologies for conversion of biomass into energy and higher value products instead of biomass combustion. They are mainly classified as biochemical and thermochemical routes as presented in Figure 2.9. The biochemical process led to biodiesel and bio-ethanol productions which are the most modern biomass- based transportation fuels globally. Biodiesel is produced from

transesterification of vegetable oil with alcohol and is known as a renewable replacement to petroleum-based diesel. Meanwhile, bio-ethanol is a petrol additive or substitute and is derived from alcoholic fermentation of sucrose or simple sugars, which are produced from cellulosic biomass by hydrolysis process [9].

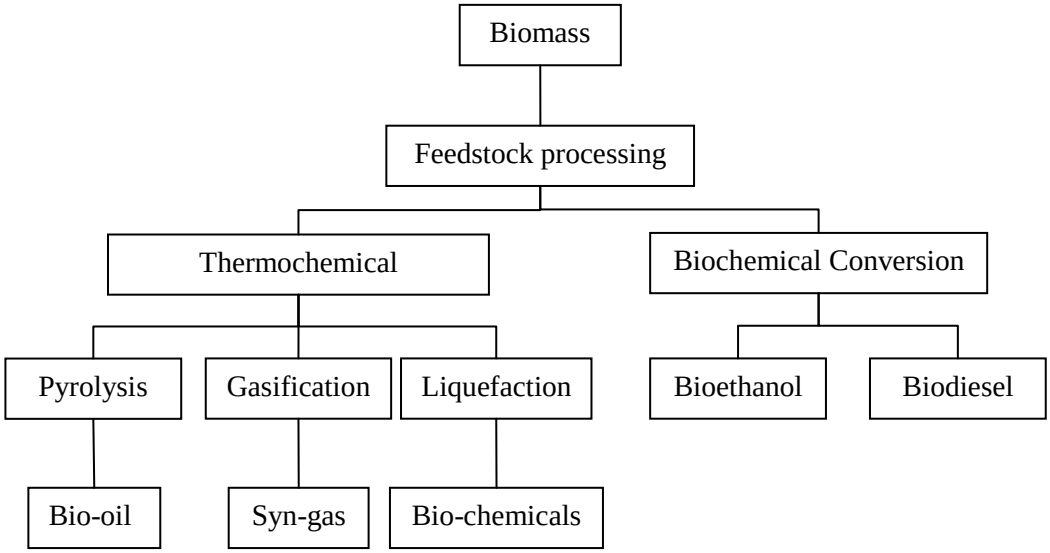

Figure 2.9 Main biomass conversion processes [9]

In the case of thermochemical processes, biomass can be converted into energy through pyrolysis, gasification and liquefaction. Gasification is the conversion of biomass into a combustible gas mixture by the partial oxidation of biomass at high temperatures, typically in the range 800-900 ºC. Meanwhile, pyrolysis is the conversion of biomass to liquid (bio-oil), solid and gaseous fractions by heating the biomass in the absence of air at temperatures around 500 ºC. Liquefaction is the conversion of biomass into a stable liquid hydrocarbon using low temperatures and high hydrogen pressures [47]. Each process gives different range of products such as bio-hydrogen or syn-gas and bio-oil which currently have higher demand in both developing and industrialized countries.

Selection of a conversion technology for biomass depends on the form in which the energy is required. However, among the existing biomass thermochemical conversion technologies, biomass gasification has attracted the highest attention in the industry as it offers higher efficiencies in relation to combustion. Apart from that,

gasification technology is one of the established green technologies in the world and the most promising method in converting biomass to hydrogen energy since it can produce high purity of hydrogen [9, 22].

2.3 Hydrogen Energy

Hydrogen gas is highly attractive as a future energy carrier where it can be stored to match energy production and energy demand. Hydrogen gas can be potentially used either as a gaseous fuel for power generation or as a feedstock for clean transportation fuel where hydrogen may be used in fuel cells and internal combustion engine. Certainly hydrogen is three times lighter than gasoline or diesel fuel per unit of mass for the same energy which formulate it higher in performance. Furthermore, the reaction between hydrogen and oxygen produces only water and heat thus demonstrating that hydrogen is an environmental benign energy. Hydrogen is also crucially important as a chemical feedstock in chemical process such as petrochemical, methanol, dimethyl ether, Fisher-Tropsch oils, polymer synthesis and as an energy carrier in clean sustainable energy systems. [2, 13-15]. Figure 2.10 illustrates the H_2 formation from several resources.

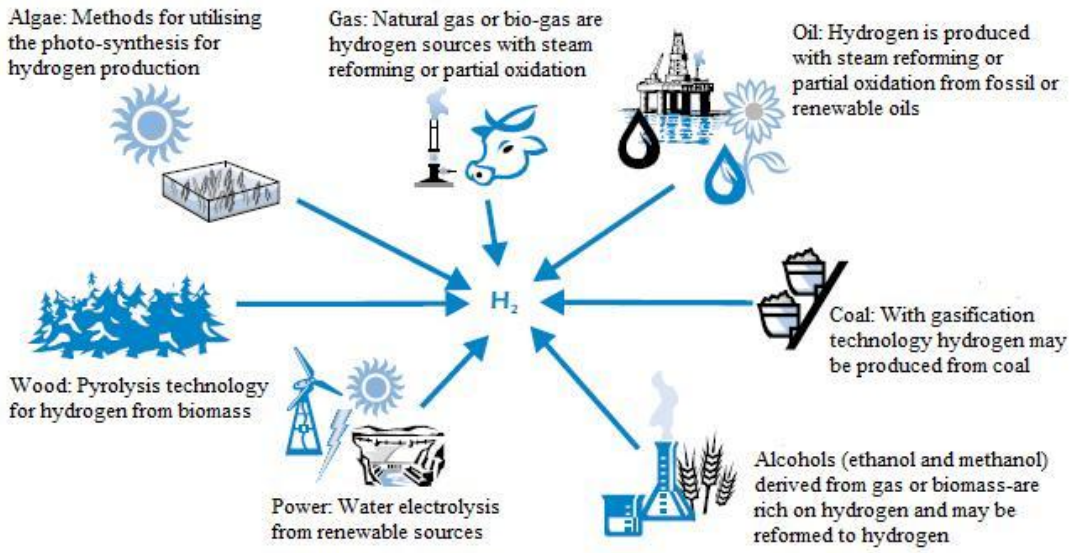

Figure 2.10 Hydrogen resources [21]

Most of the hydrogen produced globally especially for the petrochemical industry is obtained from steam reforming of naphtha or methane, natural gas, residual oil, petroleum coke and coal. The majority of hydrogen produced extensively is achieved by steam reforming of methane where methane from natural gas is reacted with steam to produce synthesis gas. The second approach commonly used to produce hydrogen is the partial oxidation of natural gas followed by coal gasification. Coal is reacted with oxygen and steam at high pressure and temperature to produce a gas mixture consisting mainly of H_2, CO and CO_2 [19-21].

However, utilization of these fossil fuels as a feedstock for hydrogen production is not effective due to the release of CO_2 gas into the environment during the gasification process through partial combustion with O_2 and air. Therefore, due to environmental problems and scarcity of these fossil fuel as well as economic standpoint, biomass can be viewed as a key economically viable component to a renewably based hydrogen economy. Besides, competition between natural gas and coal as energy source mainly for petrochemical and electricity significantly demonstrate that biomass is a good prospective for the replacement of fossil fuel in hydrogen production [2, 20].

Another method available for hydrogen production is through water electrolysis and photosynthetic microorganisms. Water electrolysis is the process whereby water is split into hydrogen and oxygen in the presence of electric current. It is the first process to produce pure hydrogen in the late 1920s. The electricity required for electrolysis can be generated using renewable energy technologies, such as wind, solar, geothermal and hydroelectric power. Hence, water electrolysis potentially reduce the production cost and yet is typically suitable for short term process. Photosynthetic microorganisms can produce biological hydrogen directly from solar energy. When microbes, such as green algae and cyanobacteria consume water in the presence of sunlight, they produce hydrogen as a by-product of their natural metabolic processes. However, this method depends heavily on the consistent supply of sunlight, which forced its limitations [21].

The hydrogen production derived from biomass is super clean and has many advantages over conventional hydrogen production. This is because the hydrogen

produced from fossil fuel or natural gas contributed more to environmental degradation if compared to clean energy derived from biomass. Various harmful pollutants are released including sulphur oxides (SO_x), nitrogen oxides (NO_x), carbon monoxide (CO), carbon dioxide (CO_2) particulate matter (PM) and volatile organic compounds (VOC). Apart from that, the release of greenhouse gases such as CO_2 to the atmosphere caused greenhouse effects and pollution of the environment and ecosystem of the world [2,7]

Hydrogen derived from biomass has been identified as one of the major sources of energy in the future mainly due to its high conversion efficiency which is estimated between 75-80%, stable element and non-corrosive as well as non-polluting nature [11, 14]. Producing hydrogen through biomass gasification releases near-zero net greenhouse gases because biomass resources consume CO_2 in the atmosphere as part of their natural growth process. Therefore, due to characteristic of biomass which is unique and renewable, the hydrogen production cannot be depleted, thus sustainable for the long term. Widespread use of bio-hydrogen as an energy source could also improve global climate change, energy efficiency and air quality. In addition, hydrogen production from biomass will also create an additional income and working field to the industry such as increase the demand for agricultural commodities [2, 14, 23].

2.4 Biomass Gasification

The combustion products from complete combustion of biomass generally contained CO_2 and H_2O. However, in biomass gasification as shown in Figure 2.11, incomplete combustion of biomass is known to produce hydrogen rich gas, CO, CO_2, CH_4 and various light hydrocarbons [8]. According to the previous study, the compositions of the gaseous product from gasification are depends on the gasification system, the method of operation and the process operating conditions i.e. types of gasifier, gasifying agent, temperature, pressure, catalytic decomposition, biomass species, particle size, heating rate and equivalence ratio [1, 11].

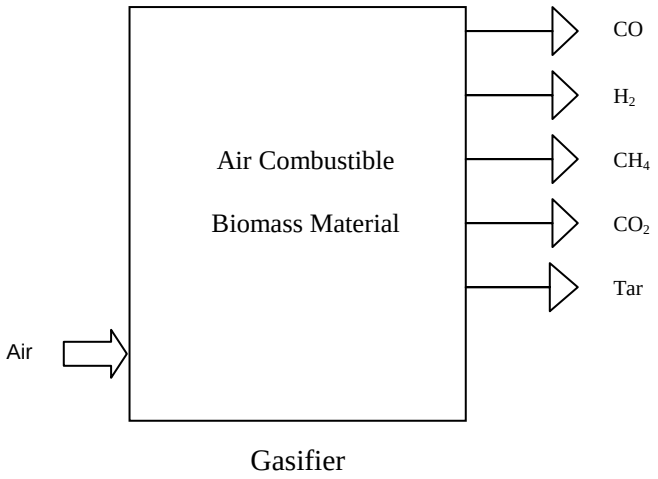

Figure 2.11 Products of gasification [48]

Air, oxygen, steam or their mixture is normally used as a gasifying agent. Usage of oxygen as a gasifying agent could produce a better quality syngas of medium heating rate but it requires a pure oxygen supply which increases the cost and safety issues [49]. The heating value and H_2 content in the syngas can be increased if steam is utilized as a gasifying agent. However, the operational costs will also increase due to demand for an external heat source for steam production [50]. Therefore, air is usually widely used as the main gasifying agent due to its low cost even the quality syngas is reduced due to large amounts of nitrogen content [51].

Nevertheless, biomass derived gasification also produces several undesirable amounts of ash particle, char, volatile alkali metals and tar. Tar can be defined as a complex mixture of acids, aldehydes, ketones, alcohols, phenols and aromatic hydrocarbons [24] meanwhile char is a solid carbonaceous materials. The formation of tar and char may cause the most severe problems in the biomass gasification because the components are very harmful and would limit the hydrogen production. Moreover, the continual build up of tar present in produce gas can cause blockage and damage to the equipment which will then reduce the efficiency of the gasification system [25].

The reactor for biomass gasification can be called as a gasifier. There are two types of gasifier normally used which is fluidised-bed and fixed-bed. However, Rapagna *et al.* [33] have indicated that fluidised-bed steam gasification is capable of

maximising the gaseous product yield and efficiency of tars and char cracking as compared to fixed bed gasifier. In addition, Effendi *et al.* [52] have studied the steam reforming of methane over Ni/Al_2O_3 in the fluidised-bed and fixed-bed reactors. Conducting the reforming in a fluidised-bed increased the conversion of CH_4 between 7-15% and reduced the coke formation as compared to fixed-bed reactor.

Apart from that, fluidised-bed units are also sufficiently flexible to be able to deal with a wide range of biomass and composition as well as effectively distribute uniform temperature in the gasification zone. There are two main types of fluidised-bed gasifier normally used which are circulating fluidised bed and bubbling bed. In the case of fixed-bed, the gasifier classification depends on the direction of air or gasifying agent flow such as downdraft, updrarft and crossdraft [11].

2.5 Gasification Process

There are a few different exothermic and endothermic reactions processes which take place either sequentially or simultaneously in the gasification system. Furthermore, the reactions are also different in fundamental chemical and thermal reactions. For endothermic reaction, external heat is supplied in a process by indirectly heated gasification. Typically, a small amount of air or oxygen is admitted for the purpose of partial oxidation, which releases sufficient heat for endothermic chemical reactions [1, 48].

Drying is the main beginning process in the gasification when biomass enters the gasifier. However, high moisture content in the biomass will give a significant effect on the reactions such as increasing the yield of char. Therefore, the desirable moisture content of biomass when used as a feedstock should be less than 10-15% before gasification [11, 48].

Generally, the gasification of biomass at high temperatures yield a product gas composed of CO, CO_2, H_2O, H_2, CH_4, higher hydrocarbons, tars, char, and ash as shown in Eq. 2.1. The presence of tar is harmful, however tar may be decomposed to

produce CH_4, other higher hydrocarbons and also H_2. The gasification reactions can be represented as follows [49, 53]:

$$Biomass + heat \rightarrow CO + CO_2 + H_2O + H_2 + CH_4 + higher\ hydrocarbons + tar + char + ash \quad \text{[Eq. 2.1]}$$

Methanation reaction: $C + 2H_2 \leftrightarrow CH_4$ [Eq. 2.2]

Then, CH_4 produced from biomass gasification and methanation reaction may react with water or steam to produce H_2 and CO. Under this reaction condition, CO is also produced by catalytic conversion of char. The conversion process is expressed as [1, 11, 53]:

Steam methane reforming: $CH_4 + H_2O \leftrightarrow CO + 3H_2$ [Eq. 2.3]

Water gas reaction: $C + H_2O \leftrightarrow CO + H_2$ [Eq. 2.4]

Boudouard reaction: $C + CO_2 \leftrightarrow 2CO$ [Eq. 2.5]

The product gas contains approximately 12% CO where it must be substantially removed in the H_2 production process. This is accomplished primarily by the water-gas shift (WGS) reaction in the presence of steam as a medium, which converts CO into CO_2 and additional H_2 [Eq. 2.6]. During the WGS reaction, CO and H_2O react in a 1:1 molar ratio on a catalytically active metal site to form CO_2 and H_2. This is a reversible reaction and therefore steam is added in excess to shift the equilibrium towards the product side. Presumably, the CO_2 is then removed by absorption [11, 22, 53-54].

Water gas shift reaction: $CO + H_2O \leftrightarrow CO_2 + H_2$ [Eq. 2.6]

Eq. 2.1 - 2.5 are also reversible reaction depending on the reaction condition. Besides, combustion reaction also occur in the gasification process whereby the combustion of carbon dioxide and water is obtained from carbon in fuel or biomass itself and hydrogen from steam reacted with oxygen. The main reactions are [1]:

Combustion reaction: $C + O_2 \rightarrow CO_2$ [Eq. 2.7]

$$2H_2 + O_2 \rightarrow 2H_2O \quad \text{[Eq. 2.8]}$$

$$CO + \frac{1}{2}O_2 \rightarrow CO_2 \quad \text{[Eq. 2.9]}$$

2.6 Catalyst

Catalysts are the key to the effectiveness of almost all biochemical and industrial chemical processes. A catalyst can be defined as a substance that accelerates a chemical reaction without being consumed in the process. Catalysts cause reactions to proceed more rapidly and they can be regenerated and reused for several times. A catalyst usually works by forming chemical bonds with reactants and assisting their conversion to form the final product [35].

Figure 2.12 shows the effect of a catalyst in a hypothetical exothermic chemical reaction. Compared to uncatalysed reaction, a catalyst provides lower activation energy and new pathway for reactant molecules to be converted into product molecules. In the biomass gasification, a catalyst is used to produce a tar-free product gas and increases the reaction rate in order to obtain higher yield and content of hydrogen gas. It has been indicated that the overall efficiency of the biomass conversion process can be increased by 10% with the use of a catalyst in gasification reaction [25].

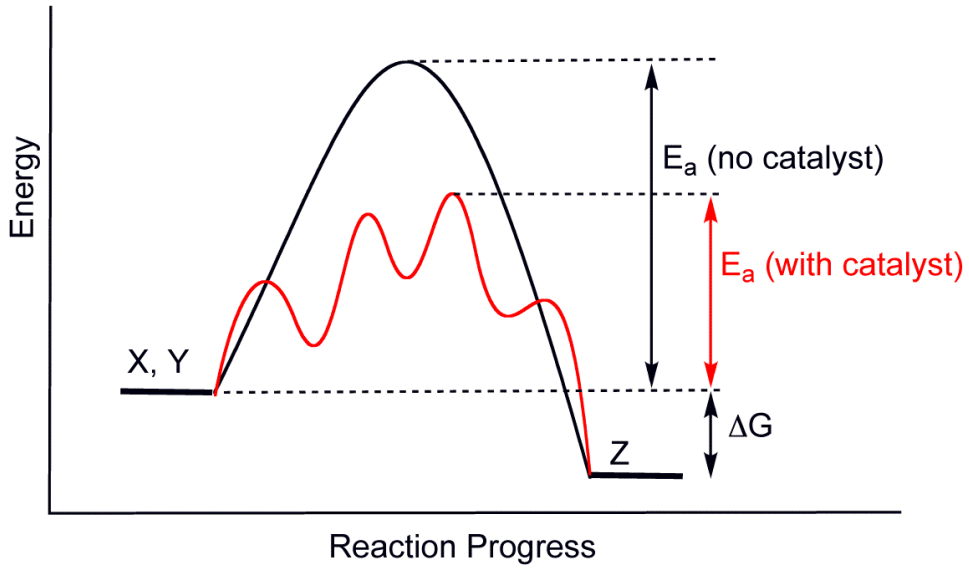

Figure 2.12 Effect of catalyst in the reaction

According to Sutton *et al.* [25], there is several criteria for consideration in choosing a suitable catalyst for biomass gasification. The catalysts must be effective

in terms of tar removal in order to obtain hydrogen rich gas in the product gases. The catalyst should also be resistant to deactivation and easily regenerated so that it can be utilized several times in the gasification process. Lastly, it should be strong as well as inexpensive for economic reasons.

2.6.1 The Nature of Supported Metals

Catalysts with highly dispersed metals on supports are preferable in the industrial process compared to metal catalysts which are very expensive. The distribution of metals is strongly dependent on the details of the catalyst preparation. The supported metal catalyst is often prepared by incipient wetness impregnation as impregnation is the easiest method of making a catalyst compared to precipitation method [54]. In incipient wetness impregnation method, an aqueous solution of a metal salt is contacted with a porous support. The solution fills the pores and some of the metals may be adsorbed depending on the polarization of the support surface, which is influenced by the pH of the solution. The resulting catalyst is then dried to allow the solution to be evaporated leaving the metal dispersed on the catalyst surface [35].

In the next step of a typical preparation, the impregnated catalyst is calcined or heated to a high temperature. The purpose of calcination is to eliminate volatile and unstable anions or cation (e.g. Cl^- from the metal salt precursor) that may also be left on the surface of the support during the preparation. In addition, calcination at high temperature is usually needed to increase the strength of the final catalyst [54].

Most reactions catalyzed by supported metals take place on the metal surface with the support usually being inert. Sometimes the support also plays a direct role in the catalysis in order to help maintain the dispersion of the metal. For further characterization of supported metal catalysts, X-ray diffraction pattern can be used to identify the crystalline phases and crystallite size. Meanwhile, Field Emission Scanning Electron Microscopy is important for estimating the shapes or morphology of metal aggregates on the support. The particles are nearly hemispherical but small aggregates especially those on strongly interacting supports may have much different shapes. Apart from that, N_2-physisorption is practical to determine the total surface

area of the particles, pore volume as well as pore distribution. Ultimately, reduction of supported metal catalysts was performed to determine the reducibility of the metal present on the catalyst surface and to investigate the interaction between the active metal and support [35].

2.6.2 Catalysis by Metal Supported Catalysts

A recent reviews by Sutton *et al.* [25], summaries the current status of catalysts in gasification. Catalysts can be divided into three groups; non-metallic oxides, alkali metals and supported metallic oxides. For non-metallic oxides, dolomite and olivine are widely investigated since they are inexpensive, abundant and can significantly reduce the tar content from a gasifier. However, the activity of dolomite and olivine is dependent on the Fe_2O_3 contents, which play an important role in lowering the rate of coke formation. Different dolomite and olivine have different activity, which may account for by different Fe_2O_3 contents and pore diameters.

Dolomite is a magnesium ore with the general formula of $MgCO_3.CaCO_3$ that contains about 30 wt.% CaO, 20 wt.% MgO and 45 wt.% CO_2 with other minor mineral impurities such as the trace minerals SiO_2, Fe_2O_3 and Al_2O_3. On the other hand, olivine is a naturally occurring silicate mineral containing oxides of magnesium, iron and silicon, namely magnesium aluminosilicate ($(Mg,Fe)_2SiO_4$) [25-26, 55].

Dolomite and olivine are significantly active only after calcination and reaction temperature conducted above 800 ºC. For dolomite, calcination removes CO_2 and forms CaO-MgO phase which improves its catalytic activity. While, calcination of olivine causes the elimination of (Mg, Fe) SiO_3 phase which is contributes to formation of Fe_2O_3. Nevertheless, the main limitation in using dolomite is that it is easily friable which causes it to disintegrate into fine particles during the reaction. In some cases, the powdered dolomite blends with tar resulting in blockage and clogging of the gasification system and as a result, affects the stable operation. Due to the lower attrition resistance of dolomite, it cannot be used inside a fluidized-bed gasifier; but it is suitable as a secondary treatment in two step gasification where it

is placed in a secondary reactor. On the contrary, olivine is a strong material and resist to attrition whereby it is more efficient to be used as a catalyst or catalyst support for fluidised-bed biomass gasification [8, 26, 53].

A few alkali metal catalysts were also studied such as potassium carbonate (K_2CO_3) and sodium carbonate (Na_2CO_3). Wang *et al.* [29] have investigated the steam gasification of coal char catalyzed by K_2CO_3. The results implied that the alkali catalyst produced hydrogen-rich gas with low formation of CO at temperatures between 700–750 °C with the catalyst loading from 10 to 17.5%. However, Sutton *et al.* [25] noted that the activity of alkali carbonate catalyst presented some operational problems during the gasification because of particle agglomeration. However, K_2CO_3 supported on alumina (Al_2O_3) was found to have significant activity and more resistant to carbon deposition although it was not as active as nickel catalyst.

The application of metal supported catalysts in biomass gasification is an effective method of reducing tar content. Among the transition metal between nickel (Ni), cobalt (Co), iron (Fe), ruthenium (Ru), platinum (Pt) and rhodium (Rh) catalyst, supported Rh catalyst shows the best performance in steam gasification. It was demonstrated that catalysts having a loading of $1.2x\ 10^{-4}$ Rh/g-cat can convert 98-99% of the carbon in biomass to gas products at 873K [13]. For economic reasons, nickel and iron based catalysts are still the preferred choice due to their wide availability and cheaper price instead of their effectiveness in terms of tar removal [8, 10, 24-25, 30]. Moreover, nickel based catalyst allows methane reforming and water gas shift activity during the gasification process, providing adjustment of the H_2/CO ratio in the product gas [31-32]. Nevertheless, the activity of the nickel based catalyst is sensitive to nickel loading and metal dispersion [25]. The reaction is frequently accompanied by coke formation and sintering of Ni metal particles, leading to catalyst deactivation.

It is possible to solve these problems by modifying the catalyst via the presence of other metals, in order to improve its properties [56]. Some studies have demonstrated that the nickel sintering could be limited when nickel oxide has strong interaction with some support [34] or prometer [32] and have a well defined structure like perovskite [33].

Several researchers have reported that nickel supported with olivine, dolomite, Al_2O_3, SiO_2 and MgO was proven to be very effective for biomass gasification and tar destruction [15, 31, 57-62]. Courson *et al.* [57] and Swierczynski *et al.* [31] have demonstrated that nickel oxide on olivine (Ni/olivine) after calcination at 1100 °C successfully increased the catalytic activity of biomass gasification whereby the catalyst enhances the gas yield and decreases the carbon deposition with increasing reaction temperatures. Natural olivine presents good characteristics to be applied as nickel support because the iron presence in olivine promotes and stabilises nickel in reducing conditions.

Ishida *et al.* [63] have investigated the effect of an inorganic alkali, Na_2CO_3 and a nickel catalyst, Ni/SiO_2 on the hydrogen generation from wood residue through hydrothermal reaction at low temperature (Figure 2.13). The process was performed in a stainless steel reactor where the reaction was conducted at 400 °C and the pressure was kept at about 25Mpa. An addition of 300 wt% Na_2CO_3 and 80 wt% Ni/SiO_2 catalyst resulted in highly effective production of hydrogen without releasing CO and small amount of CO_2 gas. Addition of larger amount of Na_2CO_3, 300 wt% significantly suppressed the formation of CO_2. However, larger amount of Na_2CO_3 was found to be uneconomical for the process.

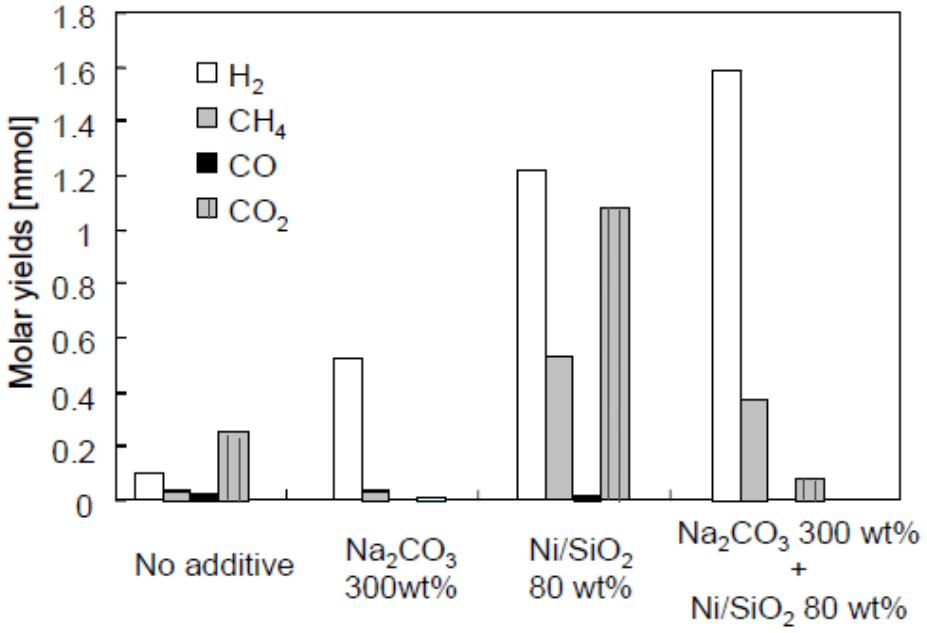

Figure 2.13 Effect of Na_2CO_3 and Ni/SiO_2 catalyst on the hydrogen production [63]

Chaiprasert and Vitidsant [32] have studied the effect of promoters on transition metal such as Pt, Co and Fe on biomass gasification using nickel/dolomite catalyst. The experiments were performed at 800 ºC with steam to carbon ratio (S/C) of 0.95. The experiment was carried out by using three types of catalysts which are 10%Ni1%Pt, 10%Ni1%Fe and 10%Ni1%Co. The effect of transition metal in catalytic activity in terms of gas composition is shown Figure 2.14.

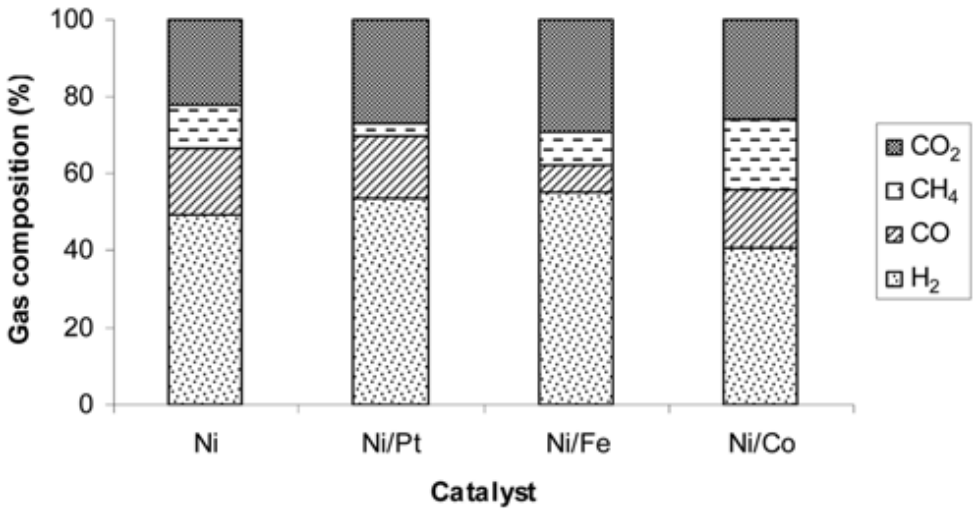

Figure 2.14 Effect of transition metal as promoter on gas composition [32]

Adding a small amount of transition metal as a promoter or second metal gives a significant effect on gas composition. The results implied that Ni/Pt/dolomite catalyst promoted steams reforming, water-gas shift reaction and increased H_2, CO, and CO_2 contents during the gasification process. Meanwhile, Ni/Fe/dolomite enhanced the water-gas shift reaction and increase H_2 and CO_2 production. The Ni/Co/ dolomite catalyst promoted methanation and reforming of methane, which increased the CH_4 and CO_2 content. The gaseous products were increased with the use of catalysts in the following order: Ni/Pt/dolomite (72.34%) > Ni/dolomite (70.34%) > Ni/Fe/dolomite (68.12%) > Ni/Co/dolomite (54%). However, in the case of coke formation stability, the order was as follow: Ni/Pt/dolomite (6.5%) < Ni/Fe/dolomite (8.3%) < Ni/Co/dolomite (9.3%) < Ni/dolomite (16.5%). Therefore, this demonstrated that the addition of noble metals may help to improve the metallic dispersion, decrease sintering and enhance the thermal stability.

Instead of dispersing active catalyst or metal on an inert support, the active catalyst species have also been inserted in a definite chemical structure in order to eliminate most of the inconvenience encountered with the sintering problem in the biomass gasification process. Rapagna *et al.* [33] have identified tri-metallic perovskite catalysts, $LaNi_{0.3}Fe_{0.7}O_3$ processing the best activity for converting methane (90% conv) at 800 ºC to produce hydrogen or syn gas. Carbon was not detected for reaction periods of up to 150h. Furthermore, the perovskite catalyst was also able to convert about 90% by weight of tar present in the raw gas at 800 ºC with no coke formation observed on the catalyst surface. This is because lanthanum hydroxyl or $LaFeO_3$ provides an oxidative character in the neighbourhood of nickel particles which participate to the destabilisation of the obtained carbonaceous species on the nickel sites [35].

Apart from that, commercially available iron metal catalysts are also active in reforming hydrocarbon and diminishing the tar content in the gas mixture. According to Nordgreen *et al.* [10], when metallic Fe is utilised as a tar-depleting catalyst in the gasification of biomass, the product gas has significantly lower tar content. Almost 100% tar were decomposed during the catalytic reaction at operating temperature of approximately 900 ºC. The capacity of Fe to diminish the tar content in the product gas has been demonstrated to be in the range of the capability of dolomite. However, as discussed previously, catalysts with highly dispersed metals or iron on supports are more preferred in the industrial process as compared to metal catalysts [35]. In the case of iron supported catalyst, surface area of the iron oxide catalyst played an important role in the catalytic tar decomposition. It was found that the addition of Al_2O_3 could improved the surface area of iron catalyst without deactivation [24].

2.6.3 Effect of Metal Loading

The changes in metal loading may affect the physical properties of the catalyst as well as its catalytic activity. Furusawa and Tsutsumi [61] have studied the effect of nickel loading in gasification process. The experiments were conducted at 1173 K with steam/carbon mole ratio of 0.6 and 2 hour reaction time. As tabulated in Table

2.4, Ni/MgO catalysts showed lower activity in this study than other work due to low steam/carbon ratio (0.6). However, 12% Ni loading yielded high carbon conversion and H_2 production as compared to 4 wt% and 36 wt%. Therefore, 12 wt% is the optimum nickel loading in the Ni/MgO catalyst for gasification process. This study illustrated that too small or too high of metal loading reduces the carbon conversion and product gas.

Table 2.4 Effect of nickel loading in gasification process [61]

Ni loading (wt%)	Carbon conversion to gas	H_2 (mol %)
0	3.7	62.5
4	4.3	64.8
12	7.9	77.2
36	5.7	75.9

2.6.4 Effect of Catalyst Preparation Method

Catalyst can be prepared using various preparation method such as impregnation (imp) and coprecipation (cop) method. However, each method gives a significant effect in the catalyst structure which influences the gasification process. According to Chaiprasert and Vitidsant [32] study, impregnation method yielded higher percentages of carbon conversion to gas as compared to coprecipitation method whereby 79.19% for Ni/Pt/dolomite (imp) and 50.51% for Ni/Pt/dolomite (cop). This is because the impregnation method gave higher BET surface areas than the coprecipitation method. High surface area provided large contact area for the reaction activity. The coprecipitation method resulted in smaller metallic surface area because metallic active species were transformed into a less active structure.

Impregnation can be divided into two preparations which are co-impregnation method (CI) and sequential impregnation method (SI). Co-impregnation is a single step impregnation process where metal, promoter and support are impregnated together before calcination while sequential impregnation involves two step impregnation processes where metal and promoter are impregnated separately to the support.

Figure 2.15 shows the catalytic performance of various Ni based catalysts in steam gasification with: 60 mgmin^{-1} biomass, 60 mlmin^{-1} N_2 flow, steam to carbon ratio (S/C) of 0.5 and 15 min reaction time. The result indicated that 4wt% $Ni/CeO_2/Al_2O_3$ catalysts prepared by CI method exhibited higher performance in the steam gasification of biomass than Ni/Al_2O_3 and $Ni/CeO_2/Al_2O_3$ prepared by the SI method. The rate of hydrogen formation was the highest and the total yield of tar and coke was the lowest as compared to other catalysts. This may be due to formation of Ni metal particles highly dispersed in CI method than SI which then provides high reactivity in the gasification process. Apart from that, the strong interaction between metals and support in CI catalyst can be evaluated by catalyst characterization whereby the results illustrated that CI catalyst has better physicochemical properties [15, 58].

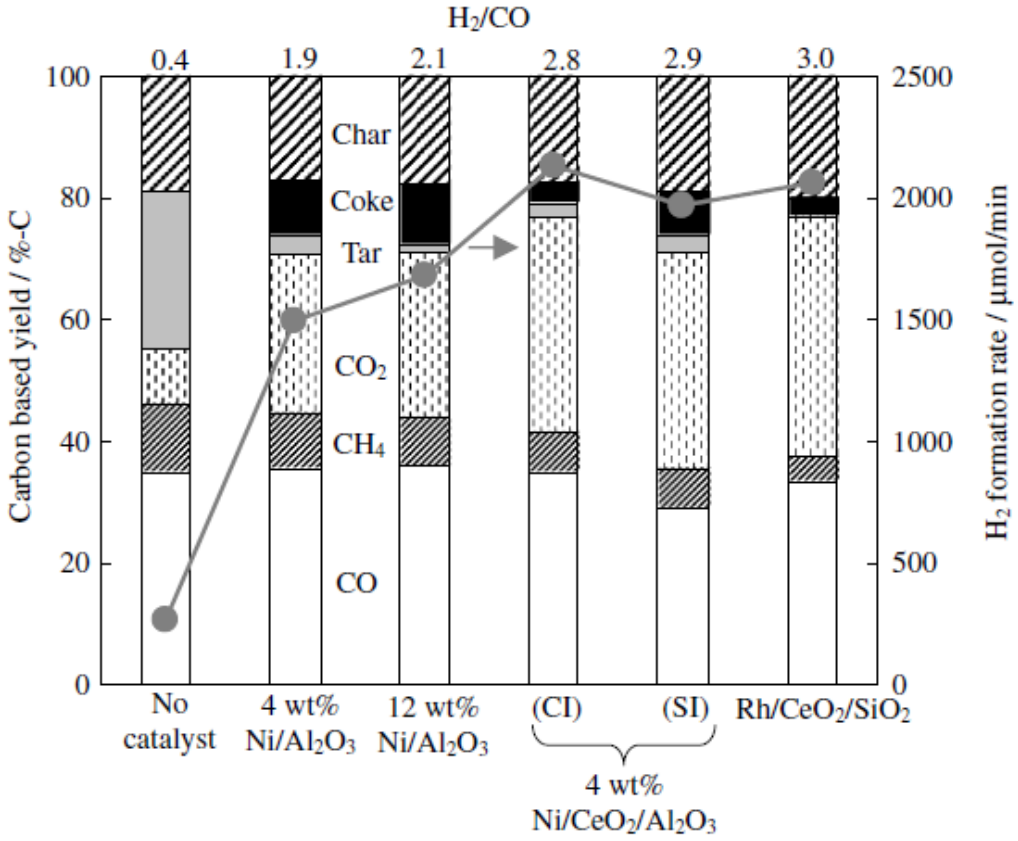

Figure 2.15 Catalytic performances of co impregnation and sequential impregnation catalysts in steam gasification of biomass at 873 K. [58]

2.7 Surface Structure of Support

Support can be defined as a carrier or an inert substance that provides a surface for active metals to be incorporated in order to help stabilize the catalytically active structure. The support may act as an inert material or involved in the catalytic activity depending on the reaction and reaction conditions [54]. In this study, zeolite beta was utilized as a support in the catalyst preparation.

2.7.1 Zeolite Beta

Zeolite beta or BEA as defined by International Zeolite Association Framework Designation is a crystalline material, hydrated aluminosilicates of alkaline or alkaline earth metals with well-defined micro- and mesopores. The frameworks are composed of $[SiO_4]^{4-}$ and $[AlO_4]^{5-}$ tetrahedral, which contains a silicon or aluminium atom in the centre [64]. Figure 2.16 illustrates the model of BEA in three dimensional networks of 12-ring pores. Since the ring is described principally by the oxygen atoms, this shows that there are 12 oxygen atoms sharing with SiO_4 and AlO_4 tetrahedra.

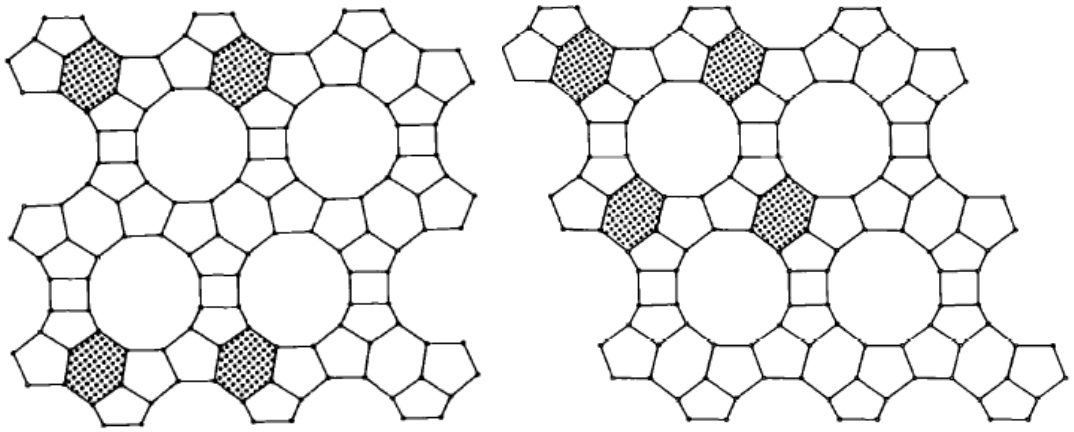

(a) (b)

Figure 2.16 Model of Zeolite Beta, BEA (a) polymorph A (b) polymorph B [65]

The BEA structure consists of an intergrowth hybrid of two distinct structures namely, polymorphs A and B. The intergrowth of the polymorphs does not significantly affects the pores in two of the dimensions. However, the pore becomes

tortuous when faulting happened [65]. The BEA model also demonstrated the pore present in small and large cavities; allowing the structure to be large enough for passage of even rather large molecules. BEA has both Lewis and Bronsted acid sites with some of the latter being very strong depending on catalytic activity [35].

Due to the excellent properties, zeolites are well-established in a number of industrial applications, ranging from low-end to high-end such as adsorbents and ion exchangers [66], pyrolysis of biomass [67] or as catalyst beds in the petrochemical industry and in the synthesis of fine chemicals [64]. BEA has been used as support for several catalysts because of their molecular sieve properties and shape selective characteristic. It has also been reported that some significant advantages can be added when amorphous support was replaced with crystalline materials such as zeolite. Selectivity will be improved due to higher density of acidic sites present in the zeolite, higher activity during reaction and additional resistance to sulphur poisoning [37]. Specifically, it is of interest to investigate the activity of metals supported on BEA for the development of catalyst for the biomass gasification because of the remarkable catalytic performance of these solids in other reaction.

2.8 Mechanisms of Catalyst Deactivation

Catalyst deactivation or the loss over time of catalytic activity is a critical problem for all industrial catalytic process. The deactivation of catalyst is unavoidable for most processes and the way it occurs are either immediate, drastic or slow depending on the process design, reaction condition, type of catalyst used as well as characteristic of the catalyst [27].

2.8.1 Poisoning

In catalytic gasification of biomass, a catalyst may be poisoned by any contaminants present in the feed. Biomass contains a variety of catalyst poisons such as sulphur, chlorine and alkaline metals depending on the type of biomass [30, 68]. The presence of poisons could react with catalyst forming non –active surface which will then

caused loss of activity in the reactions. The poisoning process may be rapid or slow and reversible or irreversible depending on the poison concentration and the strength of poison adsorbed.

Table 2.5 shows the sulphur content in various type of biomass which could give some significant effect to the catalytic gasification. It was indicated that oil palm biomass such as empty fruit bunch, mesocarp and oil palm fronds containing large amounts of sulphur as compared to other agricultural biomass [69]. According to Sato and Fujimoto [30], biomass which contains a large percentage of sulphur will produce high concentration of hydrogen sulphide (H_2S), carbonyl sulphide (COS) and sulphur dioxide (SO_2) in the product. Indeed, sulphur will react with metal catalyst forming non-active surface sulphide, metal-S as depicted in Figure 2.17.

Table 2.5 The sulphur content in biomass [69]

Biomass	**Sulphur content (%)**
Empty fruit bunch	0.22
Mesocarp fiber	0.51
Oil palm trunk	0.08
Oil palm frond	0.13
Rubber seed kernel	0.03
Sawdust	0.04
Sugarcane residue	0.06
Rice husk	0.06
Paddy straw	0.15
Coconut fiber	0.09
Coconut shell	0.05

There are four mechanisms of poisons that may affect catalytic activity: (i) adsorbed poison physically blocking one or more catalytic sites, (ii) adsorbed poison modifying the nearest neighbouring atoms and affect the catalyst abilities to react, (iii) adsorbed poison controlling the adsorbent surface causing dramatic changes in catalytic properties and (iv) adsorbed poison blocking access of adsorbed reactants and finally prevents or slows the surface diffusion of adsorbed reactants [27].

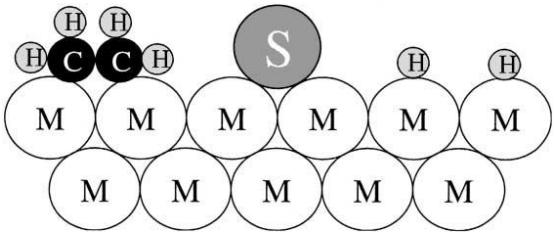

Figure 2.17 Conceptual model of poisoning on metal surface by sulphur atoms [27]

The deactivation of Ni catalysts through sulphur poisoning has been studied extensively by [30, 70-73]. Sato and Fujimoto [30] have successfully developed a Ni/MgO-CaO steam reforming catalyst promoted with WO_3 for sulphur resistance. Studies showed that WO_3 prevents the surface of the catalyst from sulphur adsorption, thus improving resistance to H_2S deactivation. Engelen *et al.* [70] synthesized 1-0.5 wt% Ni/CaO catalysts to study the ability of this catalyst to remove tar model compounds, such as benzene and naphthalene, from a simulated biomass gasification gas containing 50 to 200 ppm H_2S. The results observed that higher concentration of H_2S decreased the catalytic activity of the catalysts prepared.

Moreover, Tomishige *et al.* [71] also have studied the effect of H_2S addition in the gasification of cedar wood over Ni catalyst and $Rh/CeO_2/SiO_2$. It was demonstrated that the activity of Ni catalyst was reduced drastically in the presence of H_2S. However, $Rh/CeO_2/SiO_2$ exhibited higher and more stable activity in the presence of high concentration of H_2S (280 ppm).

In addition, Barbier [74] have investigated that the addition of small quantity of metal into other metal catalyst in bimetallic form will increase the poisoning resistance, particularly for reactions occurring at high temperatures. Therefore, small quantities of additives can greatly modify the resistance of metallic catalyst to sulphur poisoning. Table 2.6 tabulates the calculation of the desulphurizing temperature of various metals in the presence of 20 ppm of H_2S.

Table 2.6 The desulphurizing temperature of several metals commonly used as active phase in a catalyst formulation [74]

Metal	Desulphurizing temperature (°C)
Co	427
Cu	649
Fe	649
Ir	371
Mo	538
Ni	371
Pb	482
Pd	371
Pt	371
Ru	482

2.8.2 Fouling, coking and carbon deposition

Fouling is caused by mechanical deposition of carbon or coke on the catalyst surface, which results in loss of activity due to blockage of catalyst pores. Carbon is typically a product of CO disproportionation while coke is produced by decomposition of hydrocarbons on catalyst surfaces. Possible effects of fouling by carbon or coke on the functioning of a supported metal catalyst are illustrated in Figure 2.18.

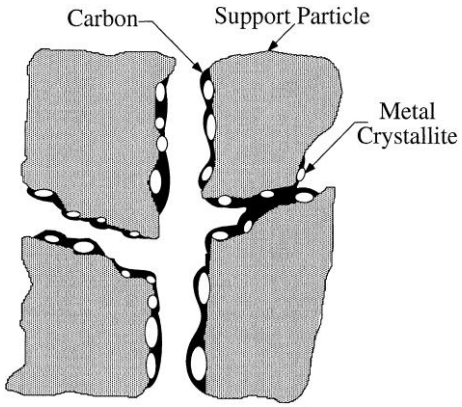

Figure 2.18 Conceptual models of fouling, pore plugging and crystallite encapsulation of catalyst due to carbon deposition [27]

Carbon may chemisorb strongly as a monolayer or multilayer and consequently blocking the metal surface sites. Moreover, carbon may also plug the pores leading to disintegration of catalyst and totally encapsulating the metal particle for deactivation [27].

The formation rate of carbon or coke can vary significantly with catalyst structure, promoter and catalyst support. It has also been reported that catalyst with oxide promoters (CeO_2, MgO) or oxide supports such as SiO_2, Al_2O_3 and MgO could control the rate of undesirable carbon or coke accumulation [8, 15, 27-28, 62]. This is because oxygen atom supplied from oxide promoters and supports are able to oxidize and gasify the carbon or coke accumulated on the catalysts surface [15].

In the case of supported bimetallic catalyst, different kinds of coke may form on the metal and the oxide support. Augustine *et al.* [75] have observed the formation of soft coke on Pt or Pt-Re metals and hard coke on the alumina support in their studies on Pt-Re/Al2O3 catalyst. They suggested that the coke precursors may be formed on the metal through hydrogenolysis following which they migrate to the support and undergo polymerization and cyclization reactions. As a result, the coke accumulated on the support causing loss of isomerisation activity, hence the catalyst was deactivated.

2.8.3 Thermal Degradation and Sintering

Thermal degradation and sintering of catalysts will result in loss of catalytic surface area and chemical transformations of catalytic phases to non-catalytic phases. Loss of catalytic surface area occurs mainly due to crystallite and atomic migration over the support surface as illustrated in Figure 2.19. Crystallite migration involves the migration of entire crystallites over the support surface followed by collision and coalescence, while atomic migration involves detachment of metal atoms from crystallites. Moreover, sintering of the catalysts also occur when the surface area of the support is lost due to collapse of the support and pore structure [27]. Furusawa *et al.* [62] have confirmed that the decrease in metal surface area is attributed to the deactivation of the catalyst.

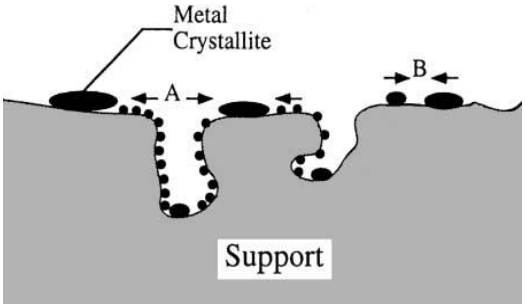

Figure 2.19 Two conceptual models for crystallite growth due to sintering by (A) atomic migration or (B) crystallite migration [27]

Sintering rates are dependent on the nature of the support surface and metal, nature of surface impurities as well as temperature. Sintering process generally takes place at temperatures above 500 ºC and are generally accelerated by the presence of water vapour. Typically, the catalyst sinter rapidly in the presence of oxygen due to carbonization and slowly in the presence of hydrogen. Most commercially available Ni catalysts display a moderate to rapid deactivation due to sintering effect. At high temperature, the metallic particles tend to migrate and form larger aggregates, reducing the dispersion and consequently the catalyst activity [8].

2.8.4 Vapour-Solid and Solid State reactions

There are several chemical routes leading to catalyst deactivation based on gas/vapour-solid and solid state reactions. Gas/vapour-solid reactions involve reactions of the vapour phase with the catalyst surface to produce inactive bulk. On the other hand, solid state condition can be categorized as reaction between metal, support and promoter as well as transformations of the catalytic phases during reaction. These forms of chemical deactivation can be avoided through careful control of reaction conditions and appropriate design of the catalyst [27, 68].

2.8.5 Mechanical Failure

Mechanical failure in terms of crushing the catalyst, attrition of catalyst agglomerates by reduction of catalyst size into fine particles and attrition of

catalyst particles at high fluid velocities in fluidized-bed are the common factors for catalyst deactivation [27]. Among the catalysts usually applied in the gasification process, dolomite catalyst is easily friable and eroded. This phenomenon causes it to disintegrate into fines particles consequently disturbing the operation of the fluidised-bed gasifier [8, 53]. As such, it is crucial to develop stronger and more attrition resistant catalyst materials for biomass gasification in order to avoid any catalyst fracture during the reaction [68].

CHAPTER THREE

METHODOLOGY

3.1 Introduction

This experiment was designed to develop a suitable catalyst for steam gasification of PKS to produce hydrogen. This research has been conducted in three phases which are catalyst preparation, catalysts characterization and lastly catalysts testing.

In order to investigate the effect of catalyst properties in the catalytic steam gasification, the catalyst preparation method were varied in terms of its calcination temperature, metal loading and impregnation method. The objectives of this research will be achieved by following the research methodology as shown in Figure 3.1.

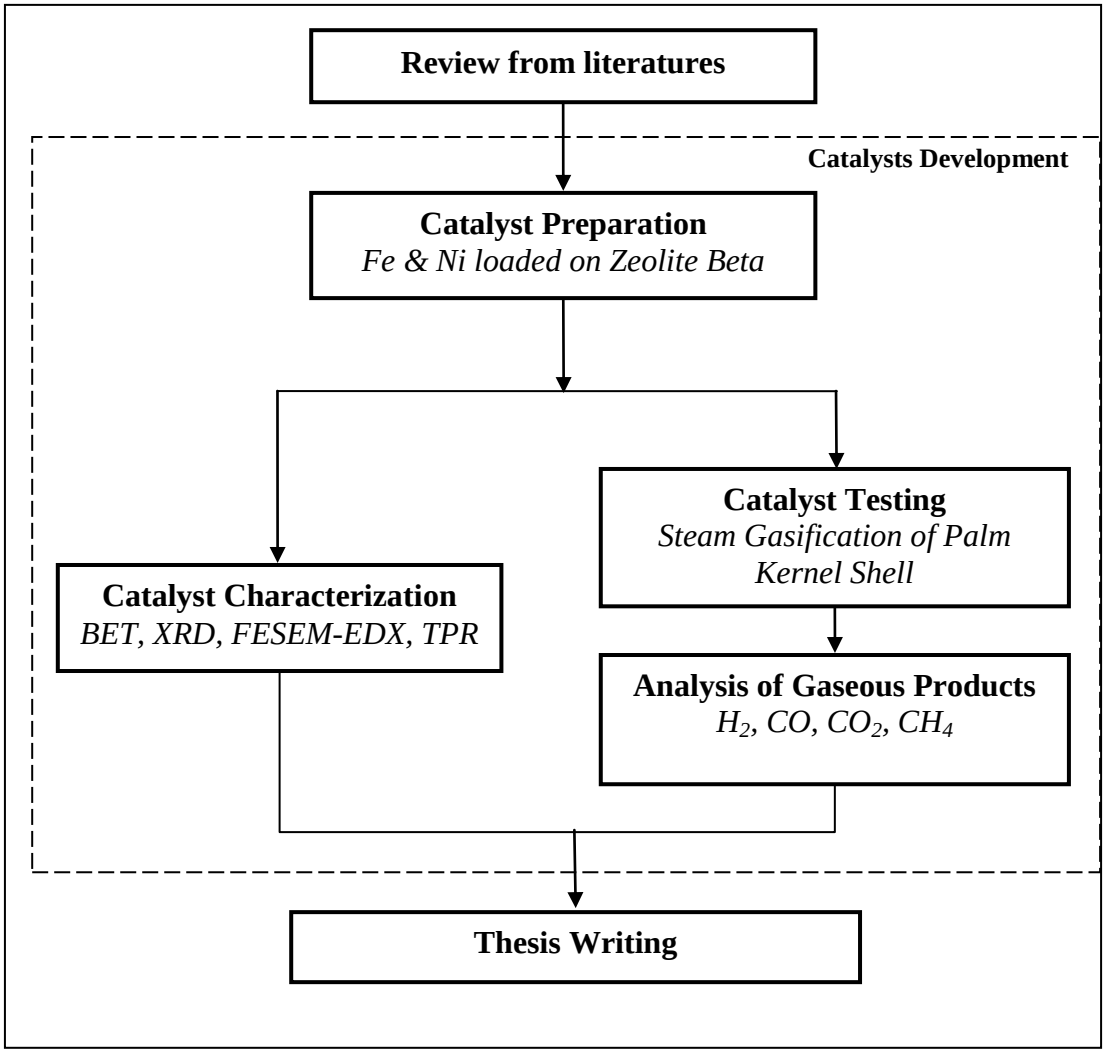

Figure 3.1 General research methodologies

3.2 Materials and Equipment

3.2.1 Reagents and Materials

The catalyst support used in this research was Zeolite Beta (BEA) with SiO_2/Al_2O_3 mole of 25 which were purchased from Zeolyst International. The metal precursors were iron (III) chloride hexahydrate ($FeCl_3.6H_2O$) and nickel (II) chloride hexahydrate ($NiCl_2.6H_2O$) were purchased from Sigma Aldrich. These reagents were used without any purification. The palm Kernel Shell (PKS) used in steam gasification reaction was collected from Oil Palm Plantation at Perak.

3.2.2 Equipment

The equipments used for catalyst preparation were an analytical balance machine to weight the chemicals, beakers to gather the mixture of chemicals, shaker or magnetic stirrer for the impregnation process, oven for drying of the samples, furnace to calcine the catalysts and crucibles to place the catalysts during calcination. For catalyst characterization, BET, XRD, FESEM-EDX and TPR instrument were utilized.

3.3 Catalyst Preparation

The catalysts prepared can be divided into two groups which are monometallic and bimetallic catalysts. For monometallic catalysts, 5 wt% of metal loading of Ni and Fe based catalysts were prepared using incipient wetness impregnation methods with BEA as the support (Figure 3.2).

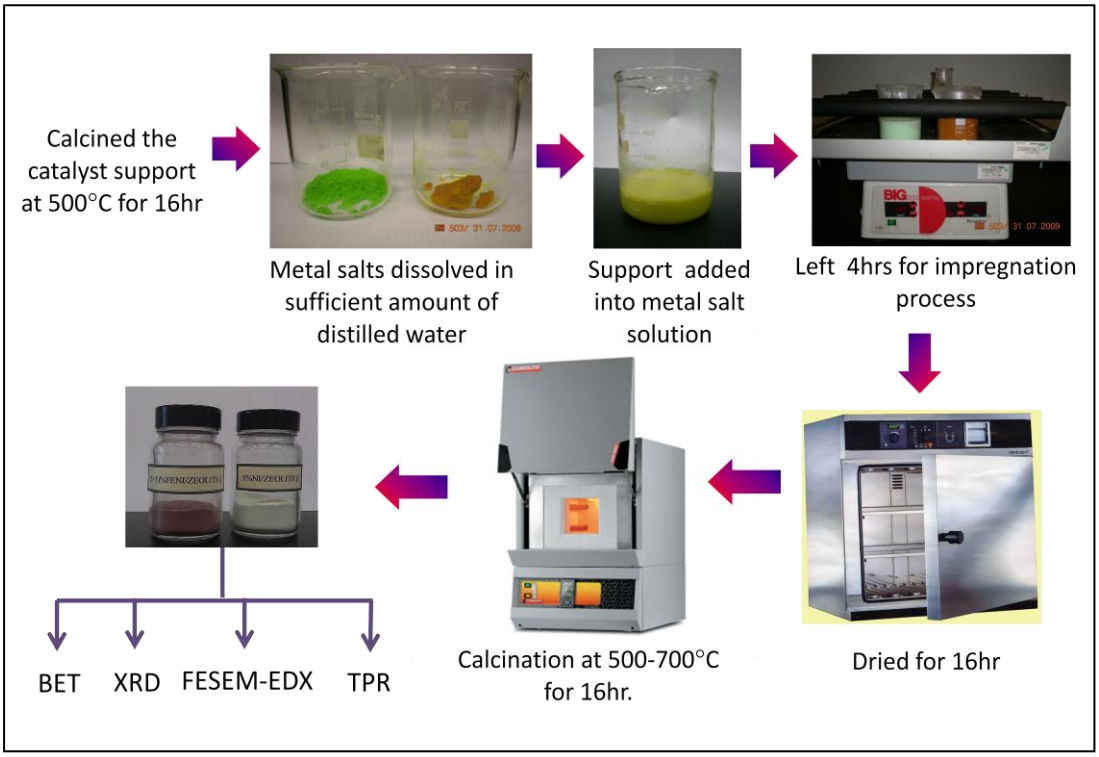

Figure 3.2 Diagram for catalyst preparation

In a typical preparation of monometallic catalysts, the BEA was calcined at 500 °C for 16 hrs before it was crushed and sieved to particles size between 250-750 μm prior to use. Then, a required amount of $FeCl_3.6H_2O$ or $NiCl_2.6H_2O$ to give 5 wt% metals in the finished catalysts was dissolved in sufficient amount of deionised water followed by addition of 95% of support to the metal salt solution under continuous stirring. The slurry formed was then left for impregnation for 4 hr under stirring and later dried at 120 °C for 16 hr. Finally, the dried sample was calcined at 500-700 °C for 16 hr. The catalysts are designated as Fe/BEA (T) and Ni/BEA (T) where T is the calcination temperature in ºC.

For preparation of bimetallic catalysts, the metals were loaded into the support via sequential impregnation method whereby the first impregnation method is the same as preparing the monometallic catalysts. 5 wt% of the second metal was introduced in the second impregnation step. The bimetallic catalysts prepared via this method are 5%Fe5%Ni/ BEA and 5%Ni5%Fe/BEA which are designated as FeNi/BEA (T) and NiFe/BEA (T). In general the catalysts are YX/BEA (T) where metal X was impregnated first followed by metal Y and T is the calcination temperature in ºC.

The bimetallic catalysts were also prepared by using co-impregnation method where the metal of 5% Fe and 5% Ni were impregnated at the same time into the support before drying at 120 °C for 16hr and calcination process at 500-700 °C for 16 hr. The catalysts are designated as Fe-Ni/BEA (T) where refers T is the calcination temperature in ºC.

3.4 Characterization Methods

Chemical and physical properties of a catalyst influence the performance of the catalyst the catalytic testing. Therefore, a wide range of these properties are determined on a routine basis. The physicochemical properties of the catalysts were characterized by typical characterization methods such as N_2 adsorption-desorption or Brunauer-Emmett-Teller (BET) to determine the total surface area, pore volume and pore distribution, Powder X-Ray Diffraction (XRD) for determination of

crystalline phases and calculation of crystallite size using Scherer equations, Field Emission Scanning Electron Microscopy (FESEM) to study the morphology of the catalysts, Energy Dispersive X-ray spectroscopy (EDX) to analyze the composition of the catalyst and Temperature Programmed Reduction (TPR) to determine the reducibility of metal present on the catalyst surface as well as to investigate the interaction between metal and support.

3.4.1 N_2 Adsorption-Desorption

In this study, BET surface area, pore volume and Barrett-Joyner-Halenda (BJH) pore size distribution of the catalysts were determined by N_2 adsorption-desorption method using Micrcomeritics ASAP 2000 at -77K.

The equipment is divided into two parts which is sample preparation or degassing and sample analysis. The samples were degassed under vacuum by flowing nitrogen gas at 120ºC overnight before analysis. The purpose of degassing is to remove the adsorbed contaminant molecules from the surface and pore in order to allow the adsorptive molecules to interact directly with the sample.

The surface area was measured by the low temperature gas adsorption technique as shown in Figure 3.3. This technique determines the quantity of nitrogen gas required to form a monolayer of molecules over the entire samples surface including the smallest open pores. Once mono-molecular layer is established, the BET equation is used to calculate the surface area of the sample. Further increase of nitrogen gas pressure causes the beginning of multilayer coverage. Therefore, continuing the process will fill the pores with nitrogen and the data collected can be used for pore volume and BJH pore distribution and calculation of average pore size.

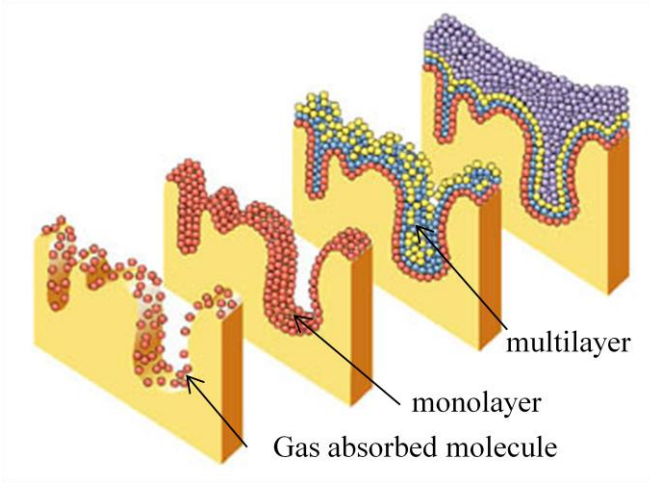

Figure 3.3 Gas adsorption technique model

3.4.2 Powder X-Ray Diffraction

The equipment used for X-Ray Diffraction is type Bruker D8 Advance. This equipment is specific only for powder and flat surface solid sample which called as 'Powder X-Ray Diffraction'. Powder diffraction is commonly used to characterize the crystallographic structure, crystallite size and orientation of powdered solid sample as well as identify unknown substances by comparing diffraction data against a database maintained by the International Centre Diffraction Data (ICDD) or formerly known as Joint Committee on Powder Diffraction Standards (JCPDS). It may also be used to characterize heterogeneous solid mixtures to determine relative abundance of crystalline compounds.

X-Ray tube, detector and sample stage are the main component in the X-Ray diffraction system. The X-Ray produced by the X-Ray tube is aligned to fall on the sample through a slit and are scattered in all directions. While, the detector scanned around the sample along the circle boundary to cut through the diffraction cones at various diffraction maxima. As a result, the X-Ray diffraction pattern will display intensity as a function of the detector angle, 2θ [76].

There are three types of information in a diffraction pattern which can be observed and related with the size and perfection of the sample crystallizations. There are the position, the intensity and the shape of the diffraction peaks. The positions of the diffraction peaks are determined by the geometry of the crystal lattice i.e. the size and the shape of the unit cell. Meanwhile, the intensities of the peaks are related to the arrangement of the specific atoms in the unit cell of the crystal.

Crystallite size, D_w (Å) can be determined from the diffractogram using Scherer equation [77]:

$$D_w = K\alpha / \beta \cos \theta \qquad \text{[Eq. 3.1]}$$

Where K is a Scherer constant usually evaluated as K= 0.9 or K= 1.0, α is the wavelength of the x-ray beam (normally used Cu Kα radiation =1.54 Å), β is the full width at half maximum of the diffraction peaks in radians and θ is the peak position at 2θ value.

3.4.3 Field Emission Scanning Electron Microscope (FESEM-EDX)

FESEM is the abbreviation of the word Field Emission Scanning Electron Microscope. FESEM is a type of electron microscope that images the sample surface by scanning it with a high-energy beam of electrons in a scan pattern. While, Energy Dispersive X-ray spectroscopy (EDX) is an analytical technique used for the elemental analysis or chemical characterization of a sample. The EDX system is commonly equipped with field emission scanning electron microscope (FESEM-EDX) for composition analyzing. In this study, the FESEM equipment used is Zeiss, model Supra with 5vp while the EDX equipment using Oxford-INCA.

Field emission scanning electron microscopy was operated at standard accelerating voltages in the range of 30-35 kV at 1000–50000x magnifications. However, in this analysis 50000x magnifications were preferred. FESEM also incorporated a cold cathode field emission gun, ultra high vacuum and sophisticated digital technologies for high resolution and quality imaging of micro structures.

Since the electron beam produced by the field emission source is about 1000 times smaller than that in a standard microscope with a thermal electron gun, it can visualise tiny structures as small as 1 nanometre with high quality images [78].

3.4.4 Temperature-Programmed Reduction (TPR)

Temperature-Programmed Reduction (TPR) determines the number of reducible species present on the catalyst surface and reveals the temperature at which the reduction of each species occurs. TPR can also be used qualitatively to investigate phenomena such as metal-support interactions and bimetal formation as well as metal distribution in a composite oxide supported precursor.

The TPR analysis begins by flowing analysis gas, hydrogen in an inert carrier gas, 5% H_2/N_2 with a flow rate of 20cm^3/min through the sample, and the temperature was programmed to increase at a rate of 10 $^oCmin^{-1}$ from room temperature to 900 ^oC. While the gas is flowing, the temperature of the sample is increased linearly with time and the consumption of hydrogen by adsorption is monitored. The H_2 consumption produced by the different reduction steps was recorded as a function of temperature.

The chemical reaction occurring during the TPR process may be described by [79]:

$$MO + H_{2\,(g)} \longrightarrow M^{2+} + H_2O_{\,(g)} \qquad \text{[Eq. 3.2]}$$

The results in a TPR experiment are obtained as a trace of the thermal conductivity detector response versus temperature. The position of the peak in the profile is determined by both the chemical nature and the environment of the reducible component and the peak area reflects the amount of reductant, typically hydrogen consumed. Based on the TPR profile, it has been proposed that higher reduction peak temperatures are indicative of stronger metal-support interactions [79].

3.5 Catalyst Testing

3.5.1 Biomass Sample and Preparation

The biomass chosen in this study was palm kernel shell (PKS). This is because PKS is the most potential feedstock for hydrogen production through gasification where it has the most suitable physicochemical properties [69]. Figure 3.4 shows the image of palm kernel shell. The PKS was dried at 110ºC before they were crushed and sieved. The particle size of PKS used in this study was 500 µm. The ultimate analysis of PKS (dry basis, wt %) were conducted using LECO 932 CHNS Analyzer and summarized in Table 3.1.

Figure 3.4 Palm kernel shell

Table 3. 1 The ultimate analysis of PKS

Elements	Composition (%)
C	49.65
H	6.13
N	0.41
S	0.48
O	39.22

Ultimate analysis shows the percentage of carbon, hydrogen, nitrogen, sulphur and oxygen in the PKS. CHNS analyzer involves qualitative conversion of the four elements (C, H, N, S) into CO_2, $H_2O_{(g)}$, N_2 and SO_2. PKS was burnt at 1000°C in flowing oxygen. The product gases were measured by infrared detectors except for N_2 which was measured by thermal conductivity detector. In the end, quantitative measurement of C, H, N and S were recorded while O was quantified by difference.

PKS was found to have high content of sulphur. Large percentage of sulphur in biomass has high probability to produce high concentration of hydrogen sulphide (H_2S), carbonyl sulphide (COS) or sulphur dioxide (SO_2) in the gaseous product. Sulphur also restraint the catalyst in attaining a stable catalytic activity during the reaction which will lead to catalyst deactivation [30]. Therefore, the proposed catalysts should have high resistance to sulphur poisoning to ensure a clean and stable production of hydrogen through catalytic PKS steam gasification.

The proximate analysis of PKS (dry basis, wt%) is shown in Table 3.2. The analysis was carried out using Perkin Elmer Pyris 1 TGA equipment. TGA measures the weight loss of PKS as a function of temperature. It provides quantitative measurement of intrinsic moisture, fixed carbon, volatile matter and ash content of the PKS. From this analysis, PKS contained about 14.52 wt% of fixed carbon and 81.03 wt% of volatile matter. These components are advantage for PKS where both carbon and volatile matter will react and contribute to more gaseous products during gasification. PKS also has less than 5 wt% of ash content. High ash content will result in ash melting in the system thus affecting the composition of the gas produced.

Table 3.2 Proximate analysis of PKS

Elements	**Composition (%)**
Volatile matter	81.03
Fixed carbon	14.52
Ash	4.44
Moisture content (wt% wet basis)	17.50
Higher heating value (MJ/kg)	20.40

Moisture in the biomass will give a significant effect on the reactions such as increasing the yield of char. However, the moisture content in the PKS is only 20 wt%. Thus, this analysis shows that PKS is a suitable biomass for gasification process.

3.5.2 Reaction System

Catalytic steam gasification of PKS was performed using a reaction system available within Prof Hengyong Xu's research group at Dalian Institute of Chemical Physics (DICP), China. Mass balance cannot be calculated due to constraint of experiment setting. The reaction only focuses on detecting composition of H_2, CO, CO_2, CH_4 and H_2S in the outlet gas.

3.5.2.1 Screening Process System

In this study, the PKS underwent a screening process before prior to steam gasification reaction in order to determine the optimum temperature for the reaction. The screening process was performed at temperatures between 600 - 900 ºC with biomass weight of 0.3 g, steam to biomass ratio of 4:1 (wt/wt) and steam to helium (He) ratio of 1:6 (vol/vol) in the absence of a catalyst. These parameters were chosen following reaction parameters reported by Asadullah et al. [80], Luo et al. [81] and Gonzalez et al. [82].

Experiments were carried out in a fixed bed quartz micro reactor with internal diameter of 15 mm heated with an electric furnace (Figure 3.5). The biomass bed was held in place by quartz wool. Two thermocouples were used to measure the temperature; one is placed at the centre of the bed in the tubular reactor and the other is placed on the outer surface of the reactor.

Helium and nitrogen were used as diluents gases and its flow was regulated by mass flow meter, in the range of 20-30 $mlmin^{-1}$. Water was introduced by a liquid pump, where it was quickly evaporated at elevated temperature and carried to the tubular reactor by state helium and nitrogen gas.

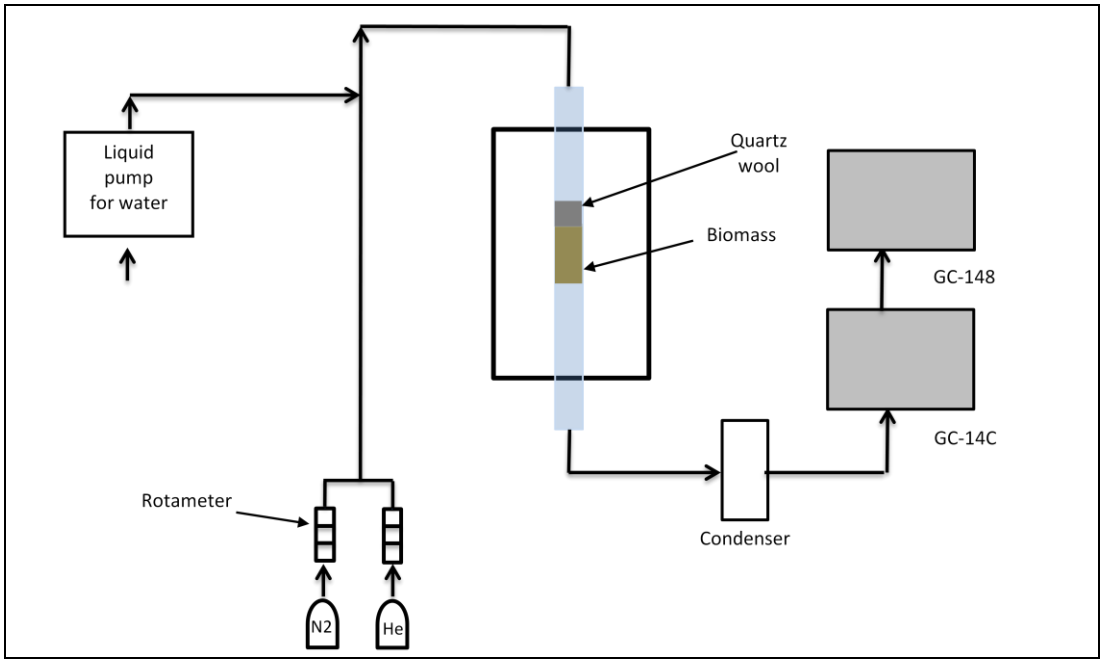

Figure 3.5 Schematic diagram of the reaction system for screening process

The outlet gas passed through ice water condenser to substantially condense the water before it entered the gas chromatograph. The gases produced in screening process (H_2, CH_4, CO_2, H_2S) were analyzed using two online gas chromatographs; GC-14C equipped with a sulphur detector (FPD) fitted with Chromosil 310 column was used to analyze sulphur compound in the product gases and the other one, GC-14B equipped with thermal conductivity detector (TCD) fitted with Carbon molecular sieve column to analyze CH_4, H_2 and CO_2 with He as a carrier gas.

3.5.2.2 Catalytic Reaction System

The catalysts were then tested for their ability to produce H_2 in the steam gasification of PKS in a fixed-bed quartz micro reactor at 700 ºC with catalyst and PKS weight of 0.3 g and 0.9 g, respectively. The steam to PKS ratio was maintained at 4:1 (wt/wt) while steam to Ar ratio was 1:6 (vol/vol). Figure 3.6 shows the reaction system for steam gasification of PKS in the presence of catalysts.

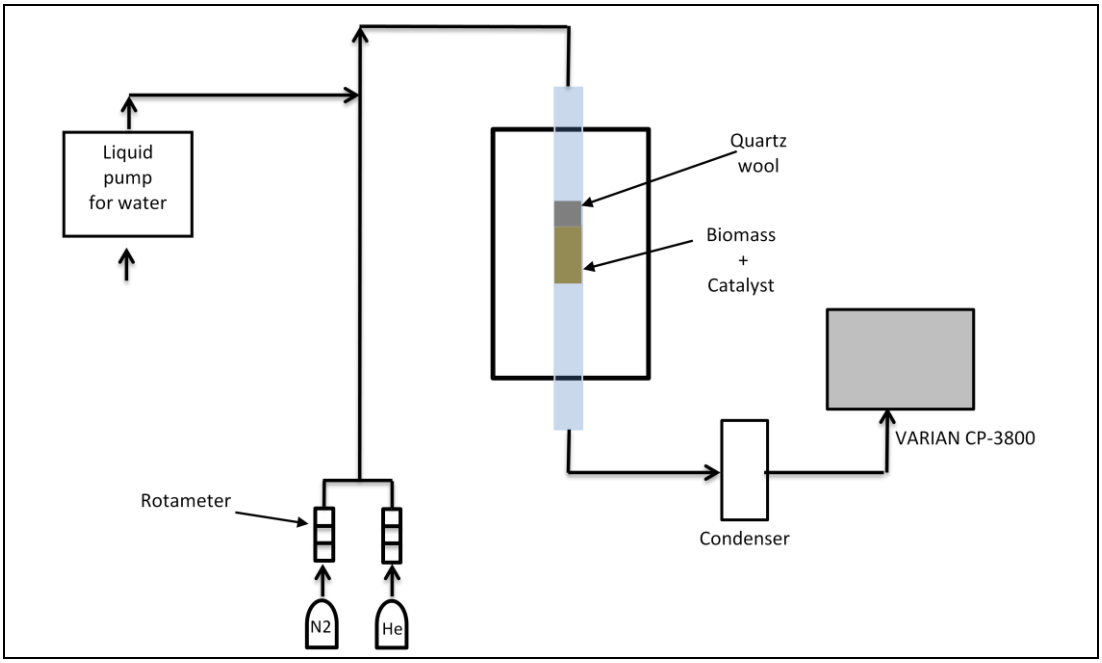

Figure 3.6 Schematic diagram of the reaction system for catalytic steam gasification

Experiments were carried out in a fixed bed quartz micro reactor with internal diameter of 15 mm heated with an electric furnace. The biomass bed was held in place by quartz wool. Two thermocouples were used to measure the temperature; one is placed at the centre of the bed in the tubular reactor and the other is placed on the outer surface of the reactor. Argon and nitrogen were used as diluents gases and its flow was regulated by mass flow meter, in the range of 20-30 $mlmin^{-1}$. Water was introduced by a liquid pump, where it was quickly evaporated at elevated temperature and carried to the tubular reactor by state helium and nitrogen gas.

The gases produced from the catalytic steam gasification (H_2, CH_4, CO_2 and CO) were analyzed using an online gas chromatograph. VARIAN CP-3800 equipped with thermal conductivity detector (TCD) and fitted with TDX-01 column utilizing Argon as a carrier gas. The images of fixed-bed quartz micro reactor were displayed in Figures 3.11 and 3.12.

Figure 3.7 Fixed bed quartz micro reactor

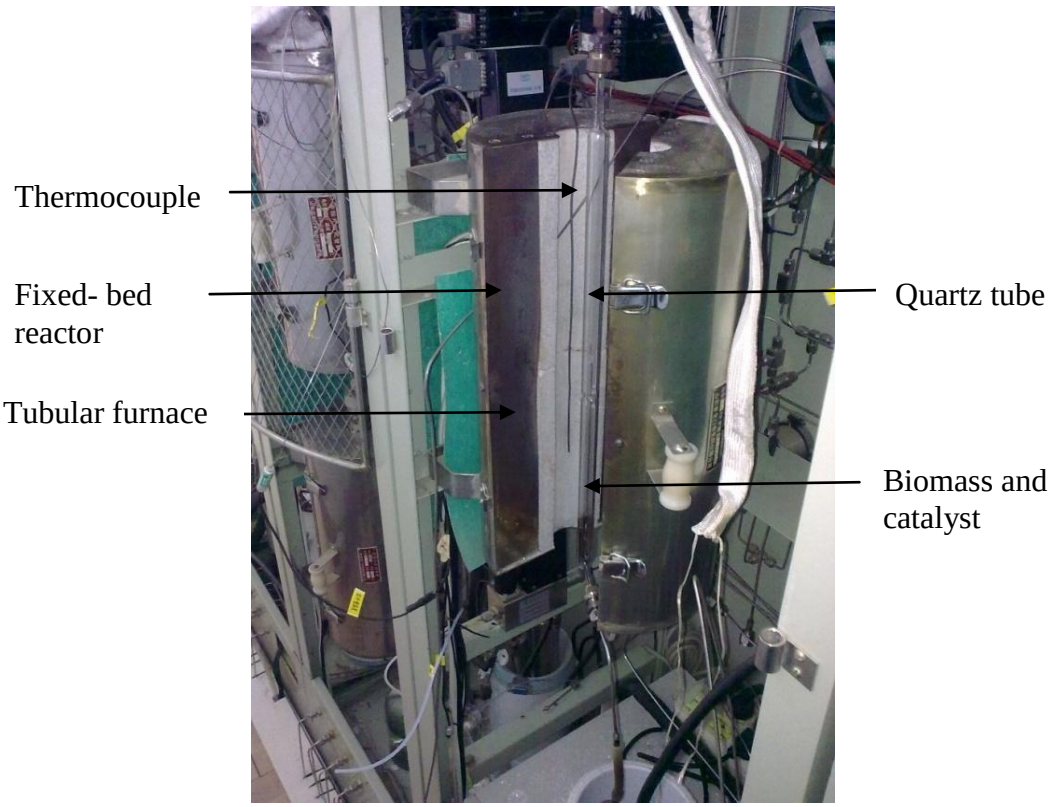

Figure 3.8 The disclosed fixed bed quartz micro reactor

CHAPTER FOUR

RESULTS AND DISCUSSIONS

4.1 Catalyst Characterization

Different metal loading, calcination temperatures and preparation method for bimetallic system used in the catalyst preparation lead to different physicochemical properties attained which may influence the catalyst's performance. Therefore, it is of importance to characterize the catalysts prepared in order to understand the effect of different parameters to the activity of the catalysts.

4.1.1 N_2 Adsorption - Desorption

According to Webb and Orr [83], pore structure is equally crucial to material performance since porosity can increase the availability of surface area which has a great influence on catalytic activity. BEA has tridirectional system of interconnected channels [84] with 12-ring orifice [85] providing large and small cavities. The frameworks are composed of SiO_2 and Al_2O_3 with SiO_2:Al_2O_3 mole ratio of 25. The adsorption-desorption isotherms of all catalysts prepared using BEA as support are shown in Figures 4.1 - 4.4.

The isotherm plots show that Ni and Fe based supported on BEA catalysts are type IV as according to IUPAC classification. The isotherms rise comparatively rapidly at intermediate relative pressure and show a wide hysteresis loop. This behaviour is typical of mesoporous catalyst which is in accordance with the average pore diameter results of the prepared catalysts greater than 2 nm (Table

4.1) along with a wide pore distribution. The initial rise in the curve is due to adsorbing molecules interacting first with the most energetic areas of the catalyst surface and then with the less energetic areas [83]. Besides, the shapes of the hysteresis loops are also similar for all the catalysts prepared. The hysteresis loops are type H1 where the adsorption and desorption br anches are almost vertical and nearly parallel over an appreciable range of gas uptake, whereas in the latter they are nearly horizontal and parallel over a wide range of relative pressure. In terms of pore structure, H1 loops are refer to agglomerates or compacts of spheroidal particles of fairly uniform size and array [86].

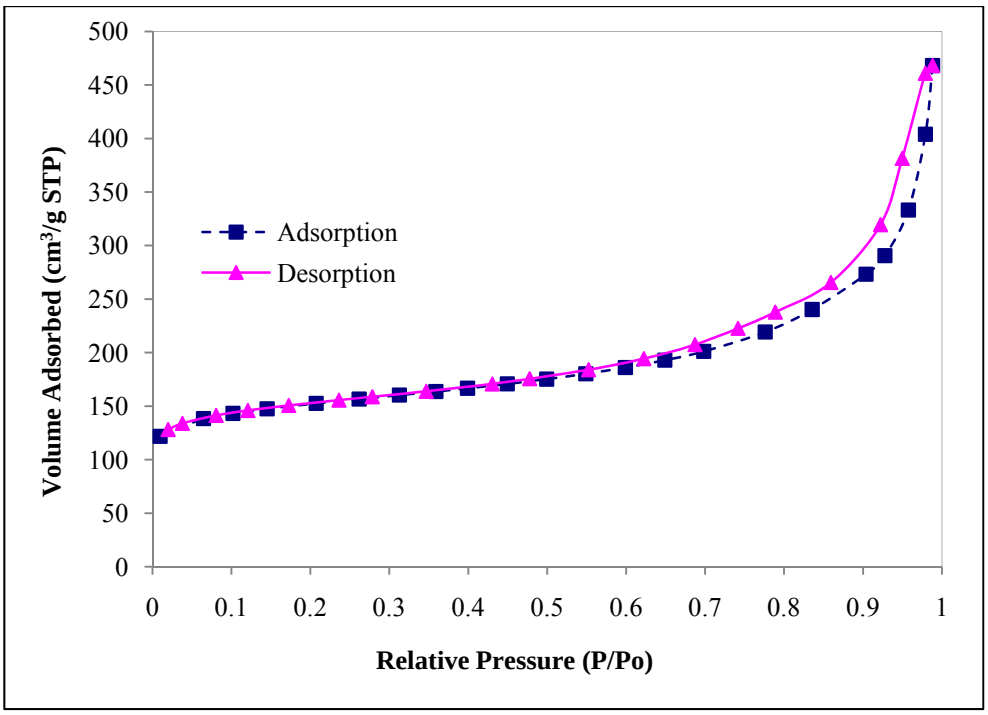

(a)

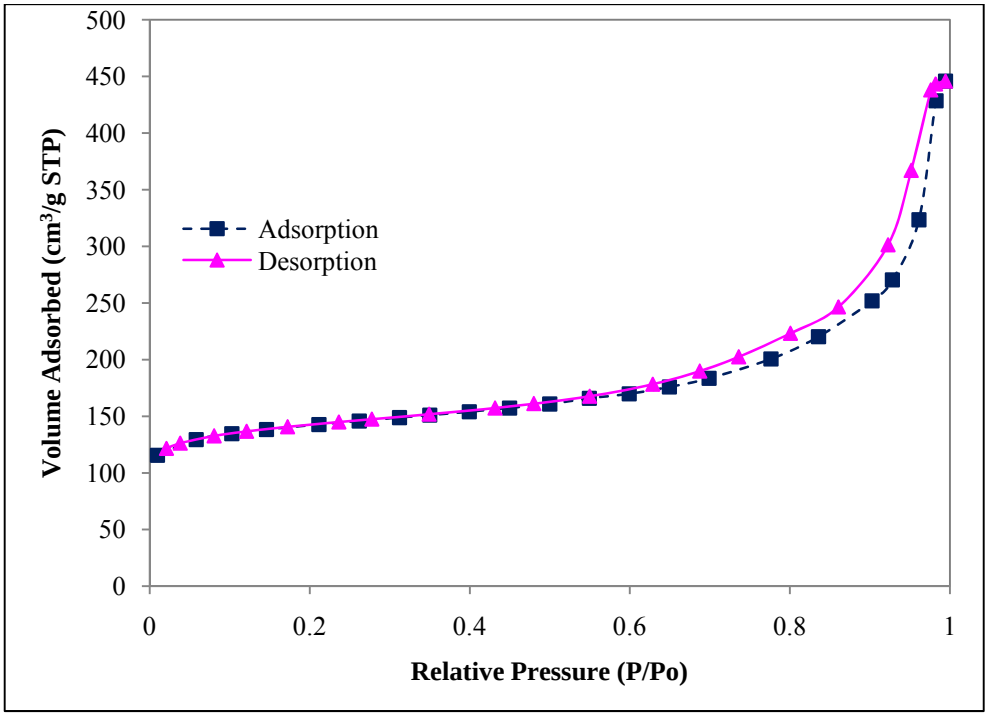
Volume Adsorbed (cm3/g STP)
500
450
400
350
300
250
200
150
100
50
0
Adsorption
Desorption
0
0.2
0.4
0.6
0.8
1
Relative Pressure (P/Po)

(b)

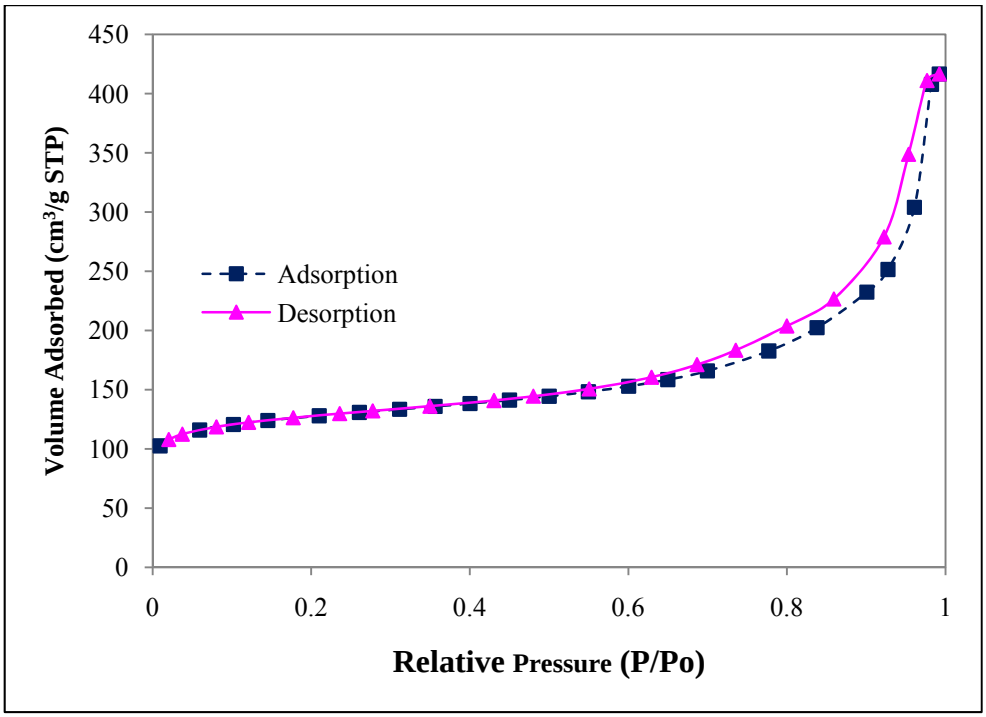
Volume Adsorbed (cm3/g STP)
450
400
350
300
250
200
150
100
50
0
Adsorption
Desorption
0
0.2
0.4
0.6
0.8
1
Relative Pressure (P/Po)

(c)

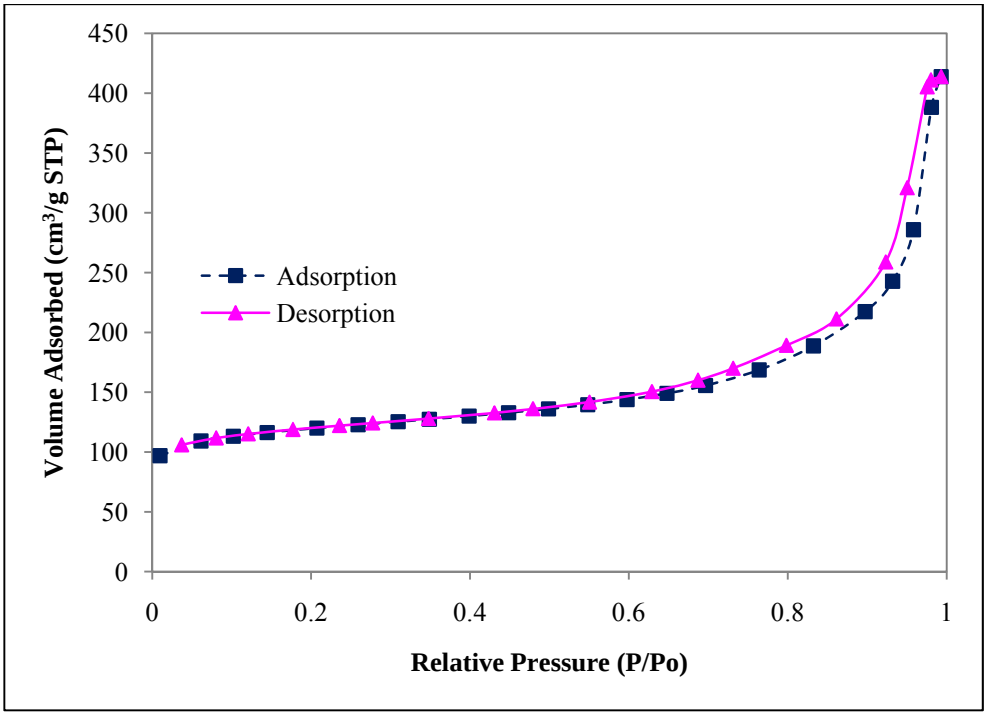

(d)

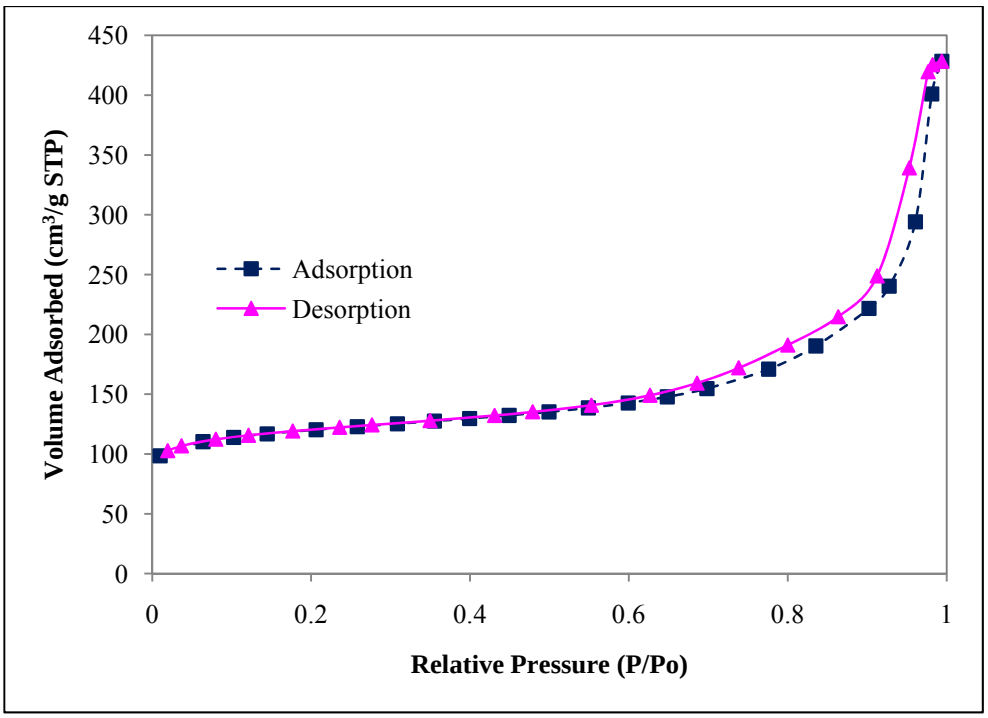

(e)

Figure 4.1 Adsorption-desorption isotherms for (a) bare BEA (b) Ni/BEA (c) Fe/BEA (d) FeNi/BEA (e) NiFe/BEA catalysts calcined at 500 ºC

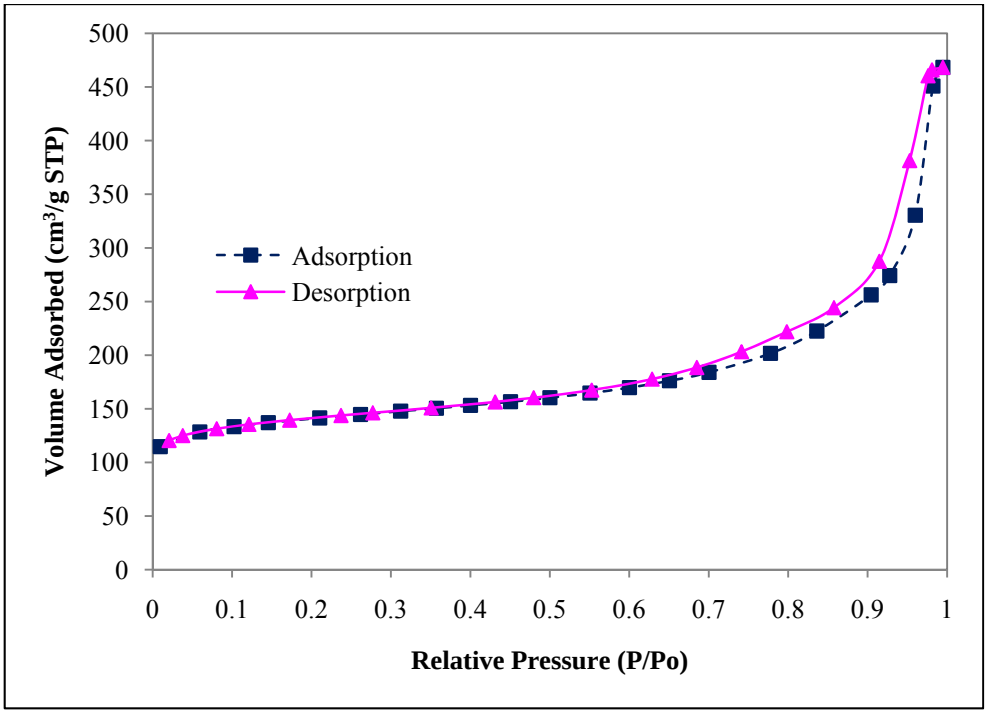
Volume Adsorbed (cm3/g STP)
500
450
400
350
300
250
200
150
100
50
0
Adsorption
Desorption
0
0.1
0.2
0.3
0.4
0.5
0.6
0.7
0.8
0.9
1
Relative Pressure (P/Po)

(a)

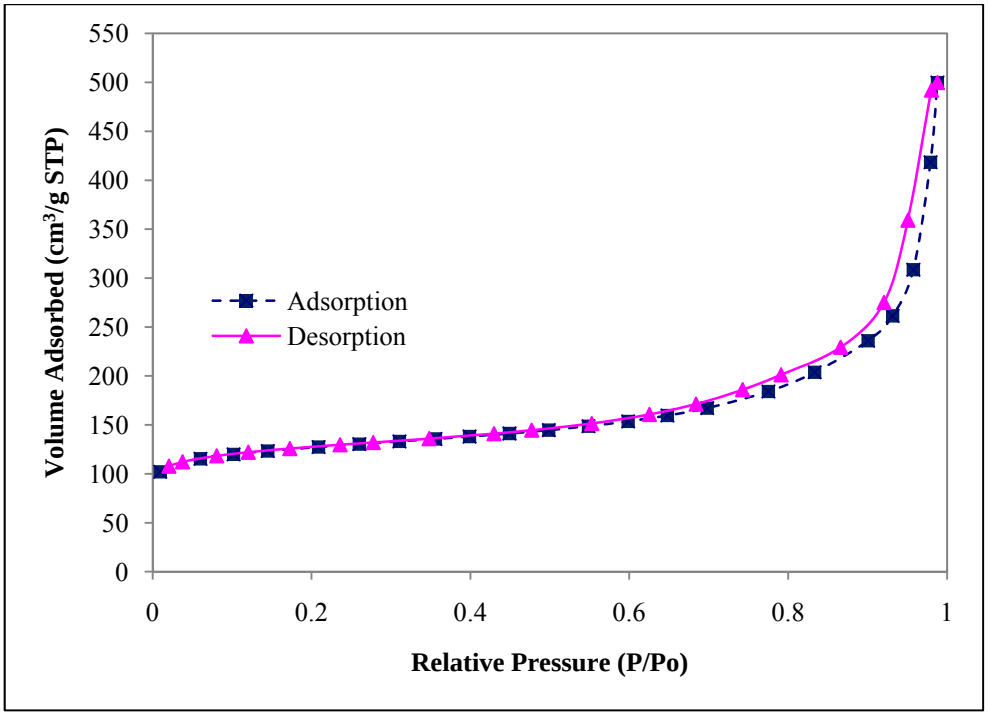
Volume Adsorbed (cm3/g STP)
550
500
450
400
350
300
250
200
150
100
50
0
Adsorption
Desorption
0
0.2
0.4
0.6
0.8
1
Relative Pressure (P/Po)

(b)

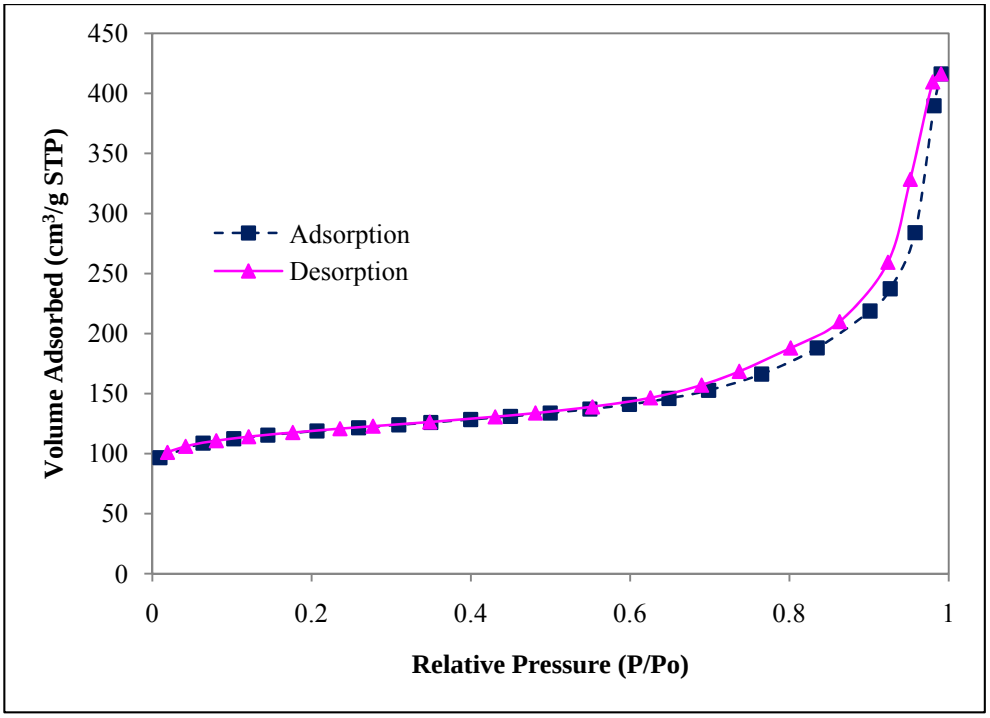

(c)

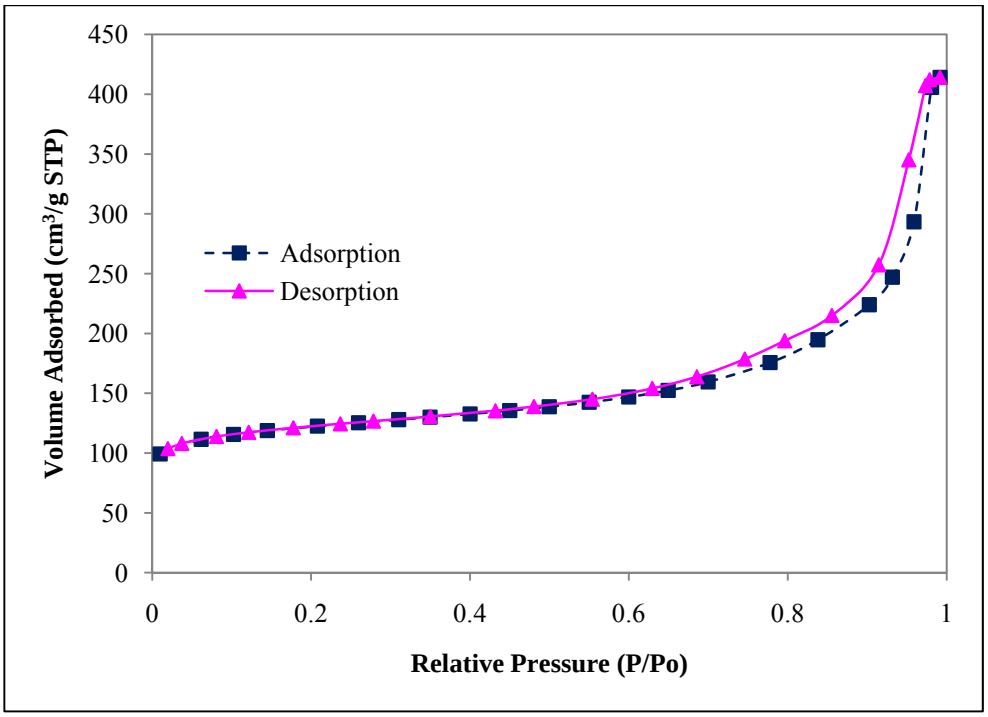

(d)

Figure 4.2 Adsorption-desorption isotherms for (a) Ni/BEA (b) Fe/BEA (c) FeNi/BEA (d) NiFe/BEA catalysts calcined at 600 ºC

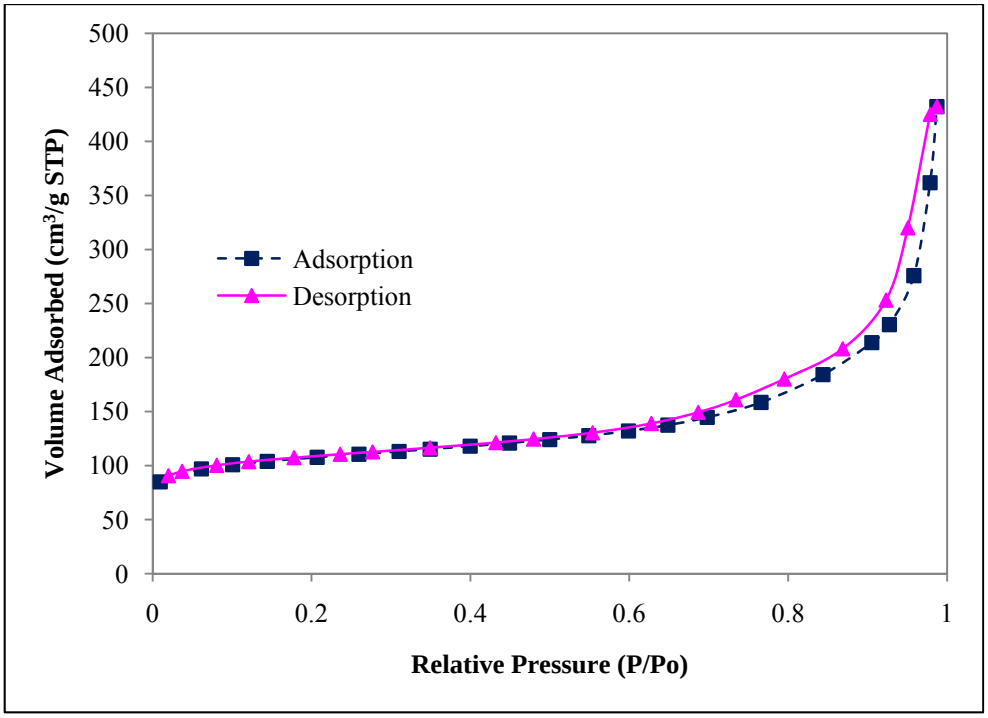
Volume Adsorbed (cm3/g STP)
500
450
400
350
300
250
200
150
100
50
0
Adsorption
Desorption
0
0.2
0.4
0.6
0.8
1
Relative Pressure (P/Po)

(a)

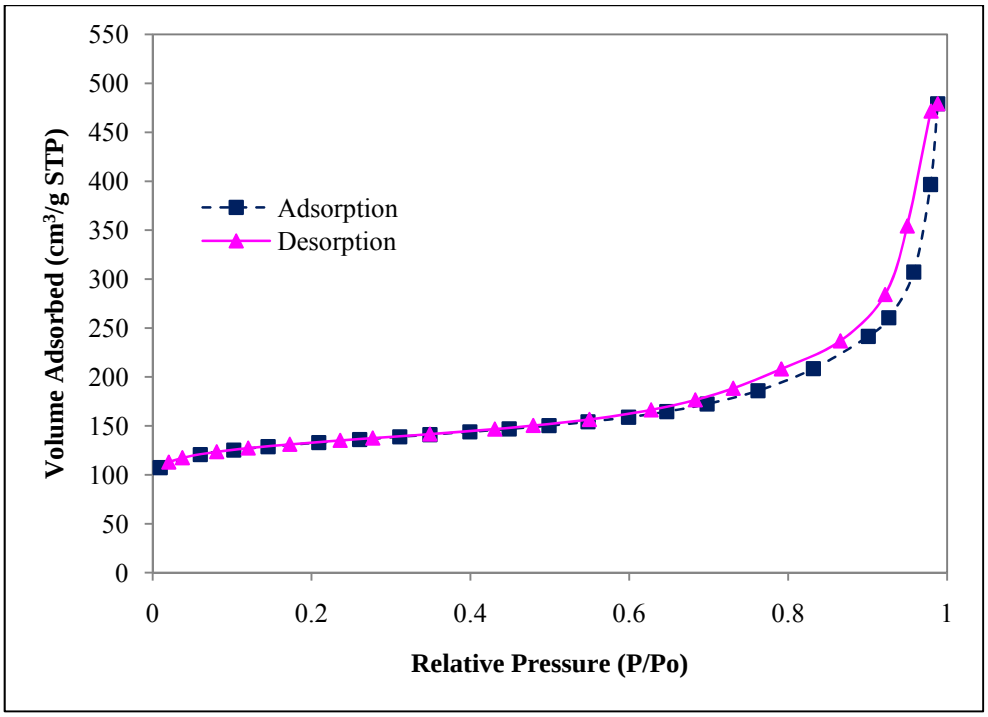
Volume Adsorbed (cm3/g STP)
550
500
450
400
350
300
250
200
150
100
50
0
Adsorption
Desorption
0
0.2
0.4
0.6
0.8
1
Relative Pressure (P/Po)

(b)

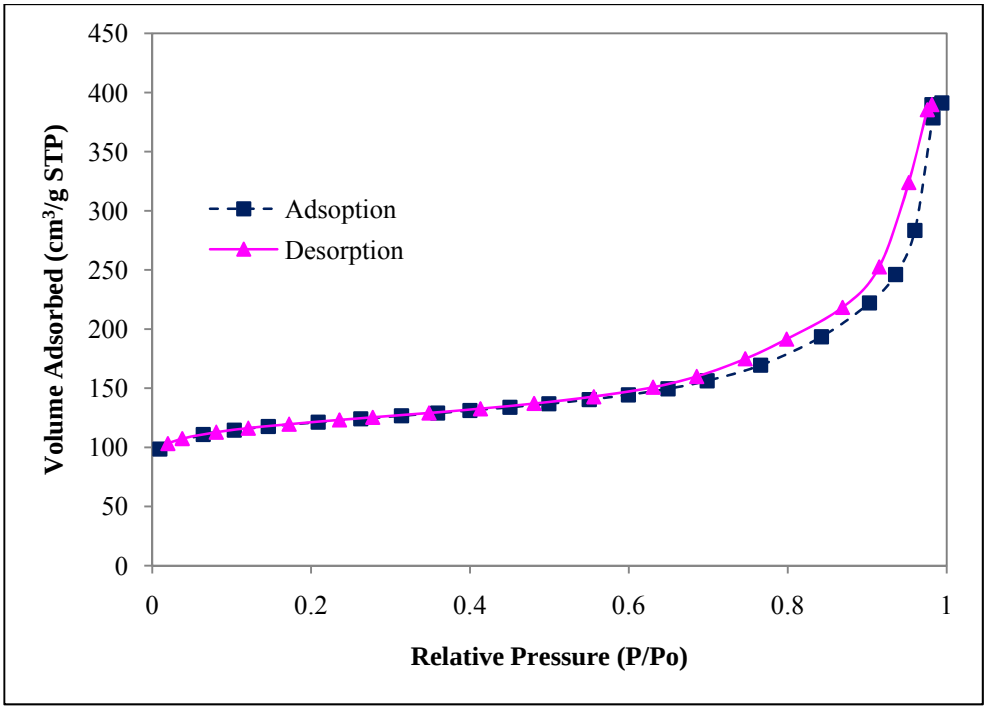

(c)

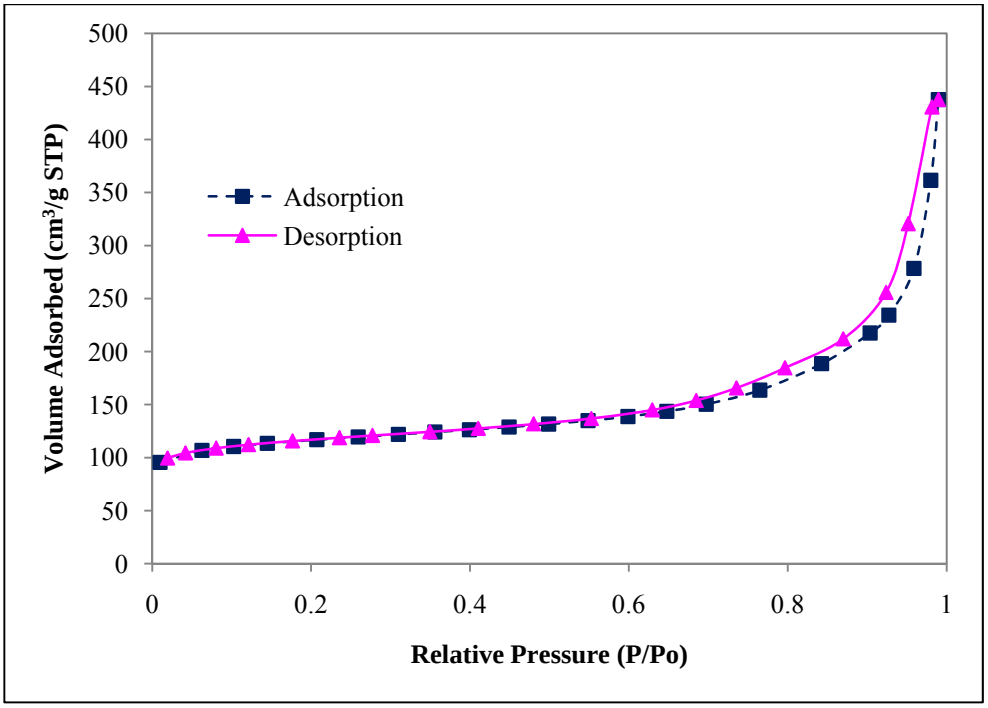

(d)

Figure 4.3 Adsorption-desorption isotherms for (a) Ni/BEA (b) Fe/BEA (c) FeNi/BEA (d) NiFe/BEA catalysts calcined at 700 ºC

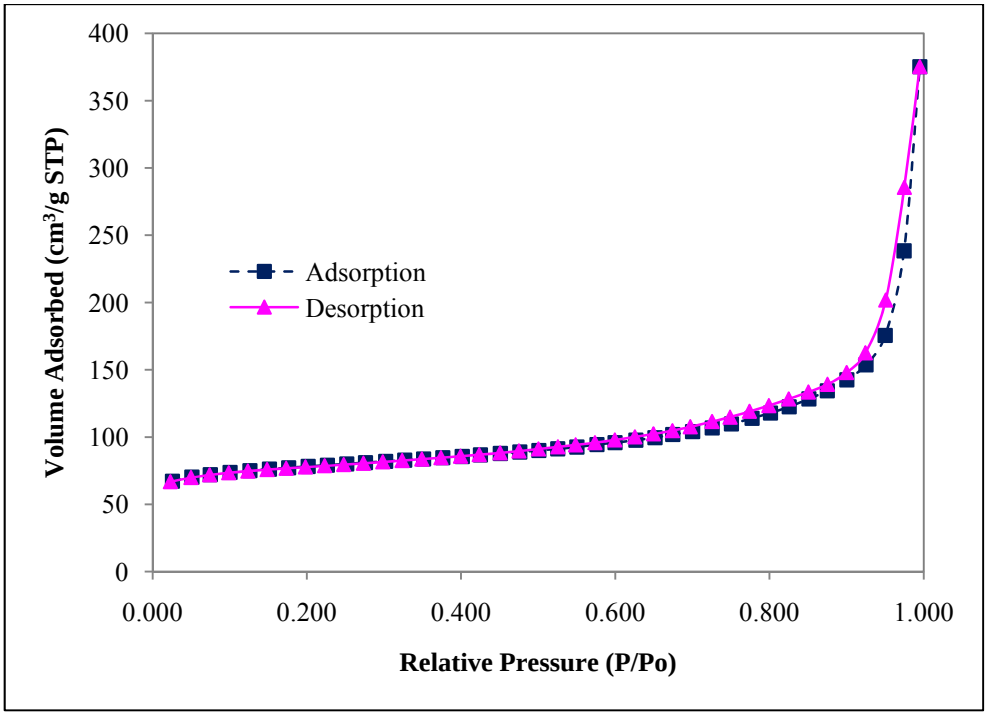
400
350
300
250
200
150
100
50
0
Volume Adsorbed (cm3/g STP)
Adsorption
Desorption
0.000
0.200
0.400
0.600
0.800
1.000
Relative Pressure (P/Po)

(a)

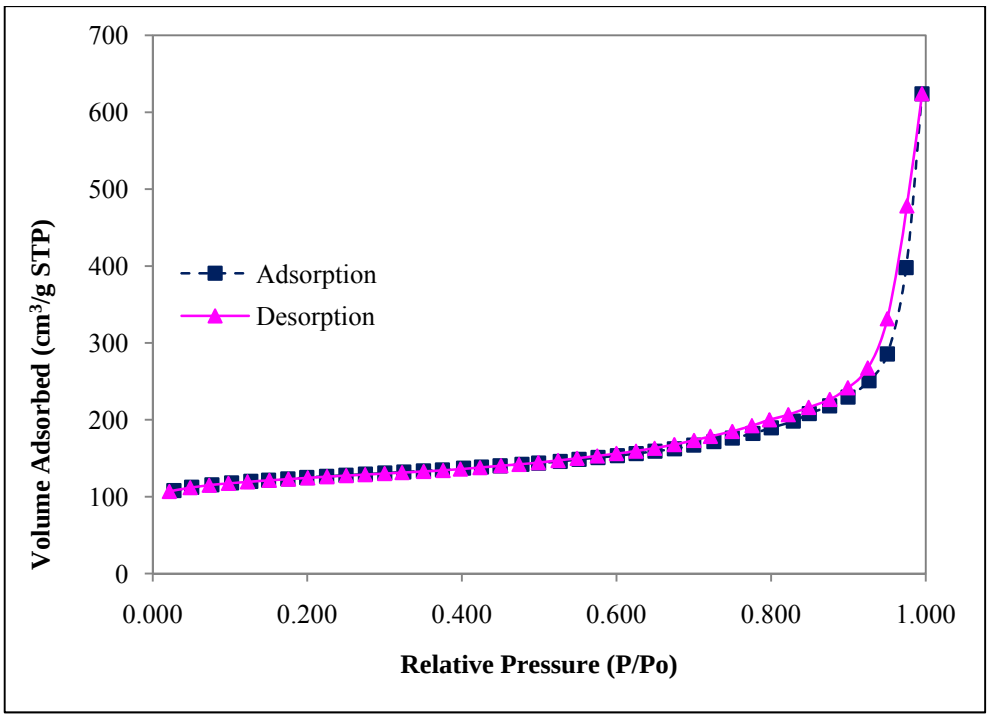
700
600
500
400
300
200
100
0
Volume Adsorbed (cm3/g STP)
Adsorption
Desorption
0.000
0.200
0.400
0.600
0.800
1.000
Relative Pressure (P/Po)

(b)

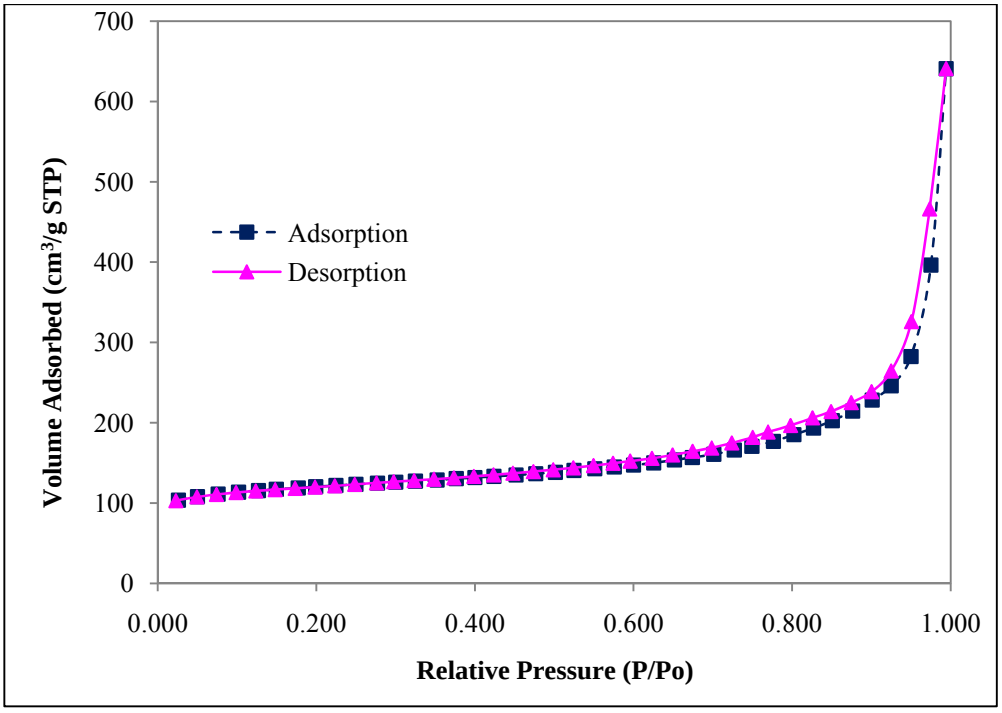

(c)

Figure 4.4 Adsorption-desorption isotherms for co-impregnation bimetallic Fe-Ni/BEA catalysts calcined at (a) 500 ºC (b) 600 ºC (c) 700 ºC

In the present study, the Ni and Fe based catalysts supported on BEA exhibit a wide pore distribution plot (Figure 4.5) which scattered in the mesopores (2-50 nm) and macropores (50-130 nm) region. This is due to the characteristics of BEA itself which has large and small cavities which, resulted in wide pore distribution.

Therefore, both monometallic and bimetallic catalysts contain a model of mesopores system as well as a macropores structure of BEA. Since a majority of the pores are in mesopores regions, it can be concluded that the average pore diameter of BEA and the prepared catalyst are mesopores type as tabulated in Table 4.1. N_2 volume uptake increases as the number of pores in the range of 20-60 nm increase when BEA was incorporated with active metals. According to Chen *et al.* [87], higher in N_2-physisorption promotes both adsorption and diffusion of the products from the reaction sites, which may be closely related to high catalytic activity in the gasification reaction.

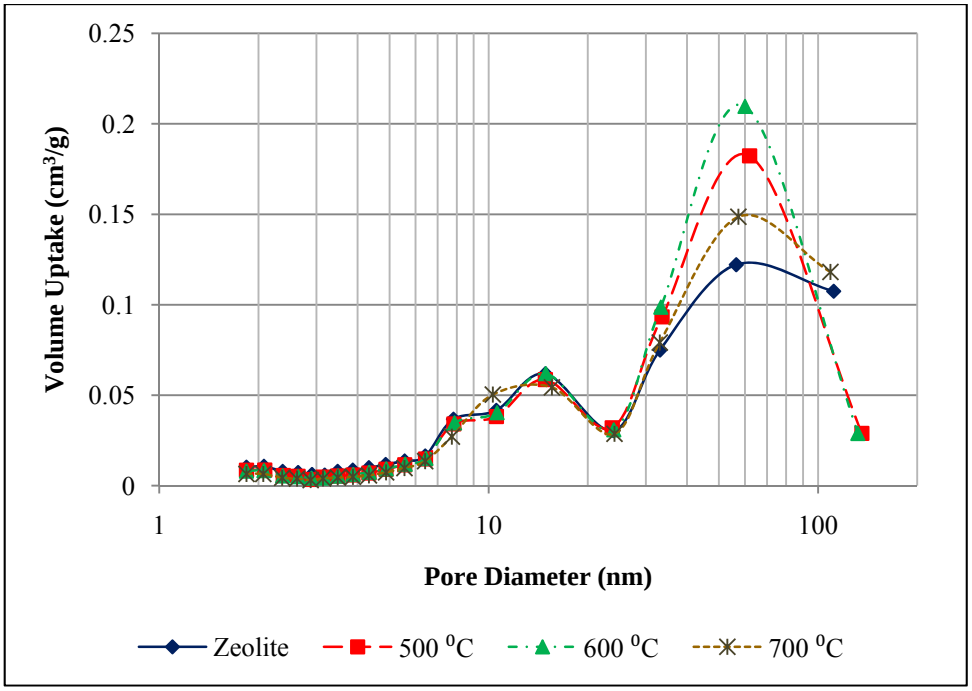
0.25
0.2
0.15
0.1
0.05
0
Volume Uptake (cm³/g)
1
10
100
Pore Diameter (nm)
Zeolite
500 °C
600 °C
700 °C

(a)

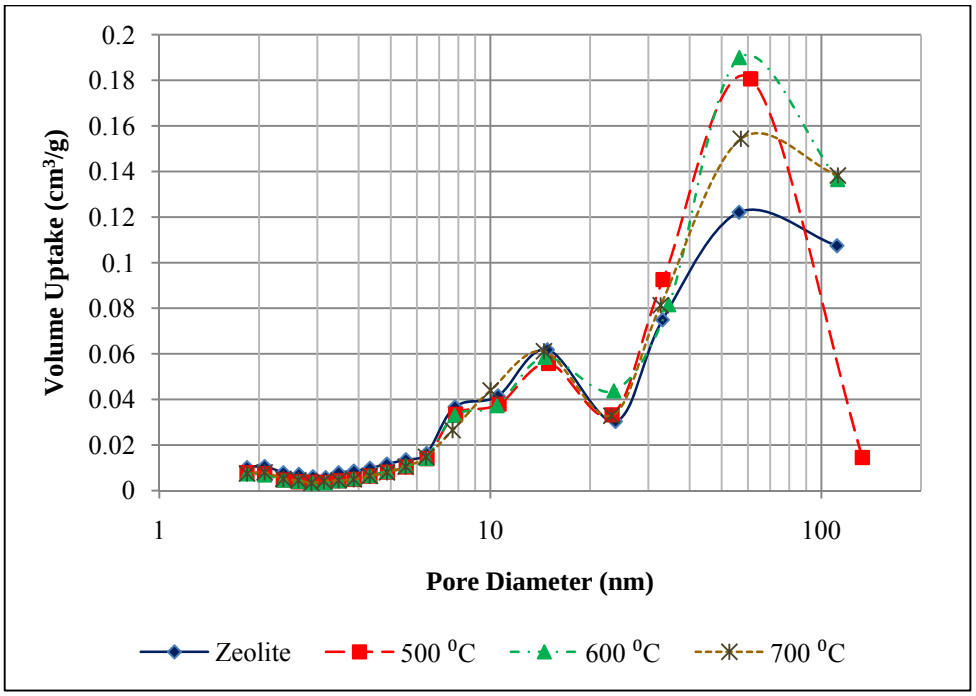
0.2
0.18
0.16
0.14
0.12
0.1
0.08
0.06
0.04
0.02
0
Volume Uptake (cm³/g)
1
10
100
Pore Diameter (nm)
Zeolite
500 °C
600 °C
700 °C

(b)

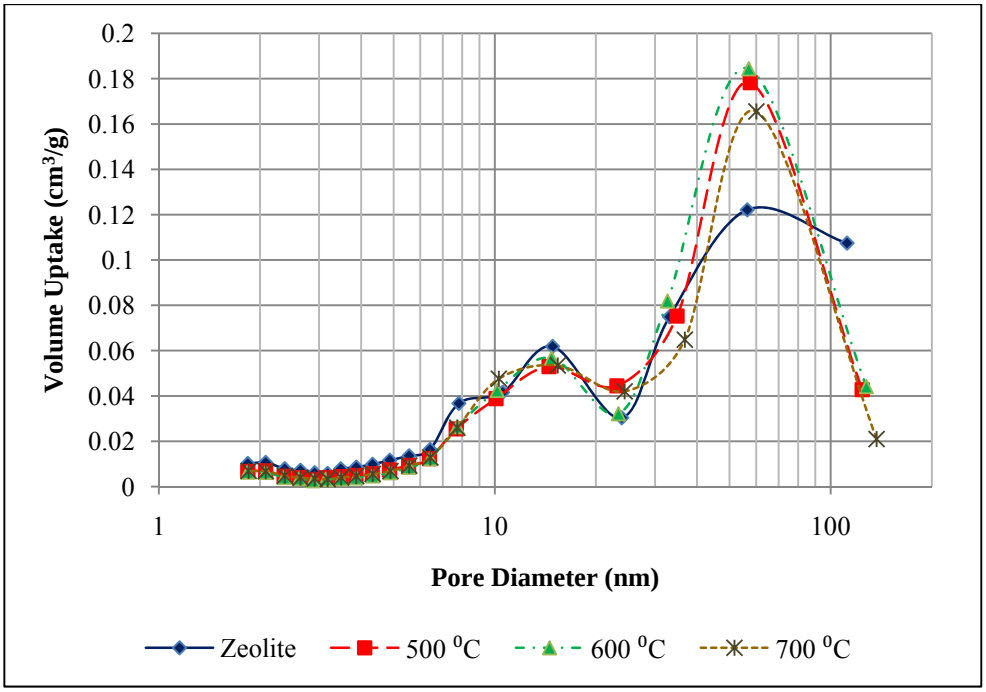
0.2
0.18
0.16
0.14
0.12
0.1
0.08
0.06
0.04
0.02
0
Volume Uptake (cm3/g)
1
10
100
Pore Diameter (nm)
Zeolite
500 °C
600 °C
700 °C

(c)

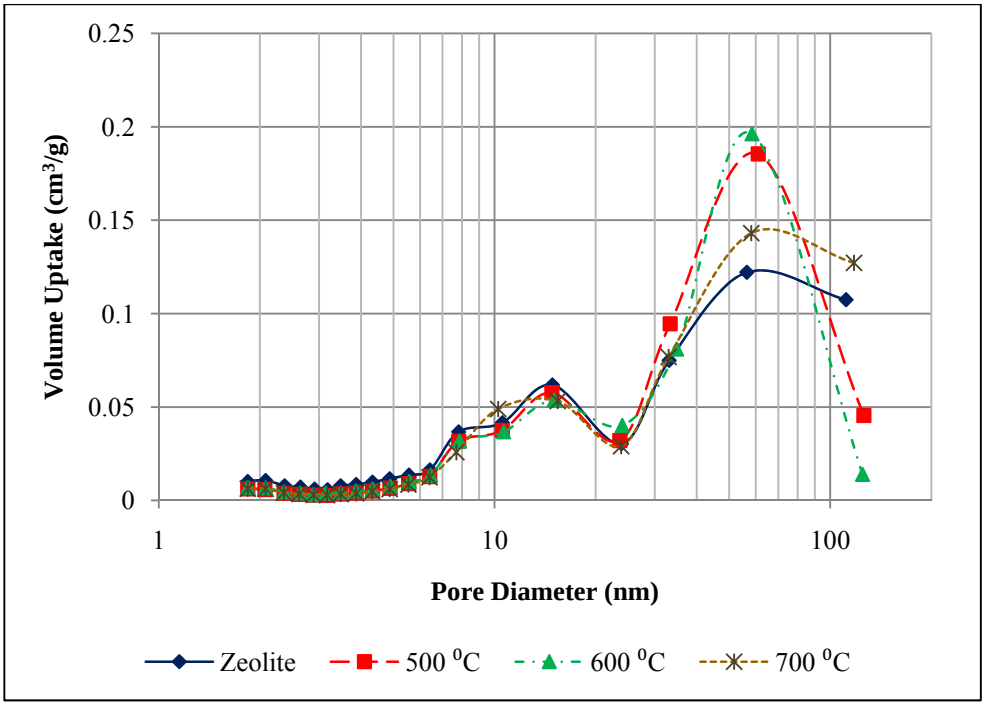
0.25
0.2
0.15
0.1
0.05
0
Volume Uptake (cm3/g)
1
10
100
Pore Diameter (nm)
Zeolite
500 °C
600 °C
700 °C

(d)

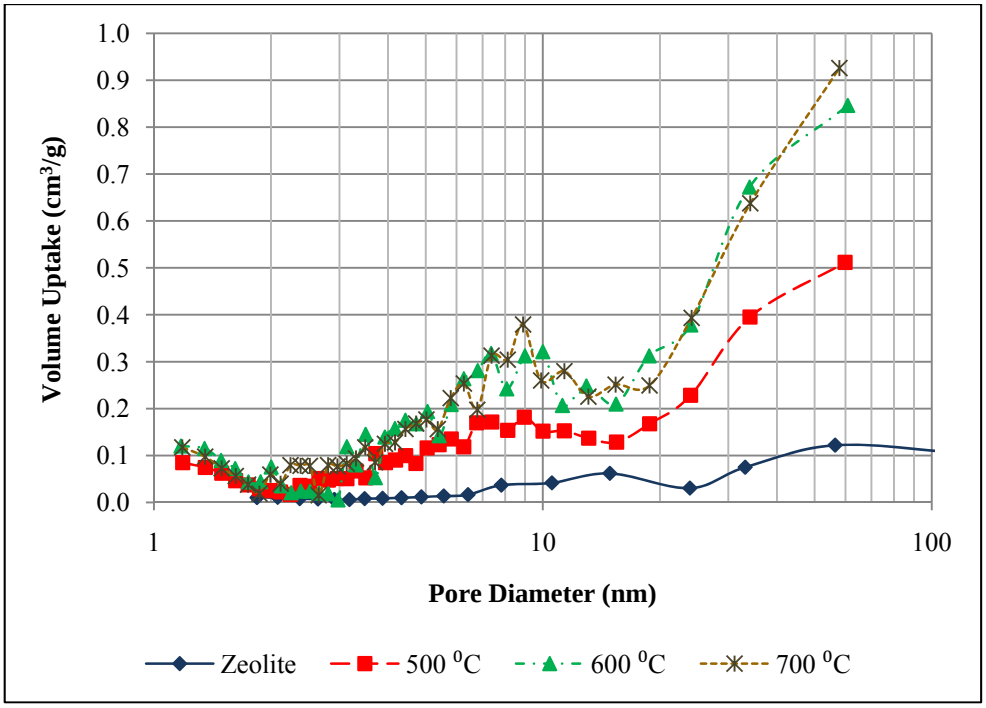

(e)

Figure 4.5 Pore diameter distribution of monometallic and bimetallic catalysts calcined at 500 – 700 ºC (a) Ni/BEA (b) Fe/BEA (c) FeNi/BEA (d) NiFe/BEA and (e) Fe-Ni/BEA

Based on N_2 adsorption-desorption, the textural properties like BET surface area, pore volume and pore diameter of the catalysts prepared using BEA as support are summarized in Table 4.1. The surface areas of the catalysts vary widely where the bare BEA has the highest surface area (529 m^2g^{-1}) as compared to the prepared catalysts. Once BEA is incorporated with active metal, the surface area of the monometallic catalysts was reduced. The effect becomes more significant in the bimetallic systems. The influence is so pronounced in some instances because Fe and Ni have occupied the BEA pores which resulted in the reduction in surface area.

The decrease in the surface area for Ni/BEA catalyst is less than 1% when the catalyst were calcined at 500 and 600 ºC while the reduction becomes more drastic (25%) when the catalyst was calcined at 700 ºC. According to Hassan *et al.,* [88], less reduction of Ni/BEA at low calcination temperatures probably due to the hydrophobic nature of high silica (SiO_2/Al_2O_3 = 25) in the presence of Ni metal species.

Table 4.1 Textural properties of the catalysts

Catalysts		BET Surface Area (m^2g^{-1})	Pore Volume (cm^3g^{-1})	Average Pore Diameter (nm)
500ºC	BEA	529	0.150	4.30
	Ni/BEA	528	0.148	5.19
	Fe/BEA	474	0.132	5.43
	FeNi/BEA	445	0.123	5.71
	NiFe/BEA	447	0.127	5.88
	Fe-Ni/BEA	243	0.581	9.56
600ºC	Ni/BEA	523	0.146	5.50
	Fe/BEA	471	0.129	6.55
	FeNi /BEA	441	0.124	5.83
	NiFe/BEA	454	0.126	5.61
	Fe-Ni/BEA	395	0.967	9.78
700ºC	Ni/BEA	397	0.104	6.72
	Fe/BEA	492	0.136	6.02
	FeNi/ BEA	449	0.093	5.34
	NiFe/BEA	434	0.090	6.23
	Fe-Ni/BEA	381	0.993	10.43

Nevertheless, the reductions are 15.8%, 16.6% and 15.0% respectively after Ni/BEA was impregnated with Fe as a second metal. On the other hand, the reductions in surface area of the Fe/BEA catalysts are 10.4, 11.0 and 7.0% after calcinations at 500, 600 and 700 ºC, respectively. However, when Ni was added as a second metal, the reduction in surface area became 15.5%, 14.2% and 18.0% with increase in calcination temperatures. Theoretically, the reduction in the surface area of bimetallic catalysts should be twice than that of monometallic catalysts. However, the results show less than twice the reduction indicating that the metals are overlapping on each other instead of occupying different sites on the BEA surfaces and pores.

Moreover, the trend in reduction of surface area of the catalyst is similar to the trend in reduction in the pore volume where the pore volume is reduced when more active metals were impregnated with BEA. In general, the prepared catalysts have lower surface area (397-528 m^2g^{-1}) and smaller pore volume (< 0.15 cm^3g^{-1}) as compared to the bare BEA except the bimetallic catalysts prepared by co-impregnation method. According to Webb and Orr [83], catalysts with more available surface area are generally more active, more adsorptive, and promoting high activity in biomass steam gasification.

In addition, the average pore diameter for the bare BEA is 4.30 nm which is smaller than the average pore diameter of the prepared catalysts which are ranging from 5.19 to 10.43 nm. This could be due to acidic nature of metal salts used for impregnation which attacked the pore opening of the support leading to a bigger pore size and deformation of some of the continuous surface into smaller non-continuous surface [89].

In terms of different preparation method for bimetallic catalysts, the co-impregnation method yield catalysts with lower surface area (243 - 395 m^2g^{-1}), higher pore volume (0.581 - 0.993 cm^3g^{-1}) and larger pore diameter (9.56 - 10.43 nm) as compared to the sequential impregnation method. From the physical and chemical view, this phenomenon occurred because of the the strong interaction between nickel oxide and iron oxide results agglomeration of the metal particles during the co-impregnation (Figure 4.6). Chen *et al.* [87] has suggested that larger pore volume and pore diameter of catalytic material are usually potential benefit for large molecule reaction.

Figure 4.6 illustrates the agglomeration of metal particles after impregnated with bare BEA. Both sequential and co-impregnation bimetallic catalysts show the combination of metal particles from monometallic catalysts integrated in the BEA lattice. In the sequential impregnation method, Fe and Ni occupied the BEA pore by following the order of impregnation. However, in the co-impregnation method, Fe and Ni particles have to compete with each other to occupy the BEA lattice. This observation demonstrated that the different approach to impregnate the metals with support will give some significant effect to the structure of the catalysts prepared.

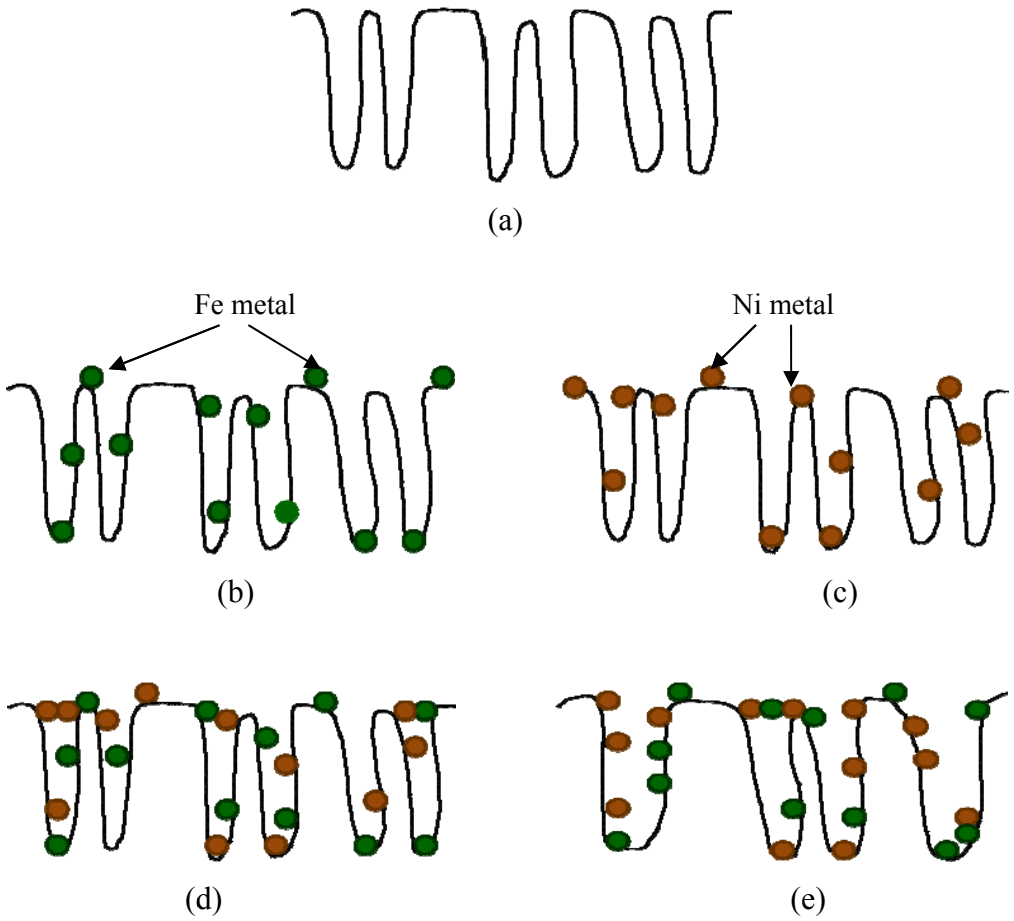

Figure 4.6 The agglomeration of metal particles (a) bare BEA (b) Ni/BEA (c) Fe/BEA (d) bimetallic sequential impregnation and (e) bimetallic co-impregnation

4.1.2 Powder X-Ray Diffraction (XRD)

The XRD patterns of the bare BEA supported monometallic and bimetallic catalysts are displayed in Figure 4.7. The bare BEA shows two major diffraction peaks at 2θ= 8° and 22.5° [65, 87]. The intensities of these peaks are high and the peaks are quite broad illustrating that the peaks contain Si-O-Al phase.

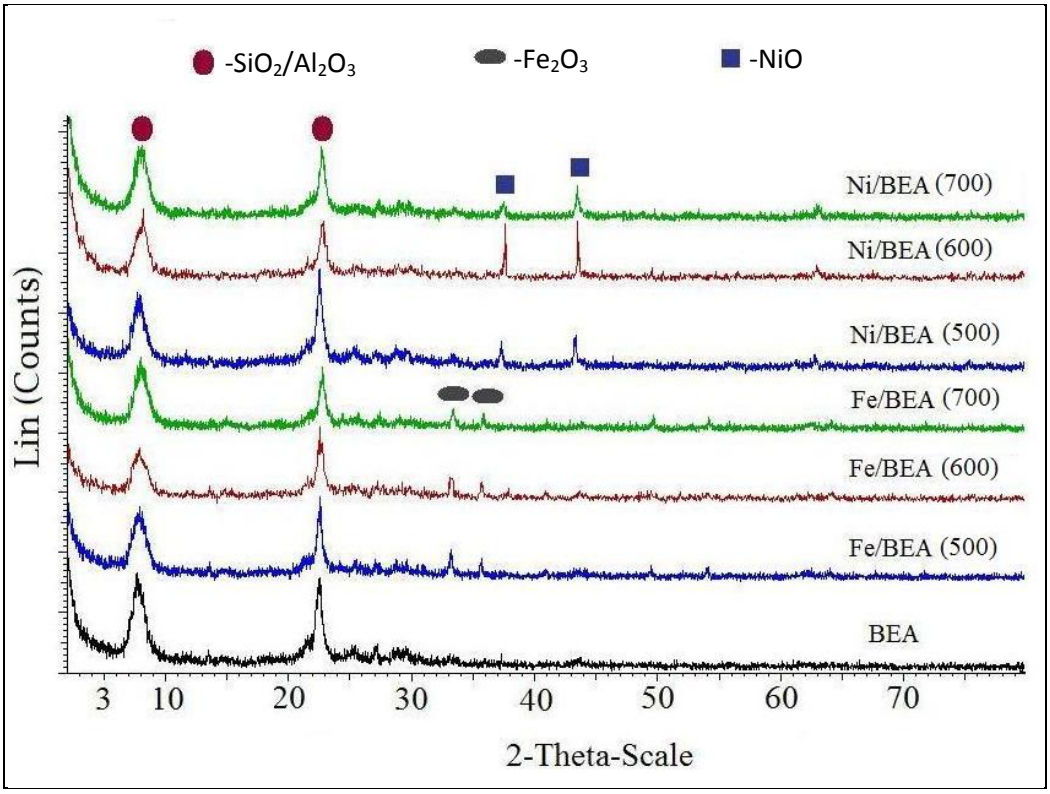

(a)

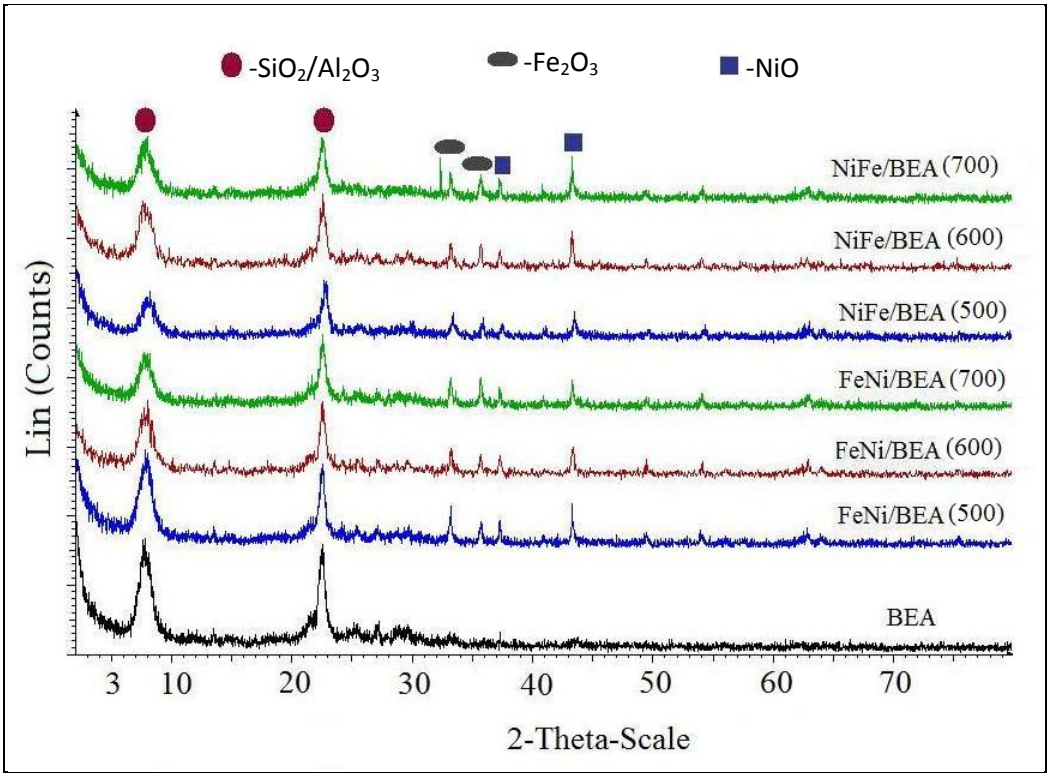

(b)

Figure 4.7 XRD patterns of BEA supported catalysts (a) monometallic (b) bimetallic prepared by sequential impregnation method

Ni and Fe revealed two diffraction peaks which are corresponding to bunsenite, (NiO phase) and hematite, (α-Fe_2O_3 phase), respectively. The strong interactions between these two elements in bimetallic catalysts presumably allow for a better control of the degree of reduction of the catalyst, prevent the oxidation of metallic Ni sites and provide partial protection against catalyst deactivation as reported by Rapagna *et al.* [33]. The peaks for NiO phase are represented by the appearance of (111) and (200) plane at the 2θ values of 37.3º and 43.3º, while the diffraction peaks corresponding to Fe_2O_3 phase are represented with the appearance of (104) and (110) plane positioned at the 2θ values of 33.1º and 35.6º. These planes are in agreement with data reported in the JCPDS card and from a previous study [84, 90-91].

Presence of NiO and α-Fe_2O_3 phase in the monometallic catalysts affects the diffraction peak of BEA. The diffraction peaks are shifted to higher 2θ value and the intensity is reduced. However, when a second metal was incorporated into BEA, the intensity of BEA diffraction peaks are significantly lowered further and shifted to higher 2θ value as compared to monometallic catalysts. This may due to the formation of interacted species between Fe and Ni with Al_2O_3 or SiO_2 in BEA. Nevertheless, nickel aluminate ($NiAl_2O_4$) and iron aluminate ($FeAl_2O_4$) phase were not detected, which could be due to lack of crystallinity as formerly observed by Zielinski [91] and confirmed by Salagre *et al.* [92]. According to Rynkowski *et al.* [90] $NiAl_2O_4$ diffraction peak can be observe at 2θ= 44.4º and 51.8º once the Ni supported catalyst was reduced or when the catalyst controlled was impregnated with Ni content of more than 8wt% [93].

Temperature is important factor which influence the product components and shapes where it can break up the precursor and eventually decelerates the crystallization process. Referring to the prepared catalysts calcined at temperatures from 500 to 700 ºC, the diffraction peaks corresponding to BEA, NiO and Fe_2O_3 are slightly shifted higher to 2θ. The intensities are lowered except for NiFe/BEA due to the agglomeration of the particles. This indicates that the temperature also contributes to the crystallization of the prepared catalysts. Referring to the JCPDS cards, the catalysts have hexagonal structure (89-0596) for α-Fe_2O_3 and cubic structure (47-1049) for NiO, respectively.

Figure 4.8 shows the XRD diffraction patterns from the bimetallic catalysts prepared by co-impregnation method. It can be seen that the diffraction pattern are similar to that of sequential impregnation catalysts except the crystallization of hematite, α-Fe_2O_3. The intensity of diffraction peak for α-Fe_2O_3 phase corresponding to the (104) plane positioned at 2θ= 33.1º is higher after calcination at 500 ºC but the peak intensity starting to reduce at 600 ºC and finally disappear at 700 ºC calcination temperatures. On the other hand, the intensity of diffraction peaks for α-Fe_2O_3 corresponding to (110) plane positioned at 2θ = 35.6º increases with increasing in calcination temperatures. In the case of NiO phase, the diffraction peaks are represented with the appearance of (111) and (200) plane at the 2θ = 37.3º and 43.3º. The diffraction peaks observed are slightly shifted to lower 2θ value with increasing of calcination temperatures.

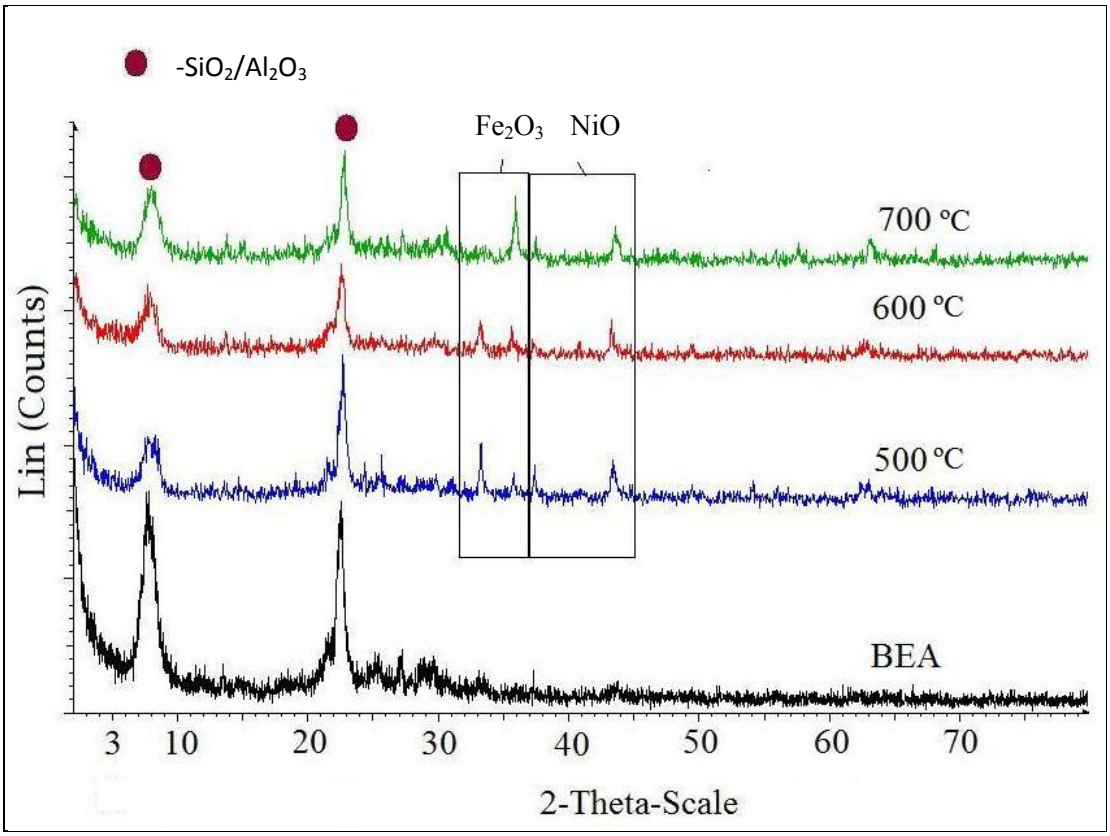

Figure 4.8 Diffractograms displayed by Fe-Ni/BEA calcined at 500-700 ºC

The diffraction peak at 2θ=35.9º detected in all diffractograms displayed by bimetallic catalysts can also be assigned to trevorite ($NiFe_2O_4$). The intensity of this

peak in the diffractogram displayed by FeNi/BEA (700) is quite high as compared to the intensity of the same peak in the diffractogram displayed by other catalysts. Miki *et al.* [94] and Wang *et al.* [95] have demonstrated that, high crystallinity of Fe and Ni catalyst resulted formation of NiO and $NiFe_2O_4$ phase. Formation of Fe_2O_4 is not detected probably due to NiO dispersed finely in $NiFe_2O_4$. Therefore, this peak is more appropriate to be assigned as $NiFe_2O_4$ in Fe-Ni/BEA (700) catalyst.

A possible reason for this phenomenon is that the Ni and Fe metals were simultaneously dissolved and impregnated with the support resulting in competition by the metals to occupy in the BEA pore. After calcination at high temperatures, the Ni and Fe melt and some chemical reaction occurred between the two metals resulting formation of mixed metal oxide deposited into BEA support. This is consistent with Miki *et al.* [94], where Ni and Fe are distributed uniformly from the surface into the support. Moreover, the combination of Fe and Ni catalyst had a well-defined crystal structure when the catalyst prepared by co impregnation method and calcined at high calcination temperatures. Therefore, this observation is comparable with the textural characterization.

The crystallite size in the catalysts can be estimated based on the basis of line broadening analysis using Scherer's formula [77]. Table 4.2 shows that the value of crystallite size between monometallic and bimetallic catalysts mainly depends on the crystallization of Ni and Fe metals during integrated into BEA lattice. Most of the catalysts calcined at 700 ºC have greater particle sizes as compared to other prepared catalysts. This is attributed to agglomeration of the active metals after prolonged treatment at high temperature.

From the calculated crystallite size, it can be suggested that some of the active metals may not have been deposited in the BEA pores since the approximate crystal size is bigger than the possible pore dimension of BEA. Hence, this active metals together on the surface of support.

Table 4.2 Crystallites size of the catalysts, nm

Catalysts	NiO	Fe_2O_3	$NiFe_2O_4$
Ni/BEA (500)	76.82	-	-
Ni/BEA (600)	139.84	-	-
Ni/BEA (700)	85.33	-	-
Fe/BEA (500)	-	87.80	-
Fe/BEA (600)	-	64.75	-
Fe/BEA (700)	-	106.64	-
FeNi/BEA (500)	104.91	87.25	-
FeNi/BEA (600)	77.66	91.62	-
FeNi/BEA (700)	106.52	93.45	-
NiFe/BEA (500)	61.63	67.46	-
NiFe/BEA (600)	75.79	78.82	-
NiFe/BEA (700)	98.43	88.19	-
Fe-Ni/BEA (500)	94.92	95.14	-
Fe-Ni/BEA (600)	78.93	84.46	-
Fe-Ni/BEA (700)	93.28	-	98.43

4.1.3 Field Emission Scanning Electron Microscopy (FESEM)

Figure 4.9 shows the comparison of morphology of bare BEA with SiO_2/Al_2O_3 mole ratio of 25 with the BEA ranging from 12.5 to 60 SiO_2/Al_2O_3 ratios. It can be seen that the bare BEA consists of fine particles smaller than 100nm with unclear features morphology. However, Zhang and Li [96] and Chen *et al.* [85] demonstrated that BEA crystals appeared like discrete spherical particles even with low or high $SiO_2/Al2O_3$ mole ratio. The interaction and crystallization of the impregnated active metals with BEA are also studied where the images are displayed in Figure 4.10 - 4.11.

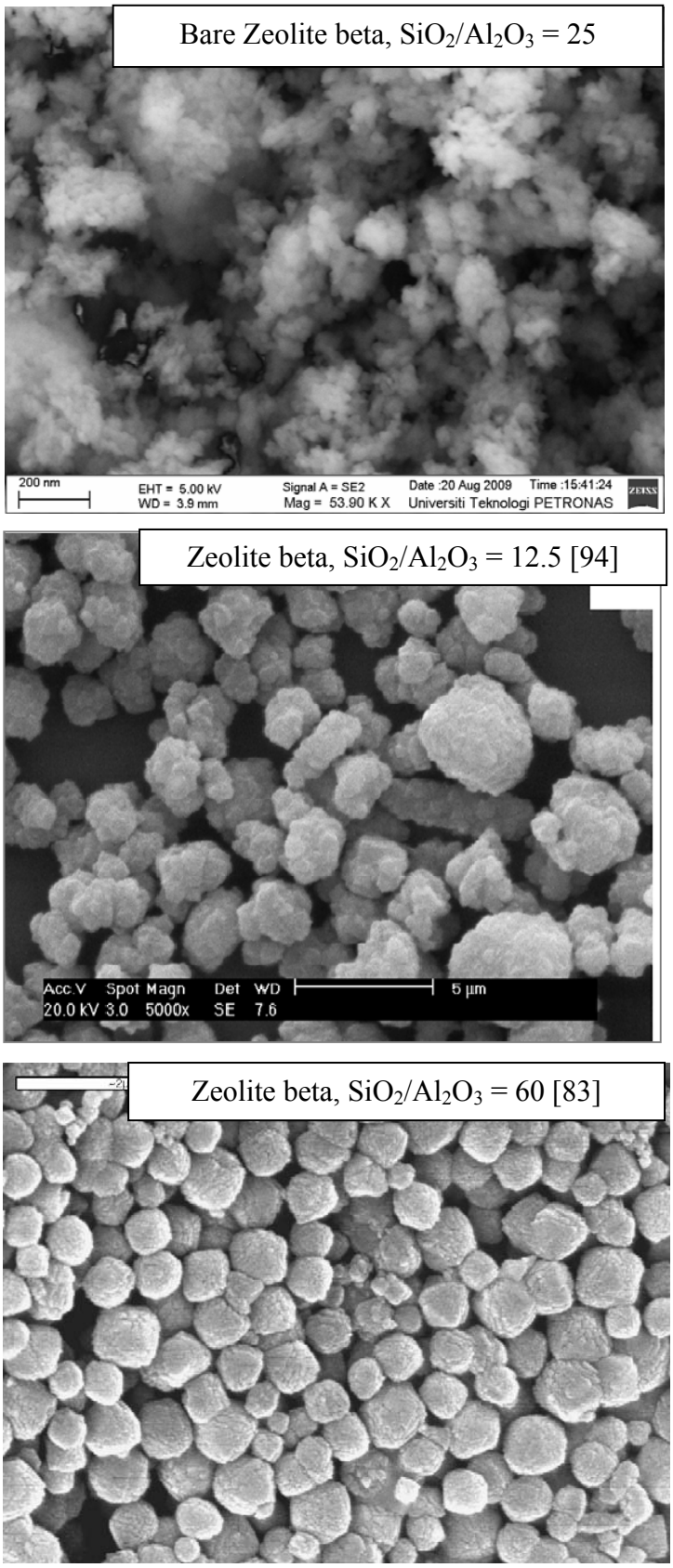

Figure 4.9 Comparison of morphology between BEA used in this study with BEA from other source

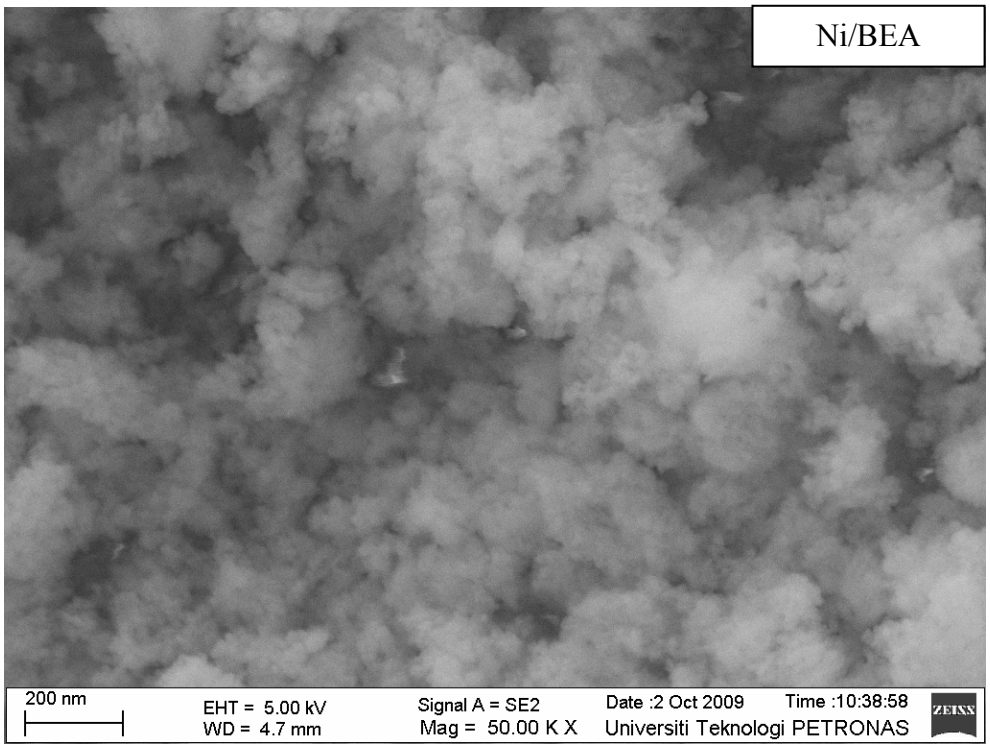
Ni/BEA
200 nm
EHT = 5.00 kV
WD = 4.7 mm
Signal A = SE2
Mag = 50.00 K X
Date :2 Oct 2009
Time :10:38:58
Universiti Teknologi PETRONAS
ZEISS

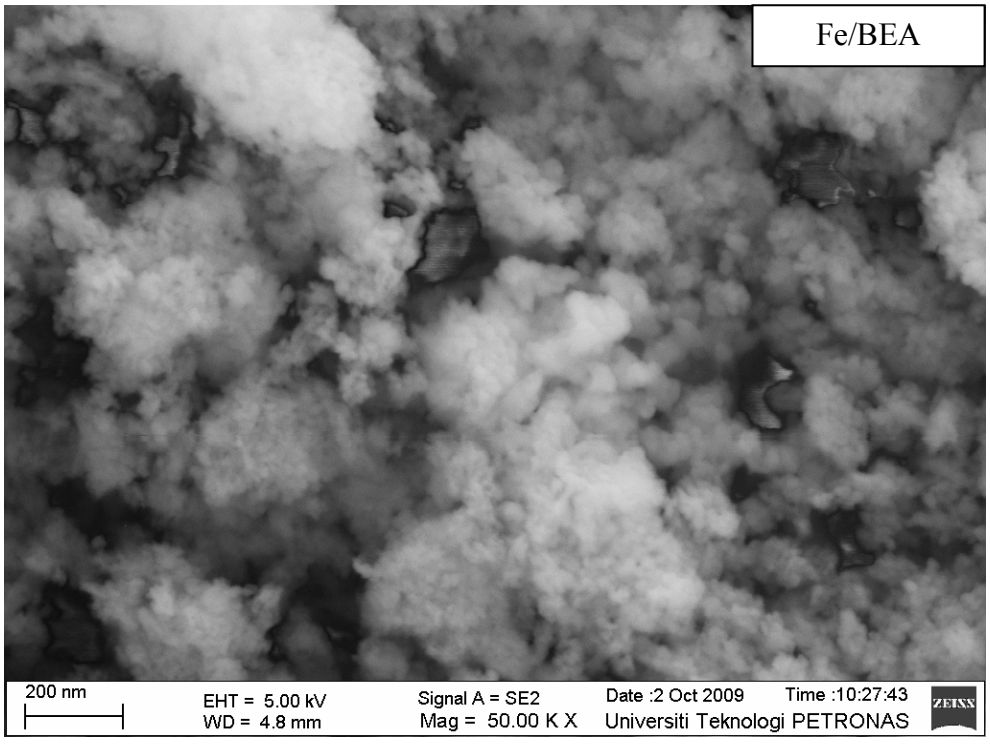
Fe/BEA
200 nm
EHT = 5.00 kV
WD = 4.8 mm
Signal A = SE2
Mag = 50.00 K X
Date :2 Oct 2009
Time :10:27:43
Universiti Teknologi PETRONAS
ZEISS

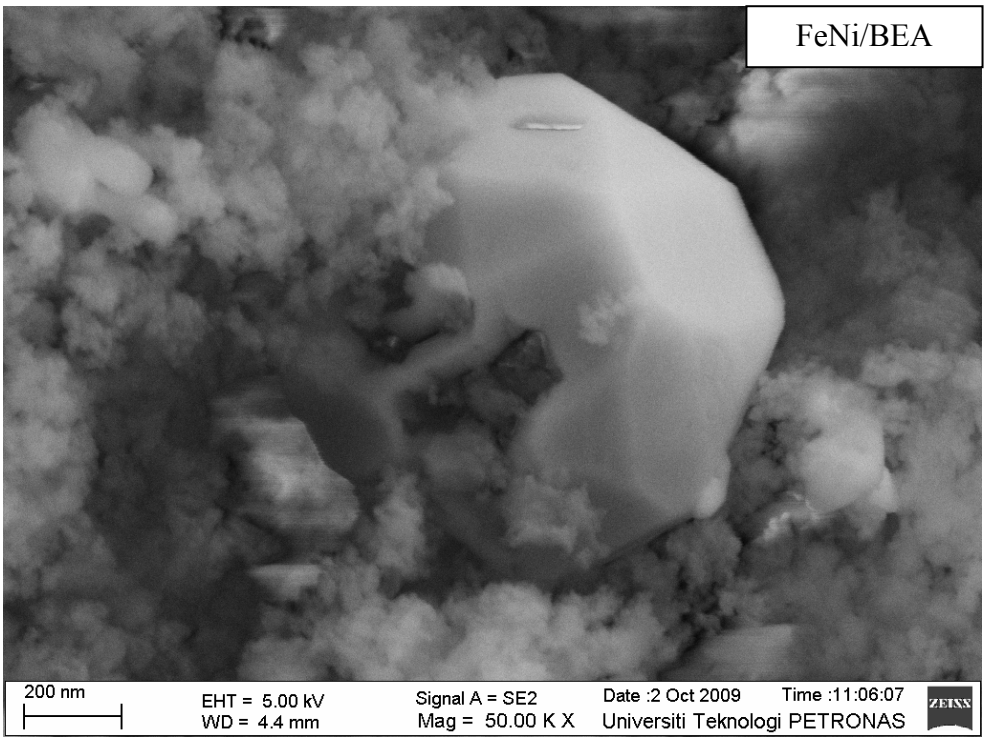
FeNi/BEA
200 nm
EHT = 5.00 kV
WD = 4.4 mm
Signal A = SE2
Mag = 50.00 K X
Date :2 Oct 2009
Time :11:06:07
Universiti Teknologi PETRONAS
ZEISS

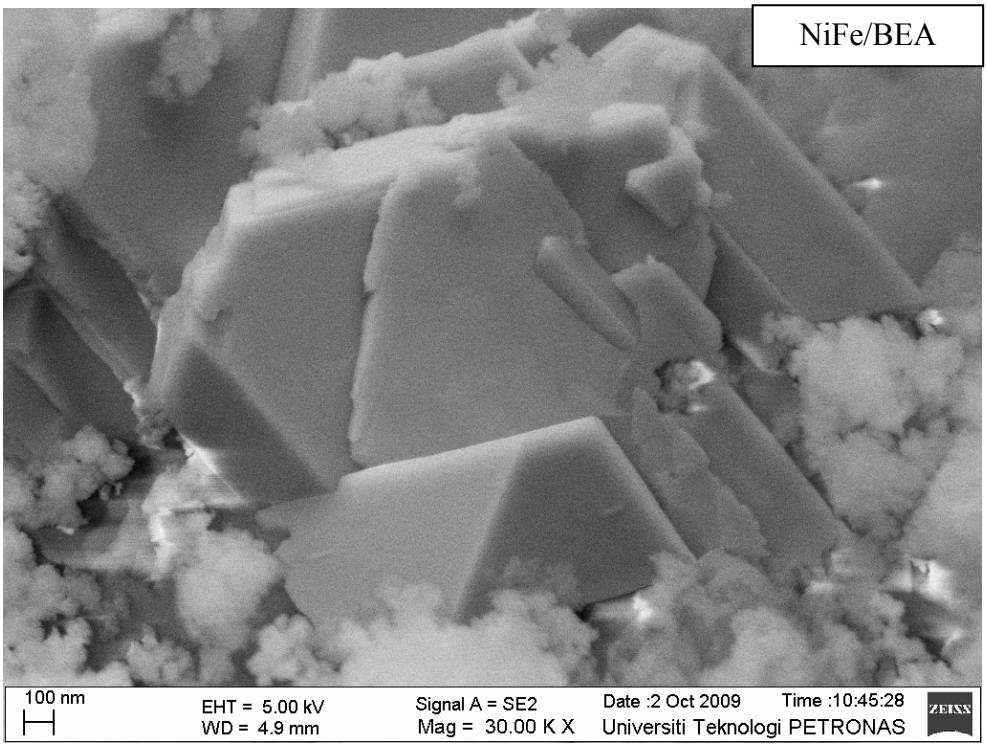
NiFe/BEA
100 nm
EHT = 5.00 kV
WD = 4.9 mm
Signal A = SE2
Mag = 30.00 K X
Date :2 Oct 2009
Time :10:45:28
Universiti Teknologi PETRONAS
ZEISS

(a)

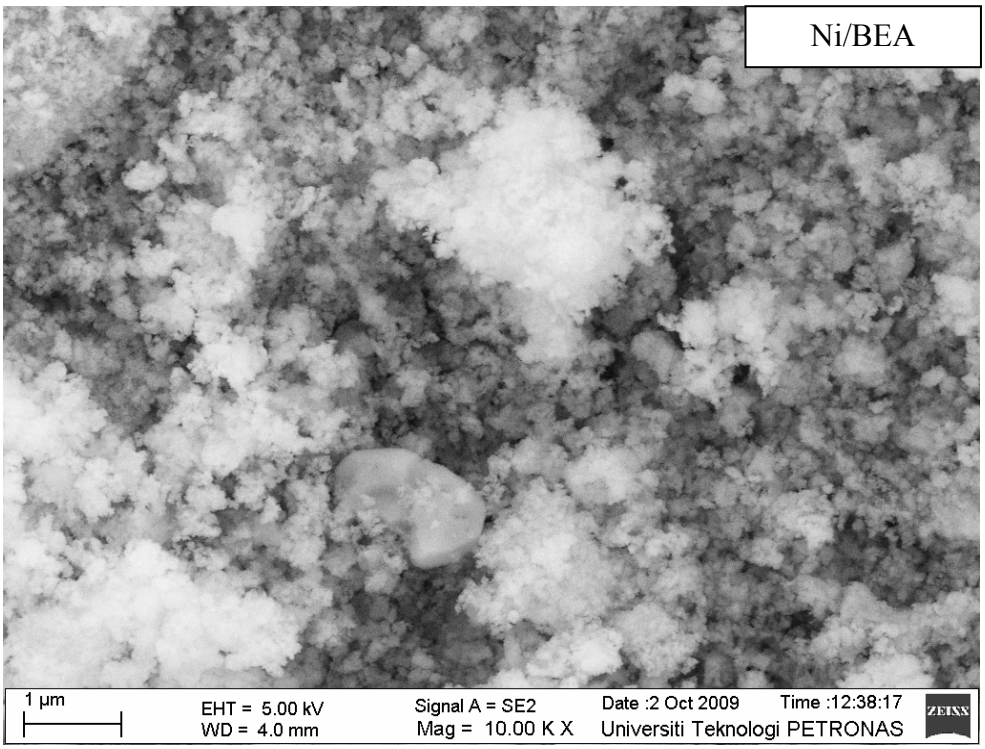
Ni/BEA
1 µm
EHT = 5.00 kV
WD = 4.0 mm
Signal A = SE2
Mag = 10.00 K X
Date :2 Oct 2009
Time :12:38:17
Universiti Teknologi PETRONAS
ZEISS

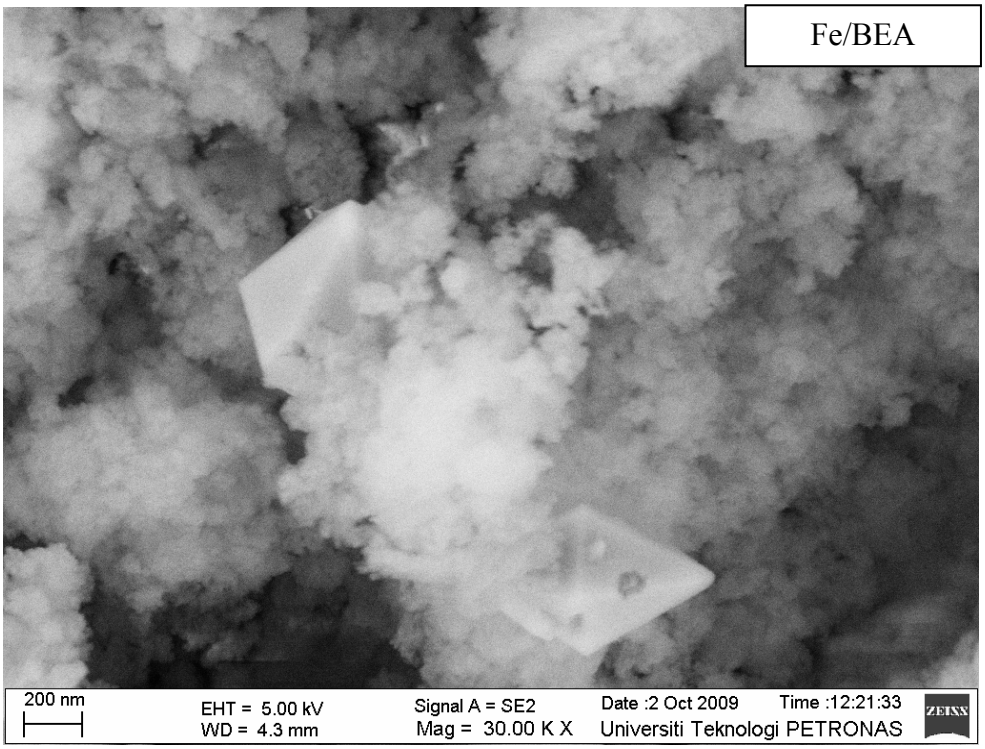
Fe/BEA
200 nm
EHT = 5.00 kV
WD = 4.3 mm
Signal A = SE2
Mag = 30.00 K X
Date :2 Oct 2009
Time :12:21:33
Universiti Teknologi PETRONAS
ZEISS

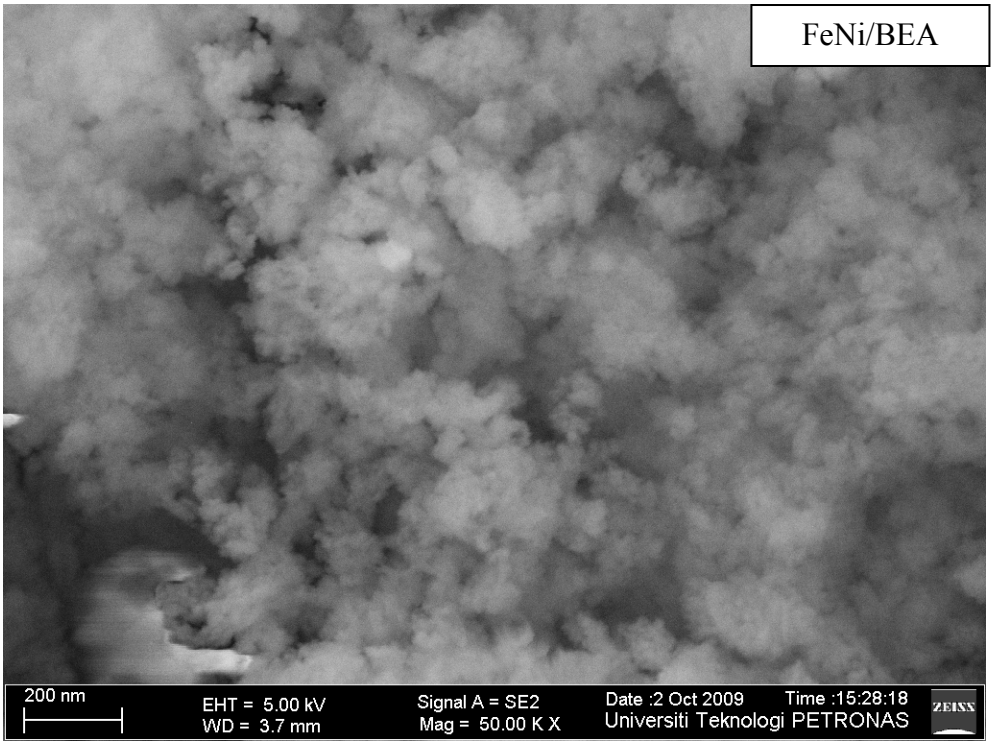
FeNi/BEA
200 nm
EHT = 5.00 kV
WD = 3.7 mm
Signal A = SE2
Mag = 50.00 K X
Date :2 Oct 2009
Time :15:28:18
Universiti Teknologi PETRONAS
ZEISS

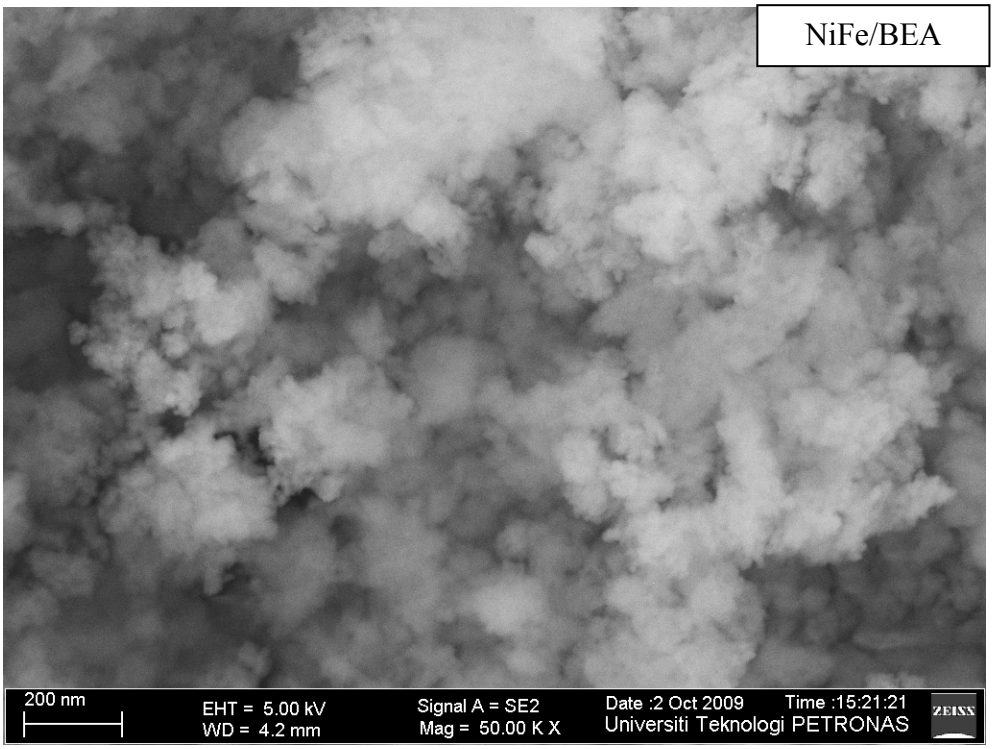
NiFe/BEA
200 nm
EHT = 5.00 kV
WD = 4.2 mm
Signal A = SE2
Mag = 50.00 K X
Date :2 Oct 2009
Time :15:21:21
Universiti Teknologi PETRONAS
ZEISS

(b)

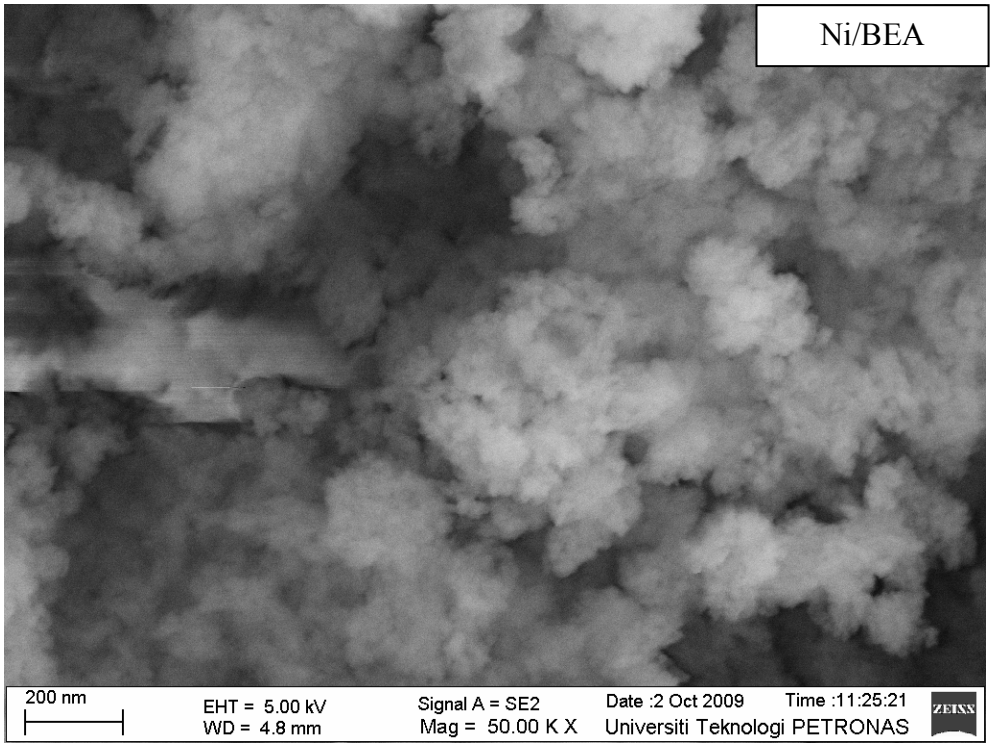
Ni/BEA
200 nm
EHT = 5.00 kV
WD = 4.8 mm
Signal A = SE2
Mag = 50.00 K X
Date :2 Oct 2009
Time :11:25:21
Universiti Teknologi PETRONAS
ZEISS

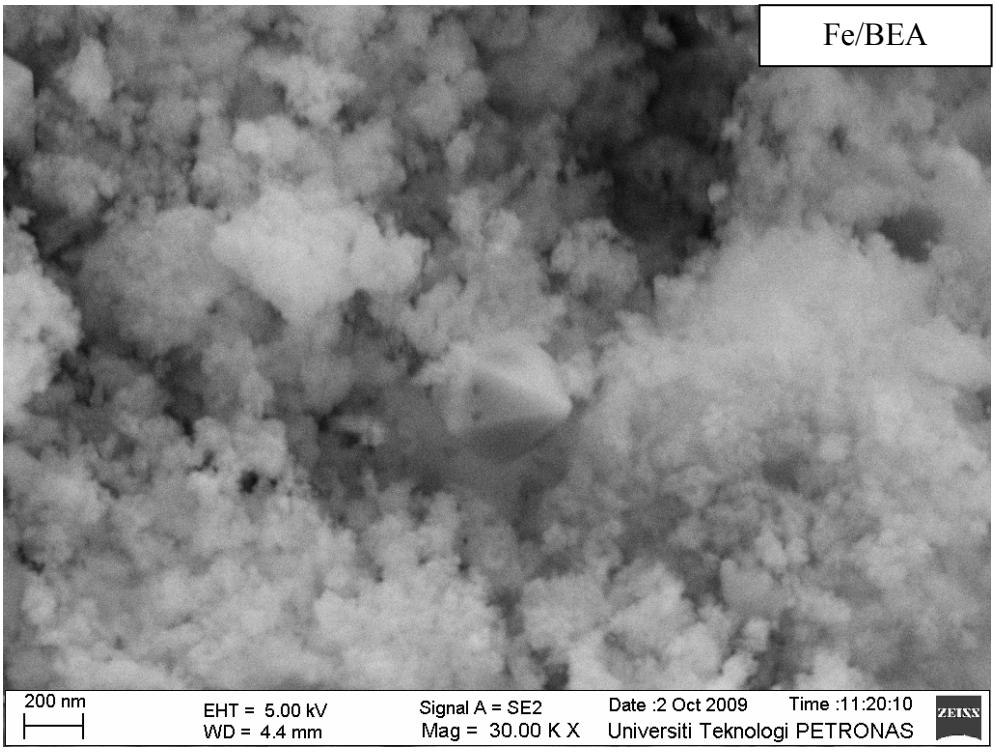
Fe/BEA
200 nm
EHT = 5.00 kV
WD = 4.4 mm
Signal A = SE2
Mag = 30.00 K X
Date :2 Oct 2009
Time :11:20:10
Universiti Teknologi PETRONAS
ZEISS

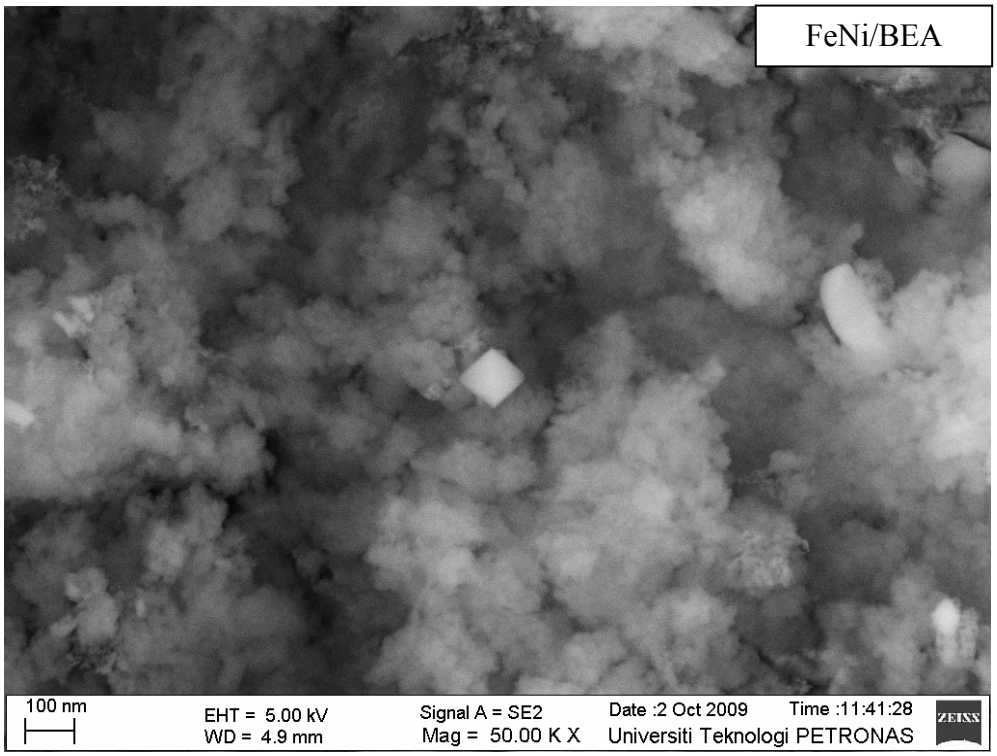

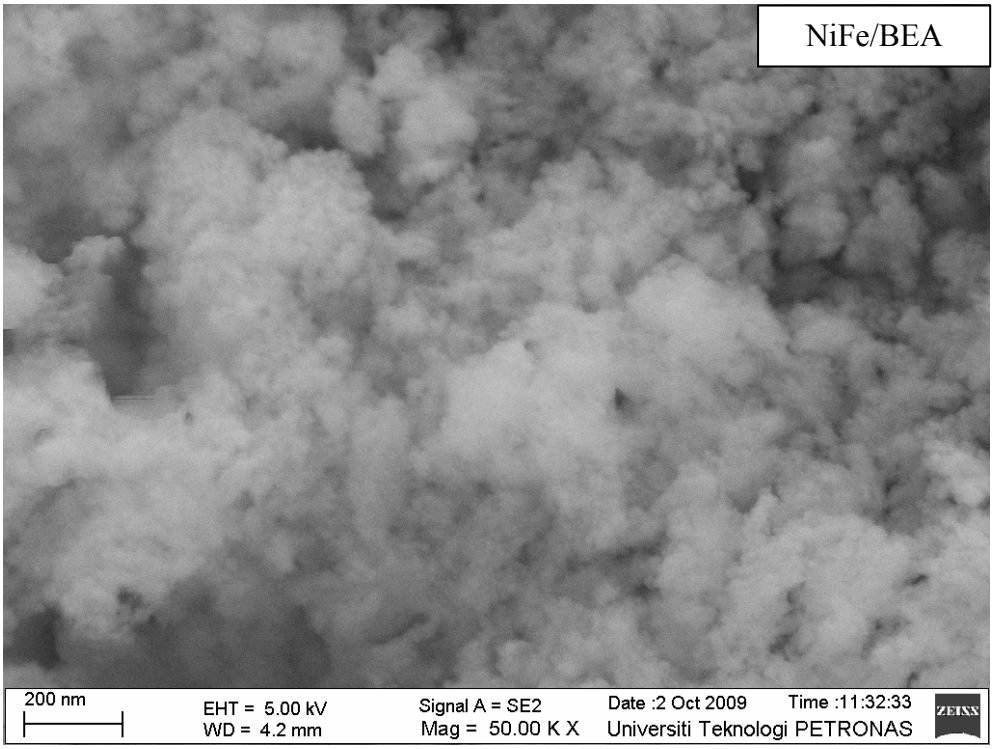

(c)

Figure 4.10 BEA supported catalysts calcined at (a) 500 ºC (b) 600 ºC and (c) 700 ºC

The morphology of BEA based catalysts does not change in the Ni/BEA and Fe/BEA catalysts even after impregnation and calcination at 500 ºC. This is because only a small amount of metal (5 wt%) was impregnated and as a result, the metals were migrating into the inner part of BEA lattice. However, the Fe/BEA catalysts revealed a crystalline phase instead of indefinite features when calcined at 600 ºC and 700 ºC. This is due to agglomeration of metal particles during the impregnation.

The crystalline phase can still be clearly observed when BEA was impregnated with both Fe and Ni and calcined at 500 ºC. The crystalline phase with hexagonal structure observed is corresponding to Fe_2O_3, and the cubic structure is corresponding to NiO as confirmed by XRD characterization. The formation of bulk Fe_2O_3 and NiO phase presumably due to the weak interaction of Fe and Ni with support [93]. The crystallization of FeNi/BEA and NiFe/BEA are improved after calcination at 600ºC however crystallization of FeNi/BEA (700) is where a minor crystalline phase can still be observed.

The morphology of the Fe-Ni/BEA catalysts is shown in Figure 4.11. The crystallization of Fe and Ni are clearly observed especially after calcination at 700 ºC. Fe and Ni particles obviously attached to each other which could arise from some chemical reaction at high temperatures. This result is in accordance with the textural properties data and XRD results for the Fe-Ni/BEA catalysts where the crystalline phase may be $NiFe_2O_4$ formation.

Thus, this ascribed to the fact that the NiO and Fe_2O_3 crystalline phase in Fe-Ni/BEA (700) submitted high contribution to the metal dispersion resulting in better interaction with the support. However, the other catalysts have less dispersion of metals due to agglomeration of metal particles. It is worthy to note that FESEM analysis is based on location of samples. Although, no pronounced crystal structure was observed in FESEM micrograph, it does not mean that the structure is unavailable within the catalyst.

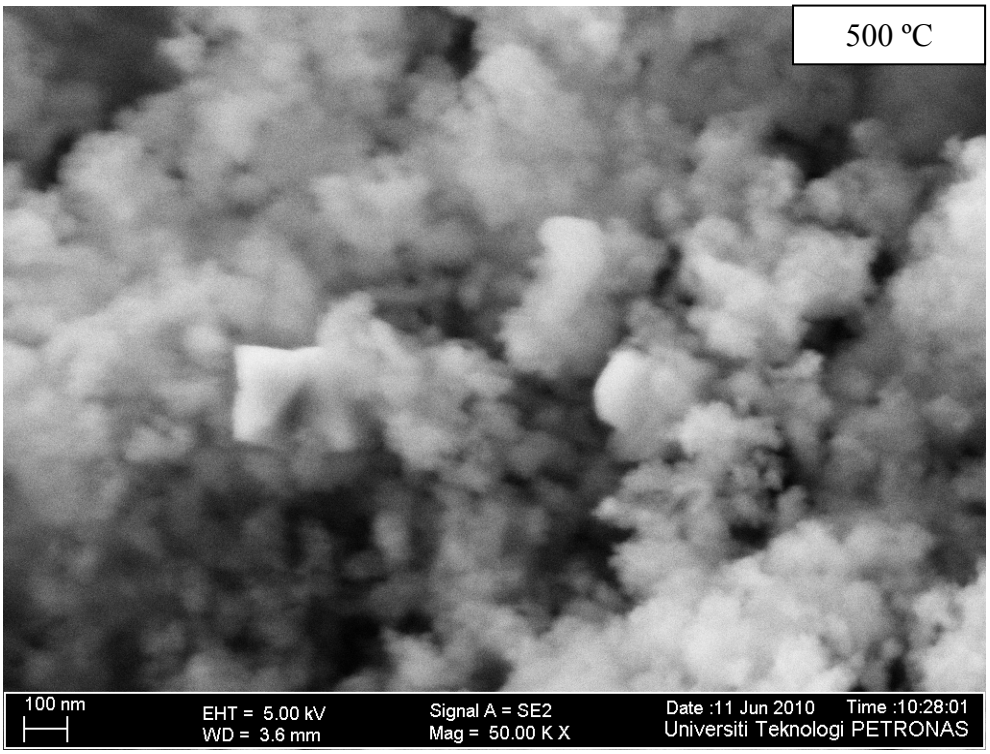
500 ºC
100 nm
EHT = 5.00 kV
WD = 3.6 mm
Signal A = SE2
Mag = 50.00 K X
Date :11 Jun 2010
Time :10:28:01
Universiti Teknologi PETRONAS

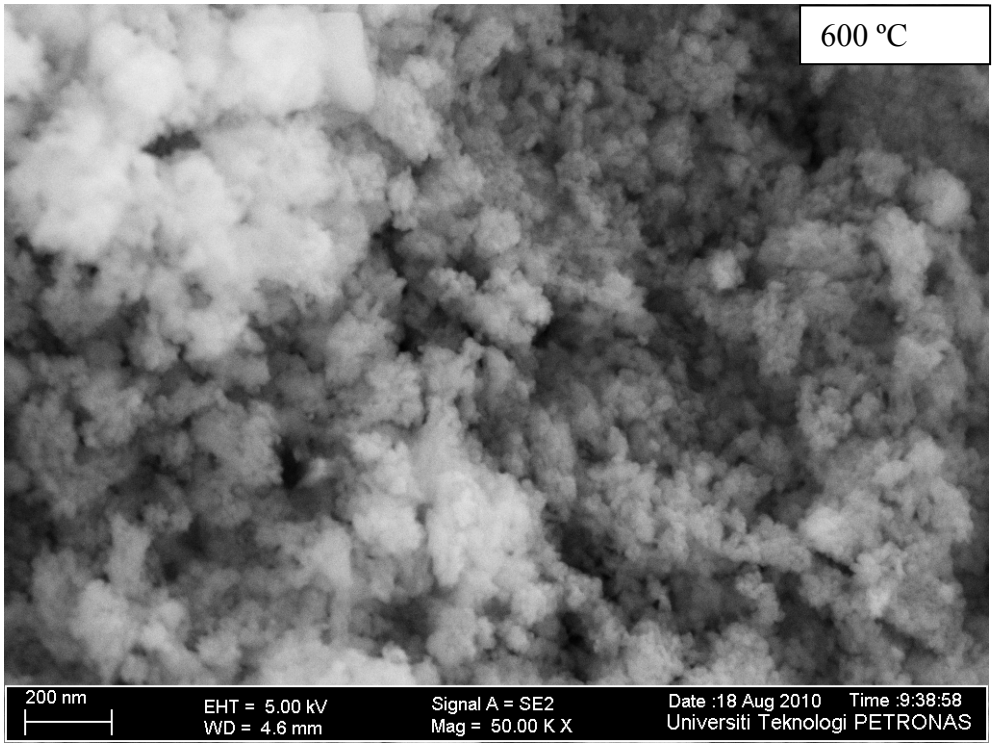
600 ºC
200 nm
EHT = 5.00 kV
WD = 4.6 mm
Signal A = SE2
Mag = 50.00 K X
Date :18 Aug 2010
Time :9:38:58
Universiti Teknologi PETRONAS

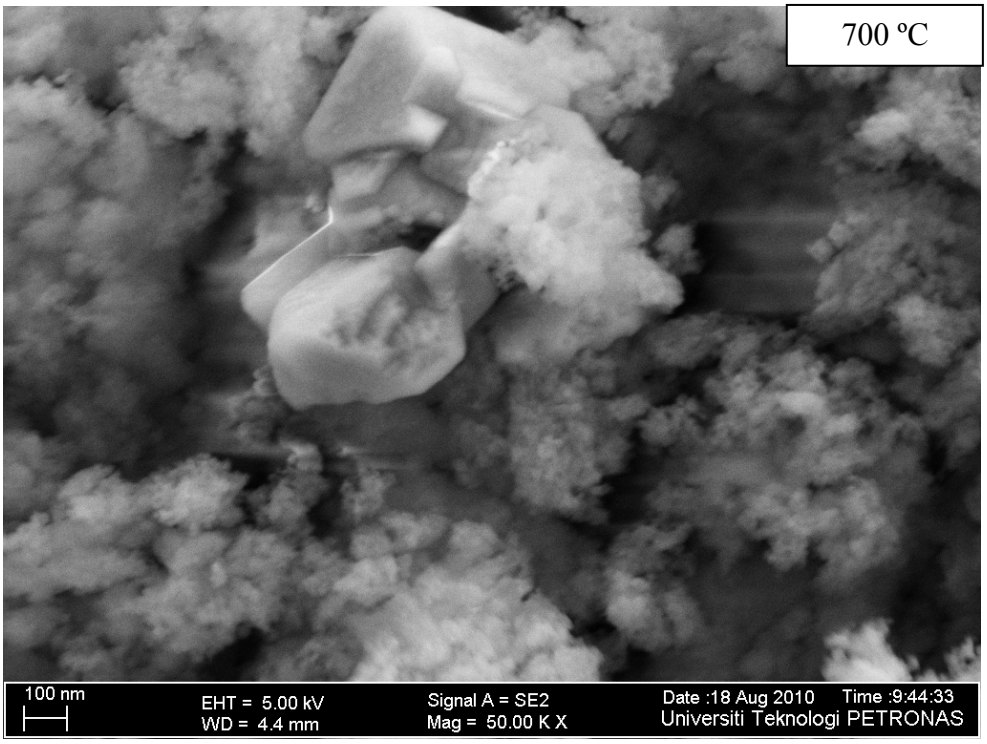

Figure 4.11 Morphology of co-impregnated bimetallic catalysts

There are three factors in favour of a high dispersion of the nickel and iron: (i) the support material is porous and easily agglomerates, which allows the active metal to contact support over a large surface area; (ii) the strong interaction between nickel oxide and iron oxide with support prevents active metals agglomeration during the impregnation; (iii) the content of nickel and iron is low which makes it easy for all the nickel and iron to diffuse into the support lattice [97].

The surface elemental compositions of the prepared catalysts were characterized by EDX analysis and the results are shown in Table 4.3. Fe and O were detected in the monometallic Fe catalyst verifying that the prepared catalyst consists of Fe_2O_3 phase and Si-O-Al which confirms the results from the XRD analysis. Meanwhile Ni and O were detected in the monometallic Ni catalyst verifying that the catalyst consists of NiO phase and Si-O-Al in the form of BEA as detected by XRD analysis. The measured elemental ratios of monometallic catalysts are slightly lower (2.68-3.92 wt%) than the starting material which is ±5 wt% except for Ni/BEA calcined at 600 ºC where 10.46 wt% of Ni was detected.

Table 4.3 Element compositions of prepared catalysts

Catalyst		Element (Weight %)					
		Si	Al	O	Fe	Ni	Cl
500 ºC	BEA	41.90	3.27	54.84	-	-	-
	Ni/BEA	40.76	2.42	53.67	-	3.15	-
	Fe/BEA	35.61	2.63	58.18	3.58	-	-
	FeNi/BEA	37.31	2.58	52.39	4.55	3.17	-
	NiFe/BEA	33.66	2.64	45.72	3.49	8.94	5.55
	Fe-Ni/BEA	35.38	1.85	57.54	3.47	1.75	-
600 ºC	Ni/BEA	36.00	2.78	50.77	-	10.46	-
	Fe/BEA	35.24	2.94	57.90	3.92	-	-
	FeNi/BEA	33.43	2.64	57.25	3.20	3.48	-
	NiFe/BEA	33.17	3.32	57.88	3.85	1.79	-
	Fe-Ni/BEA	35.26	2.37	60.19	0.75	1.43	-
700 ºC	Ni/BEA	39.85	2.94	53.85	-	3.36	-
	Fe/BEA	50.86	2.40	44.07	2.68	-	-
	FeNi/BEA	40.28	2.94	48.94	5.16	2.68	-
	NiFe/BEA	37.43	3.01	48.62	3.01	7.93	-
	Fe-Ni/BEA	22.66	5.32	52.25	10.21	9.55	-

Table 4.3 also shows that when Fe and Ni were impregnated together in BEA to form bimetallic systems, both Fe_2O_3 and NiO phases are present in the prepared catalysts. In terms of compositions of Fe and Ni, the results are not in agreement with the percentage of the metals used during preparation. In general, even though the amount of Fe and Ni used are the same, the percentage of metal used in the

second impregnation step is detected higher than the percentage of metal used in the first impregnation step. This could be due to impregnation of the second metal on top of the first metal which resulted in the first metal being covered by the second metal, thus not detected during EDX analysis. The presence of 5.55% Cl as an impurity was also detected in NiFe/BEA (500). This is because of Fe or Ni was not fully decomposed during the calcinations.

4.1.4 Temperature Programmed Reduction Analysis (H_2-TPR)

Figure 4.12 shows the TPR profile of the monometallic and bimetallic catalysts calcined at different calcination temperatures. The reduction of 5% Ni/BEA shows two reduction peaks in the region between 400-500 ºC and 600-700 ºC. Zielinski [91] indicates that the low temperature peak on the TPR curve is due to the reduction of NiO not bounded to the support which is referred to as "free nickel oxide". Meanwhile the higher temperature peak corresponds to the reduction of nickel that has reacted with the support forming $NiAl_2O_4$ or so-called "fixed nickel oxide". The reduction profile of 5% Ni/BEA is in accordance with Cheng *et al.* [98] where NiO is reducible below 500 ºC while $NiAl_2O_4$ is reducible at temperature above 600 ºC. The formation of $NiAl_2O_4$ is possible as a result of the reaction of extra-framework alumina which is present in the zeolite sample. Due to the framework silica/alumina ratio, a roughly small amount of alumina that might be present in the sample is outside of the framework and is available for reaction with NiO to form $NiAl_2O_4$ [99]. XRD data, however, have not shown any diffraction peak for existence of nickel aluminate in the catalyst which could be due to low crystallinity [91-92]. Preparation procedure such as types of nickel salt used, support and calcination temperature has been found as one of the factors which contribute to the development of fixed nickel oxide [91].

Both reduction peaks of Ni/BEA catalysts shifted to higher temperature as the calcination temperatures increases. This indicates that the metals are difficult to reduce, thus Ni/BEA (500) results high reducibility as compared to Ni/BEA calcined at 600 ºC and 700 ºC.

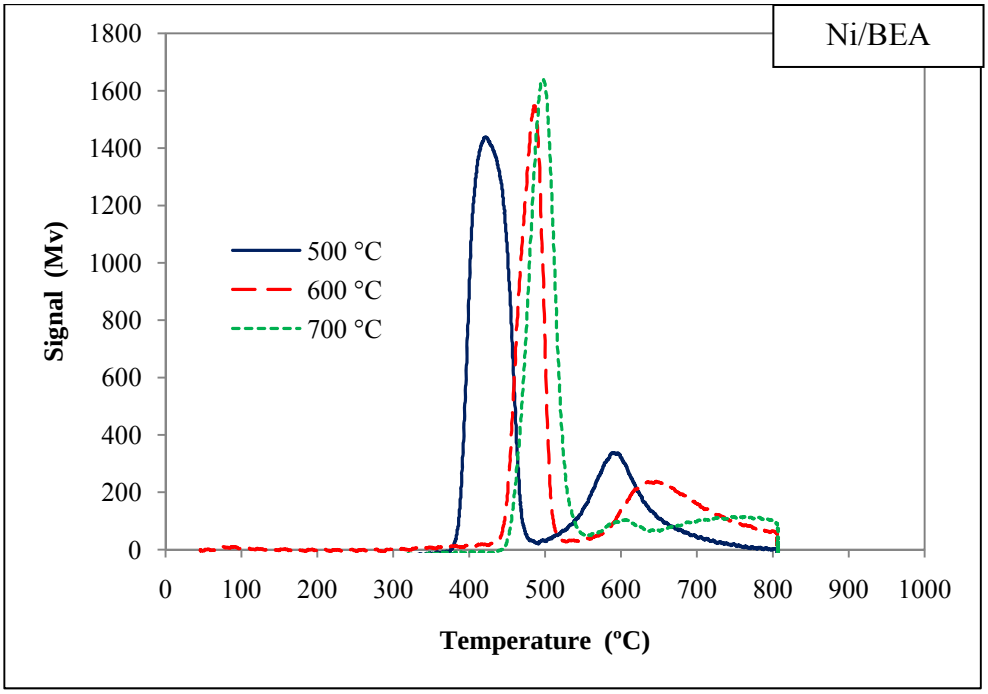
Ni/BEA
1800
1600
1400
1200
1000
800
600
400
200
0
Signal (Mv)
500 °C
600 °C
700 °C
0
100
200
300
400
500
600
700
800
900
1000
Temperature (ºC)

(a)

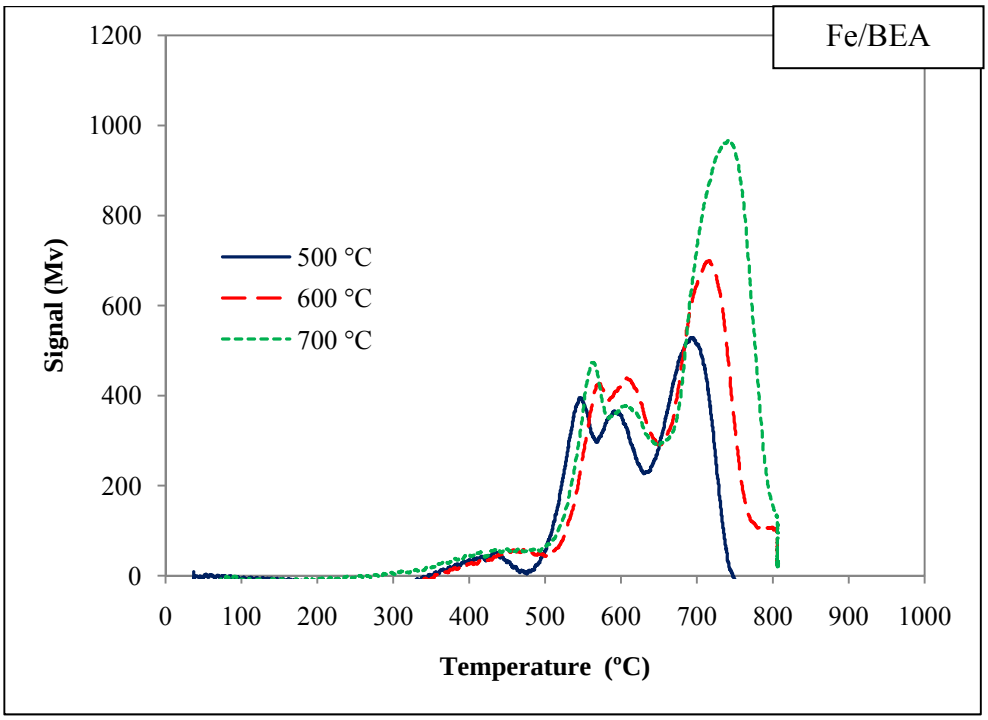
Fe/BEA
1200
1000
800
600
400
200
0
Signal (Mv)
500 °C
600 °C
700 °C
0
100
200
300
400
500
600
700
800
900
1000
Temperature (ºC)

(b)

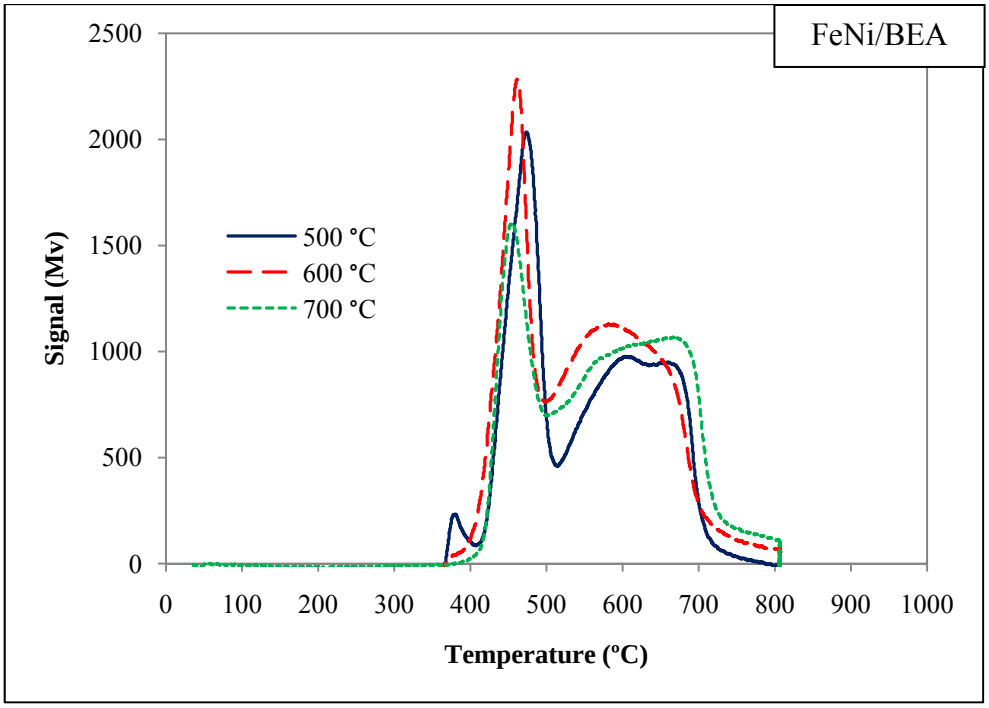
FeNi/BEA
Signal (Mv)
2500
2000
1500
1000
500
0
500 °C
600 °C
700 °C
0
100
200
300
400
500
600
700
800
900
1000
Temperature (ºC)

(c)

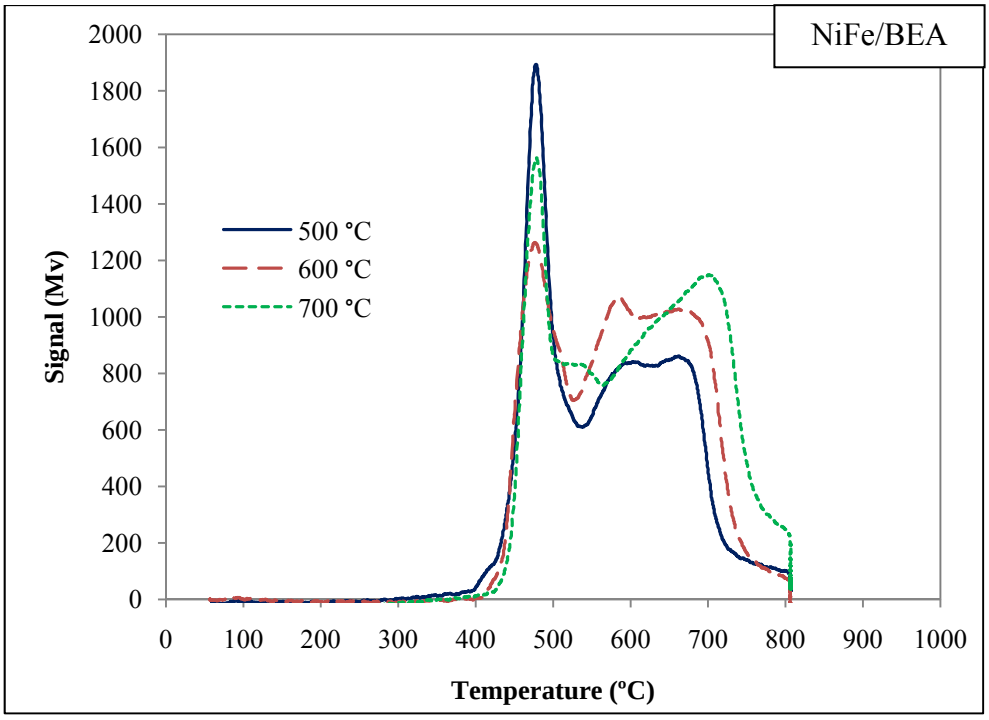
NiFe/BEA
Signal (Mv)
2000
1800
1600
1400
1200
1000
800
600
400
200
0
500 °C
600 °C
700 °C
0
100
200
300
400
500
600
700
800
900
1000
Temperature (ºC)

(d)

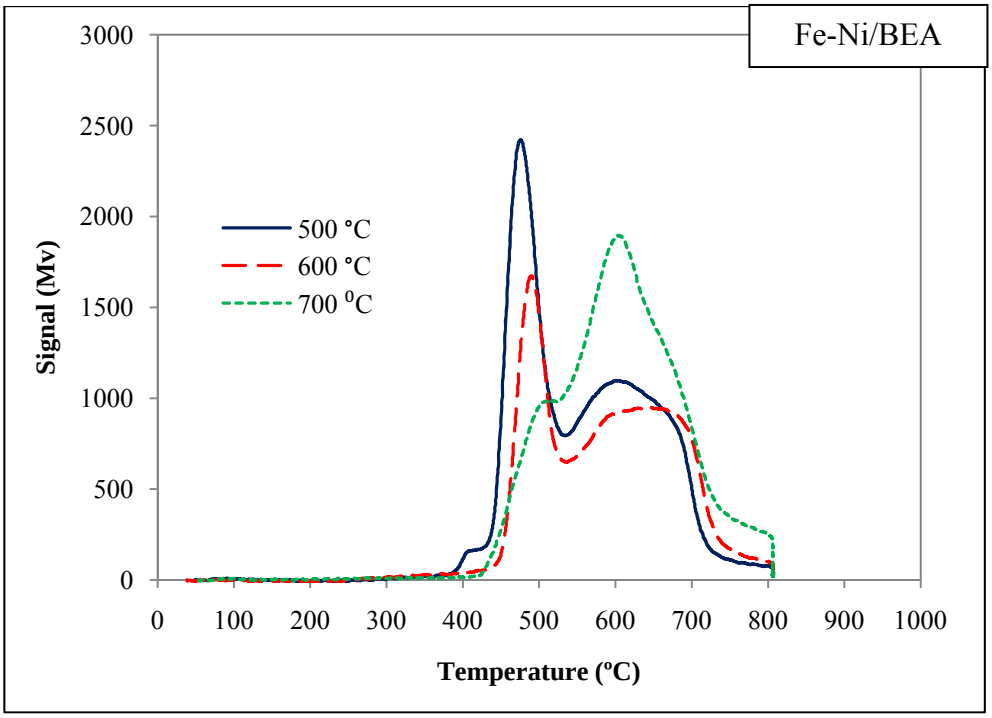

(e)

Figure 4.12 TPR profiles of monometallic and bimetallic catalysts (a) Ni/BEA (b) Fe/BEA (c) FeNi/BEA (d) NiFe/BEA (e) Fe-Ni/BEA calcined at 500-700 ºC

The phase transformation of 5% Fe/BEA during TPR process shows three reduction peaks between 500 to 800 ºC which represents several reduction phases of iron oxide. The reduction peaks between 500-650 ºC are attributed to reduction of Fe_2O_3 which has weak interaction with support. The first peak ascribed to reduction of $Fe_2O_3 \rightarrow Fe_3O_4$, whereas the second peak represents the reduction of $Fe_3O_4 \rightarrow$ FeO [100]. These reductions are also known as reduction of Fe^{3+} to Fe^{2+}. The reduction peak at temperature between 650-800 ºC is ascribed to reduction of $FeAl_2O_4$, which Fe has strong interaction with support [99]. Reduction of Fe_2O_3 ends at FeO phase rather than metallic Fe because FeO is a metastable phase of iron oxide on the support [101]. The strong interaction between Fe and Al_2O_3 provided the stabilization of FeO phase on support [102], which could further retard the transformation of FeO to metallic Fe [100, 103]. It should be noted that a lower broad peak between 300 to 500 ºC was observed and the peak is attributed to the reduction of free Fe_2O_3 as reported by Virginie *et al.* [104].

The reduction activity of Fe/BEA catalysts also increased with increasing calcination temperature which follows the sequence: 500 ºC > 600 ºC > 700 ºC. The first and second reduction peaks were observed slightly shifted at higher calcination temperature as the calcination temperatures increases. While, the third peak represents the reduction of $FeAl_2O_4$ was largely shifted towards higher temperature when the catalysts were calcined from 500 to 700 ºC. This may be attributed to the strong interaction between Fe and BEA after calcined at higher temperature results the BEA suppresses the reduction of metals in TPR process [100]. However, the intensity of $FeAl_2O_4$ reduction peak was increased indicating that a high H_2 consumption is required for reduction to the metal phase.

The variation in the TPR profiles of FeNi/BEA, NiFe/BEA and Fe-Ni/BEA catalysts shows the combination of nickel and iron phases' reduction. The reduction of 'free nickel oxide" was observed at 400 - 500 ºC. On the other hand, the reductions of nickel and iron phase at 500 - 800 ºC region were overlapped into a broad peak, which suggests the stabilization of Fe^{3+} and Ni^{2+} ions in the lattice. The reduction process transforms Fe^{3+} to Fe^{2+}, $FeAl_2O_4$ and $NiAl_2O_4$.

However, the reduction peak of FeNi/BEA (500) as illustrated in Figure 4.12c slightly splits into two peaks between 500-800 ºC. The peaks represent the reduction of Fe^{3+} to Fe^{2+} as a discrete peak and the second one representing the reduction of $NiAl_2O_4$ followed by $FeAl_2O_4$. A possible reason for this is that non-homogeneous mixing of Fe and Ni species due to less metal dispersion as observed under FESEM analysis and hence Fe could not promote the reduction efficiently [84].

The reduction peak of free Fe_2O_3 can still be observed from TPR profile of FeNi/BEA calcined at 500 ºC. However, due to strong interaction of Fe and Ni at high temperature, the reduction peak of free Fe_2O_3 is significantly intensified and disappeared. This result is in agreement with FESEM analysis where the morphology of FeNi/BEA (500) catalyst shows a hexagonal structure of Fe_2O_3 located on the support. However, the peak gradually disappeared at 600 ºC and 700 ºC calcinations temperature. This type of oxide is easily reduced and its existence can cause several difficulties during reaction such as sintering and carbon deposition on the catalyst surface which will lead to catalyst deactivation [104]. Apart from

that, the reduction peak associated to the reduction of free nickel oxide NiO to Ni^0 shifted towards lower temperature as the calcination temperatures increases. While, the reduction peak represents the reduction of several phases were shifted to higher temperature in the following order FeNi/BEA (600) > FeNi/BEA (500) > FeNi/BEA (700). Less reduction were observed for reducing Ni and Fe phase in FeNi/BEA (700) bimetallic catalyst due to agglomeration of the active metal during the impregnation as confirmed by calculation of the crystallite size using Scherrer equation [77].

In the case of NiFe/BEA (Figure 4.12d), the reduction peak representing reduction of several phases is also divided into two peaks particularly after calcination at 700 ºC. This is because in NiFe/BEA (700) catalyst, the peak represent the reduction of Fe^{3+} to Fe^{2+} is shifted to lower temperature while the peak having strong interaction with support ($NiAl_2O_4$ and $FeAl_2O_4$) is shifted to higher temperature. This indicates that addition of Ni as a second metal in this catalyst results high reducibility of Fe_2O_3 phase where it able to reduce at low temperature and active for the reaction.

The existence of free Fe_2O_3 is noticeable with a small peak at 400 ºC from TPR profile of NiFe/BEA calcined at 500 ºC. However, the absence of free Fe_2O_3 is observed when NiFe/BEA was calcined from 600 to 700 ºC. Besides that, as the calcination temperatures increases, reduction of free NiO is maintained at the same temperature with different intensity. At higher calcination temperatures the reduction of NiFe/BEA decreases in the order: NiFe/BEA (500) > NiFe/BEA (600) > NiFe/BEA (700). In considering these trends, NiFe/BEA calcined at higher temperature is difficult to reduce, thus confirming the strong interaction of Ni and Fe in the BEA lattice.

The reduction activity of Fe-Ni/BEA catalysts is shown in Figure 4.12e. Significant reduction of Fe-Ni/BEA (700) was observed where the first reduction peak of NiO is shifted to higher temperature and combined towards second reduction peaks. These reduction peaks presumably represents the reduction of $NiFe_2O_4$ as discuss previously in XRD and FESEM analysis. Therefore, this indicates that the components of Fe and Ni in prepared catalyst are well uniformed [88] and are in

accordance with Wang *et al.* [95]. Free Fe_2O_3 also occur in the reduction of Fe-Ni/BEA (500) as observed in TPR profile of FeNi/BEA (500) and NiFE/BEA (500) catalysts. Apart from that, the reduction peaks of Fe-Ni/BEA shifted towards higher temperature as the calcination temperatures increase in the order: Fe-Ni/BEA (500) > Fe-Ni/BEA (600) > Fe-Ni/BEA (700).

Fig. 4.13 illustrates the interaction of nickel or iron metal with the support which attributed to appearance of "free" metal oxide or "fixed" metal oxide and integrated between metal and support [57].

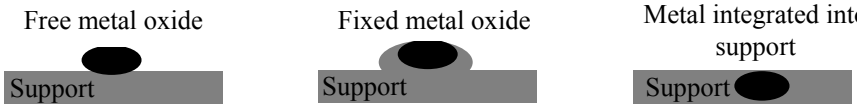

Figure 4.13 The interaction of nickel or iron metal with the support [57]

4.2 PKS Steam Gasification

The steam gasification of PKS was carried out at Dalian Institute of Chemical Physics utilizing the facilities available within Prof Hengyong Xu's research group. Due to limited access to the reactor system, the optimum temperature for the steam gasification of PKS was determined in the absence of a catalyst through screening process. The temperature at which the outlet gas composition consists of optimum concentrations of CO_2, CH_4 and H_2 was then chosen for the catalytic reaction.

4.2.1 Screening Process

The screening process was performed on PKS steam gasification at temperatures between 600-900 °C with biomass weight of 0.3 g, where the steam to biomass ratio was set at 4:1 (wt/wt) and steam to helium ratio of 1:6 (vol/vol). The gases (H_2, CH_4, CO_2 and H_2S) produced in the screening process were analyzed using two online gas chromatography; GC-14C equipped with a sulphur detector (FPD) fitted with Chromosil 310 column was used to analyze sulphur compound in the product gas and GC-14B equipped with thermal conductivity detector (TCD) fitted with Carbon

molecular sieve column was used to analyze CH_4, H_2 and CO_2 with helium as a carrier gas.

Generally, steam gasification of biomass produce H_2, CO, CO_2, CH_4 and higher hydrocarbons. In other circumstances, tar, char and sulphur gases, namely H_2S and SO_2 may also be present in the outlet gas [30]. Figure 4.14 depicts the profile of gases produced from the gasification of PKS in the absence of a catalyst at temperatures between 600-900 °C. The conversion of PKS is 100% to outlet gas with CO_2 as a predominant product.

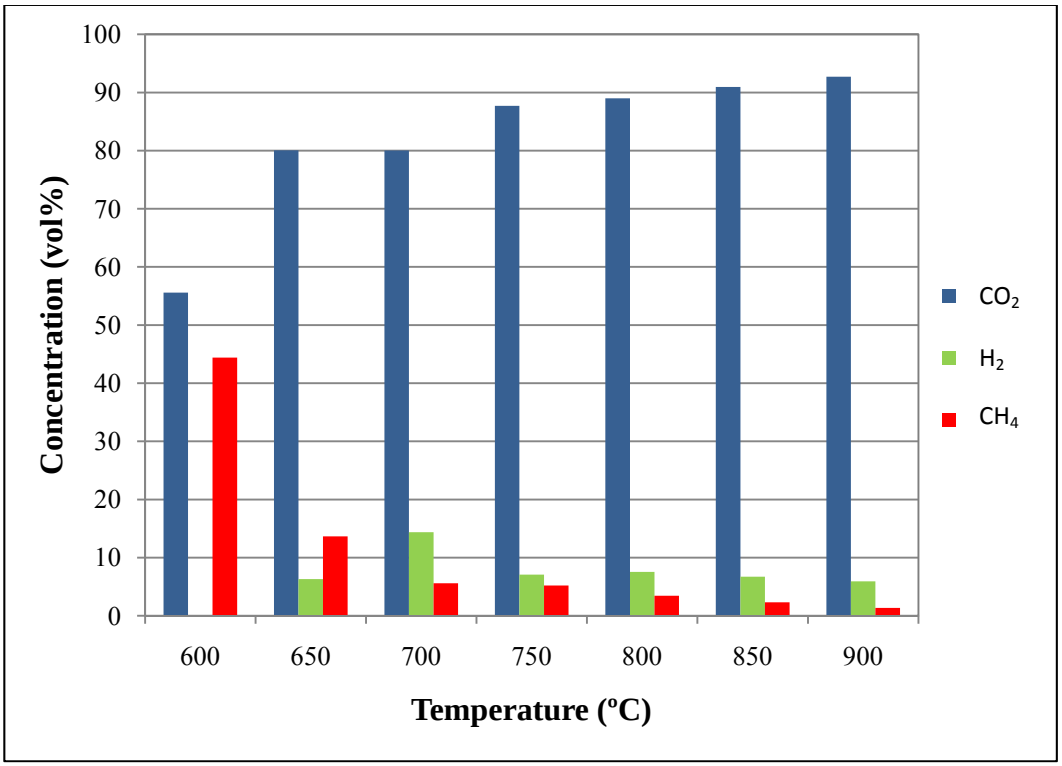

Figure 4.14 Profile of gases produced from steam gasification of PKS

At 600 ºC, only CO_2 and CH_4 were detected in the outlet gas. The concentration of H_2 at this temperature may be too low to be detected by GC. H_2 evolution was only observed starting from 650 ºC and it later reached a maximum at 700 ºC before the concentration gradually decreasing with increasing temperature. On the other hand, CH_4 concentration was the highest at 600 ºC followed by a sharp decrease at 650 ºC before gradually decreases at higher temperatures. This suggests that the CH_4 produced from steam gasification of PKS either undergoes non-catalytic steam

reforming or combustion at temperatures as low as 600 ºC, leaving only 1.36 vol% CH_4 at 900 ºC. According to Lv *et al.* [105], the concentration of CH_4 decreased with temperature due to a higher temperature strengthens the steam reforming reaction of CH_4. However, the concentration of CO_2 in outlet gas is observed to increase with increasing temperature, thus supports the suggestion that once formed, CH_4 subsequently undergoes combustion. Figure 4.14 also shows the optimum temperature for steam gasification of PKS under the experimental conditions used in this work is 700 ºC.

Asadullah *et al.* [13] have investigated the gasification of cedar wood at temperatures between 500-900 ºC in the absence of a catalyst. They observed that the carbon conversion of biomass is dependent on the operating temperature whereby both the carbon conversion and H_2 formation increase with increasing temperature. However, 700 ºC is the most favourable operating temperature when char and tar formation were considered. In addition, different types of biomass have different best operating temperature. The suitable temperature for the best performance gasification of coconut shell is 800 ºC [106] while baggase and rice straw is 650 ºC [107].

Based on the elemental analysis (Section 3.5.1), PKS contains about 0.48 wt% of sulphur which may lead to formation of hydrogen sulphide (H_2S), carbonyl sulphide (COS) and sulphur dioxide (SO_2) in the product [30]. Table 4.4 shows the concentration of H_2S detected from the PKS steam gasification in the absence of a catalyst.

Table 4.4 H_2S concentration in non-catalytic PKS steam gasification

Temp (^oC)	Concentration (ppm)
600	-
650	-
700	-
750	-
800	1.6
850	4.43
900	5.42

Formation of H_2S was detected starting from 800 °C and the concentration increases as the temperature was increased to 900 °C. The presence of H_2S could have come from ash generated after the gasification.

Tomishige *et al.* [107] have reported that the sulphur content in biomass affects the performance of gasification of biomass. The sulphur content from the gasification of cedar wood, jute, bagasse and rice straw at temperatures between 550 – 650 ºC are in the following order; cedar wood (0.02 S%) > jute (0.05 S%) > bagasse (0.05 S%) > rice straw (0.06 S%).

4.2.2 Catalytic Steam Gasification

From the screening process above, the optimum temperature for the steam gasification of PKS is determined to be at 700 ºC. Therefore, the BEA supported Fe and Ni catalysts were then tested in steam gasification of PKS at 700 °C with a catalyst weight of 0.3 g and biomass weight of 0.9 g using steam to biomass ratio of 4:1 (wt/wt) while steam to argon (Ar) ratio was 1:6 (vol/vol). However, the gases (H_2, CH_4, CO_2 and CO) produced from the catalytic steam gasification were analyzed using an online gas chromatograph (VARIAN CP-3800) equipped with thermal conductivity detector (TCD), fitted with TDX-01 column utilizing Ar as a carrier gas. The new analytical system enables a more efficient detection of H_2 due to better sensitivity in analysis. To make sure that the results for catalytic steam gasification is comparable to those of non-catalytic, the PKS was tested again in a non-catalytic steam gasification using the new reactor system. Hence, the result for non-catalytic steam gasification of PKS reported in this section will be somewhat different from those reported in section 4.2.1.

4.2.2.1 Monometallic Catalysts

Catalytic performance of the BEA supported monometallic catalysts in the steam gasification of PKS is demonstrated in Figure 4.15. The results can be understood through evaluation of the effect of catalyst on gas composition.

There are variations in the trend in the outlet gases compositions. The conversion of PKS observed in the steam gasification reaction at 700 ºC is 100% to outlet gas. Non-catalytic PKS steam gasification leads to evolvement of (vol%) 62.64% H_2, 30.41% CO_2, 5.24% CO and 1.71% CH_4. When bare BEA was used, the concentrations of H_2, CO and CH_4 in the outlet gas increase slightly to 68.25%, 6.41% and 2.17%, respectively while the concentration of CO_2 decreases slightly to 23.17%. Substantial reactions can take place on BEA active sites due to its high surface area (529 m^2 g^{-1}) and high pore volume (0.15 cm^3 g^{-1}). These results show that BEA has the potential to be the catalyst as well as the catalyst support for biomass gasification.

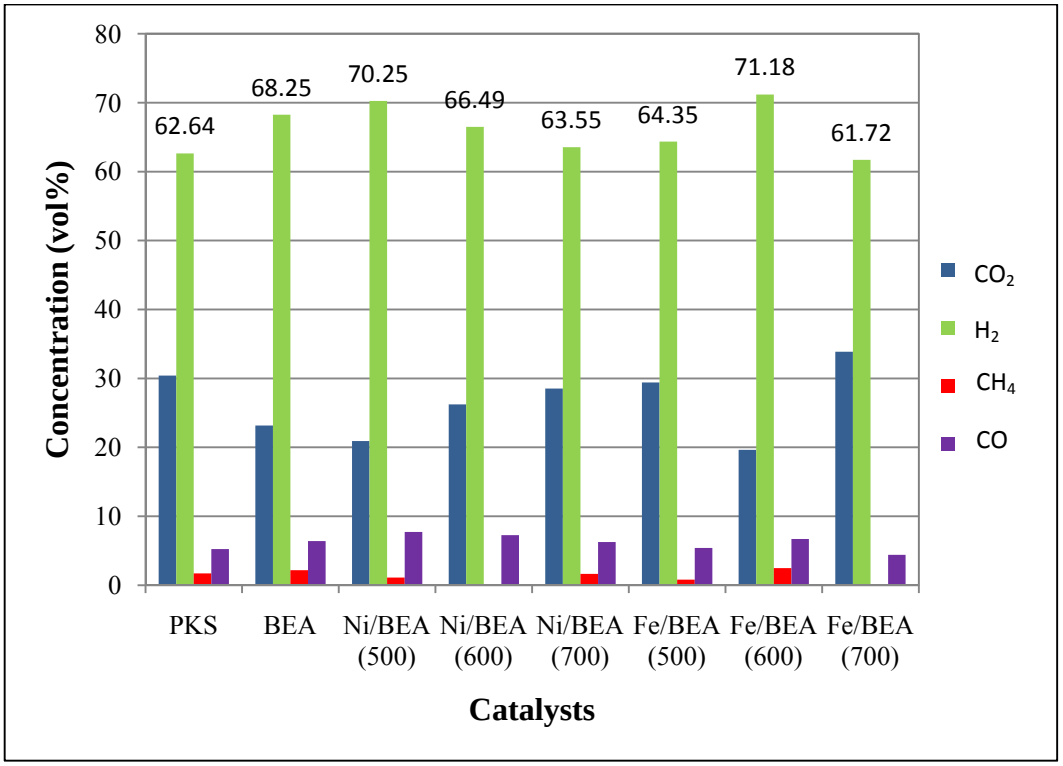

Figure 4.15 Profile of gases produced in the presence of Ni/BEA and Fe/BEA catalysts.

Calcination temperature has an effect on the performance of Ni/BEA and Fe/BEA catalysts in producing H_2. In the case of Ni/BEA catalyst, the highest H_2 concentration was observed from the steam gasification of PKS in the presence of Ni/BEA (500). As the calcination temperature increases, the H_2 and CO gas evolved

from steam gasification reaction gradually decreased which is in contrast to the concentration of CO_2 detected. On the other hand, CH_4 was not detected in the product gas when Ni/BEA (600) was used as catalyst while a small concentration (<2.0%) was detected in the presence of Ni/BEA (500) and Ni/BEA (700). In the presence of Ni/BEA (500), CH_4 may have reacted with steam during methane steam reforming to produce CO and H_2 as the concentration of these gases are increases. However, in the presence of Ni/BEA (600) as catalyst, CH_4 produced may have subsequently undergone steam reforming to produce CO and H_2 [105] or may have been oxidised to produce CO_2 and H_2O [108]. The latter may be the more appropriate reason as the concentration of CO_2 evolved increases while CO and H_2 evolved decrease when Ni/BEA (600) was used as catalyst.

The effectiveness of Ni/BEA (700) catalyst to produce H_2 from the steam gasification is reduced as compared to Ni/BEA (600) when more PKS undergo combustion to form CO_2 as can be observed with further increase in CO_2 concentration and further reduction of H_2 evolved. Lv *et al.* [105] have suggested that higher content of CO_2 caused by catalytic activity of nickel catalysts can be solved by controlling operation conditions and modifying the nickel catalyst to lower its selectivity on the water gas shift reaction, thus promoting more H_2 formation.

The Ni/BEA (500) catalyst has demonstrated its ability to produce higher concentration of H_2 as compared to other Ni/BEA catalysts. These may be attributed to the catalyst properties where Ni/BEA (500) catalyst has high reducibility and surface area. As previously discussed in H_2-TPR (Section 4.1.4), when low calcination temperatures were used, the reduction peaks are also shifted to the lower temperature. Therefore, the reduction of NiO and $NiAl_2O_4$ phases in Ni/BEA (500) are reducible to its free oxide at much lower temperature and then actively reacted with PKS to produce more H_2 gas. This observation is also in agreement with Chaipraset and Vitidsant [32] as well as Webb and Orr [83] theories whereby the catalyst with high surface area can provide large contact area for reactants and consequently enhance the reaction activity

In the case of Fe/BEA catalyst, the concentration of H_2 gas evolved from the steam gasification of PKS increases when the calcination temperature was increased

from 500 to 600 ºC but further increase in calcination temperature to 700 ºC resulted in a decrease in H2 concentration. The concentration of CO evolved follows the same trend as H_2 evolved with Fe/BEA (600) gives the maximum CO evolved in the presence of Fe/BEA catalyst. Concentration of CH_4 detected also increases when the calcination temperature of Fe/BEA catalyst was increased from 500 to 600 ºC. However, CH_4 was not detected when the calcination temperature was increased to 700 ºC. This indicates that Fe/BEA (600) promotes formation of CH_4 and methane steams reforming as the concentration of CH_4, H_2 and CO evolved were increased. Water gas shift reaction may not favourable in this process due to low transformation rate of CO. [105].

Concentration of CO_2 on the other hand decreases as the calcination temperature of Fe/BEA was increased from 500 to 600 ºC and increases again as the calcination temperature was further increased to 700 ºC. These may be attributed to lesser efficiency of Fe/BEA (700) to promote steam gasification of PKS to H_2, hence resulted in PKS undergoing combustion to produce more CO_2 or oxidation of CO to CO_2.

Further reduction of Fe_2O_3 to metallic Fe may be one of the factors contributed to poor conversion of biomass to H_2 gas [109]. Insufficient presence of steam content during the reaction will lead to over reduction of Fe_2O_3 into metallic Fe. As a result, metallic Fe facilitates the oxidation of CO to produce more CO_2 rather than undergo steam reforming as shown in Eq. 4.1 - 4.2 [108]. On the other hand, Eq. 4.3- 4.5 represents the combustion reaction which may also happen during the gasification of PKS, thus resulting in higher production of CO_2 [1].

$$CH_4 + H_2O \leftrightarrow CO + 3H_2 \quad \text{[Eq. 4.1]}$$

$$2CO \leftrightarrow CO_2 + C \quad \text{[Eq. 4.2]}$$

$$C + \frac{1}{2}O_2 \rightarrow CO \quad \text{[Eq. 4.3]}$$

$$CO + \frac{1}{2}O_2 \rightarrow CO_2 \quad \text{[Eq. 4.4]}$$

$$H_2 + \frac{1}{2}O_2 \rightarrow H_2O \quad \text{[Eq. 4.5]}$$

Fe/BEA (600) has larger pore diameter resulting in higher activity in H_2 production. Larger pore diameter of Fe/BEA (600) benefits for larger molecule reaction [87], thus allows the PKS to penetrate the active sites of the catalyst and promote the reaction. Furthermore, Fe/BEA (600) has lower crystallite size, 64.75 nm as compared to Fe/BEA (500) and Fe/BEA (700). The strong interaction between Fe and support stabilizes the small iron oxides crystallites from sintering during the high temperature calcination process [100]. Besides, presence of 'free iron oxide' at lower reduction temperature between 350 - 480 ºC (Figure 4.12b) in Fe/BEA (500) is possibly the reason for low catalytic activity of the catalyst. This is because existence of 'free iron oxide' may cause sintering and carbon deposition on the Fe/BEA (500) catalyst surface which leads to catalyst deactivation [31, 57 and 104].

4.2.2.2 Bimetallic Catalysts

From Figure 4.15, it can be seen that the concentration of H_2 evolved from the steam gasification of PKS under the experimental conditions used in this research is determined by the active metal and also the temperature used during calcination of the catalyst. Both Ni and Fe are found to be active in the production of H_2 from the steam gasification of PKS with Ni/BEA (500) as the best Ni catalyst and Fe/BEA (600) as the best Fe catalysts. It would be interesting to see the effect of adding a second metal to the BEA supported monometallic catalysts.

Figure 4.16(a) - (c) shows the concentration of gases evolved from the steam gasification of PKS in the presence of BEA supported bimetallic catalysts. The results on monometallic Fe and Ni catalysts are reported again for comparison. Addition of Fe to the Ni/BEA (500) to form FeNi/BEA (500) resulted in slight decrease in H_2 and CO evolved, which in turn increases the concentration of CO_2 while there is no significant change in the of CH_4, evolved (Figure 4.16a). This indicates that FeNi/BEA (500) is slightly less reactive in steam gasification, thus promoting combustion of PKS to CO_2. This could be due to the presence of both fixed nickel oxide ($NiAl_2O_4$) and fixed iron oxide ($FeAl_2O_4$) as seen in Figure 4.12(c) which suppresses the reduction of Fe_2O_3 and NiO with different state of interaction with BEA. Furthermore, existence of 'free iron oxide' at lower reduction

temperature between 380 - 400 ºC in the catalyst is possibly also the reason in low catalytic of FeNi/BEA (500) catalyst. This is because it promotes the carbon formation as well as loss of active phase during the reaction [31, 57 and 104].

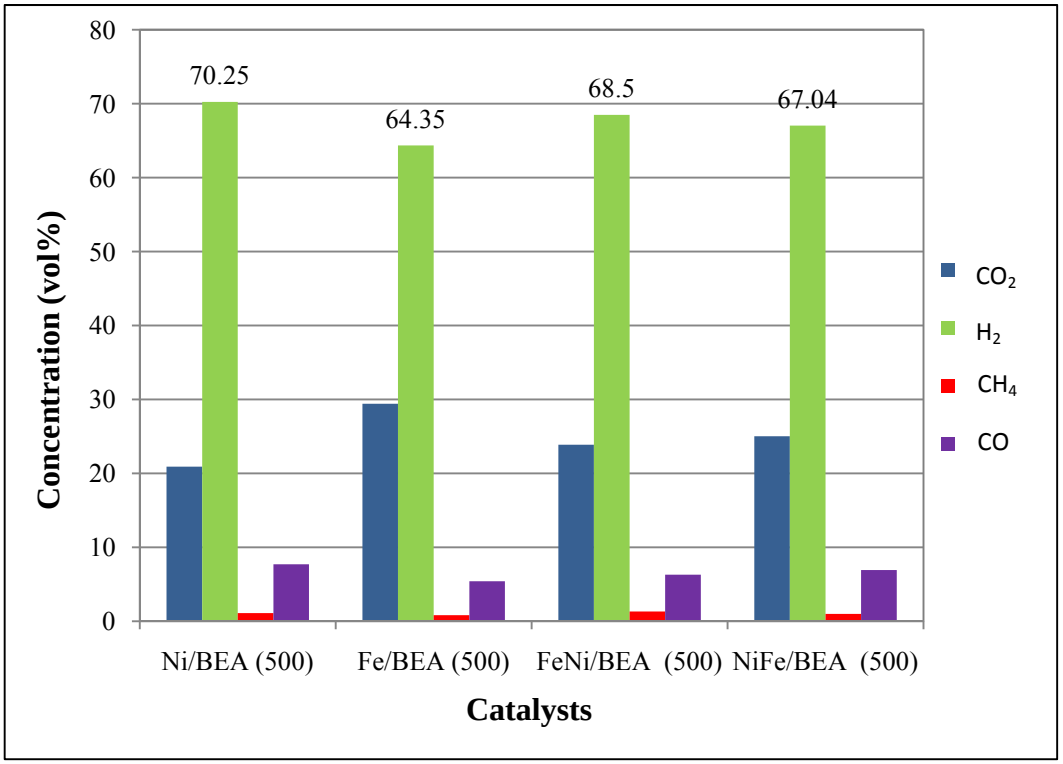

(a)

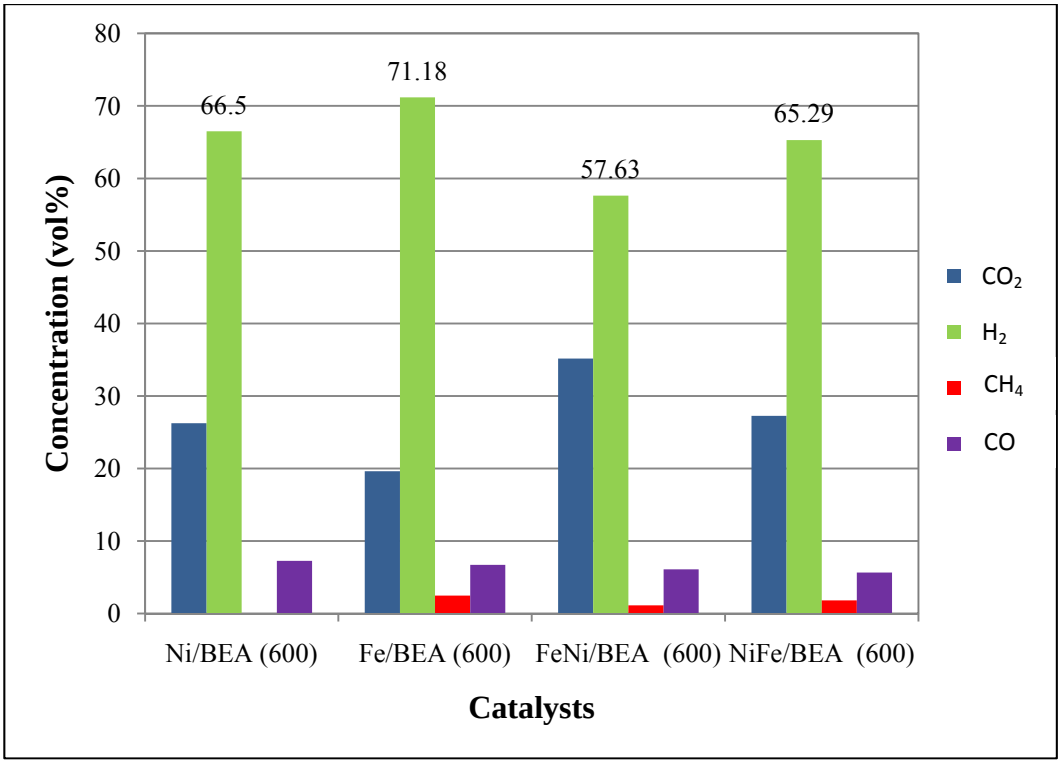

(b)

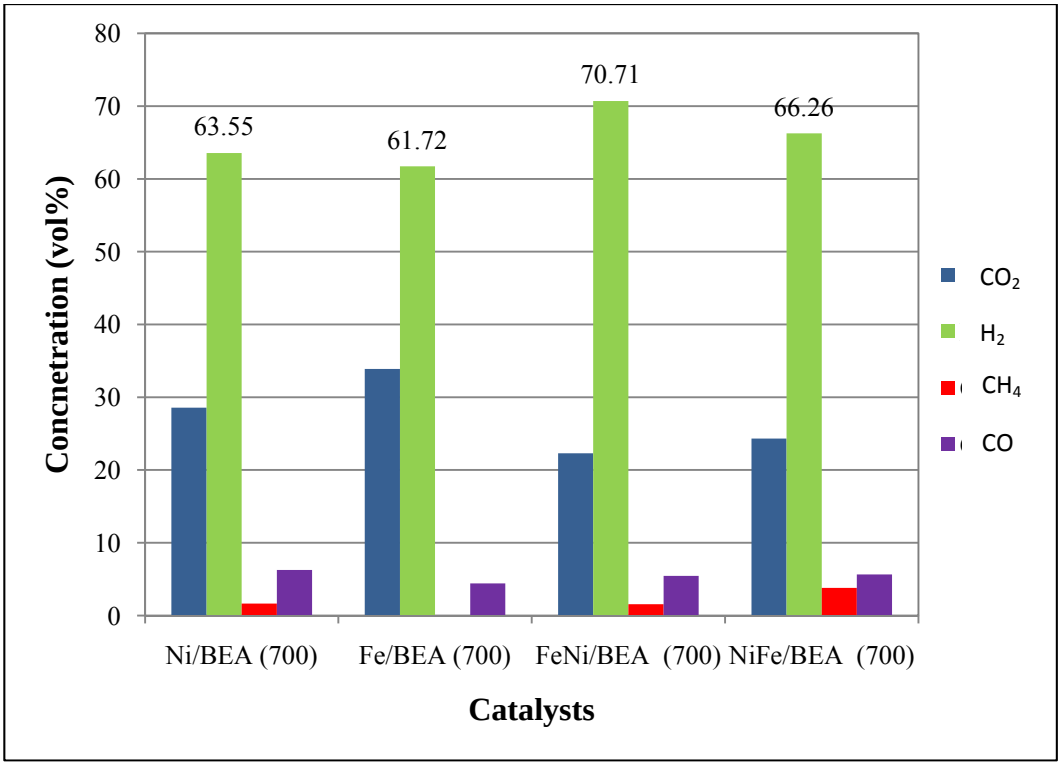

(c)

Figure 4.16 Profile of gases produced from steam gasification of PKS in the presence of BEA supported catalysts calcined at (a) 500 ºC (b) 600 ºC and (c) 700 ºC

Addition of Ni to Fe/BEA (500) to form NiFe/BEA (500), enhanced the steam methane reforming. This is due to addition of Ni as the second metal which leads to an improvement in the concentration of H_2 produced and reduction of CO_2 concentration in the product gas although there is slight increase in CO concentration. Based on Eq. 4.1, CH_4 and H_2O react in a 1:1 molar ratio on a catalyst active metal site to form a 1:3 molar ratio of CO and H_2 during the steam methane reforming [1, 11 and 22].

$$CH_4 + H_2O \leftrightarrow CO + 3H_2 \qquad \text{[Eq. 4.1]}$$

High performance of this catalyst may be attributed to bigger reduction peak at 500-700 ºC in H_2-TPR profile as compared to Fe/BEA (500) whereby this peak is attributed to reduction of Fe_2O_3. Bigger reduction peak means more H_2 consumption which means more Fe_2O_3 available within the catalyst system thus, the catalyst becomes more active for steam gasification due to availability of more active sites for the reaction to take place [95].

Addition of Fe to Ni/BEA (600) to form FeNi/BEA (600) follows the same trend as the catalysts calcined at 500 ºC whereby it becomes no longer effective to promote steam gasification of PKS to produce H_2. Instead, the FeNi/BEA (600) promotes the oxidation of CO or combustion of PKS which is shown by an increase in CO_2 concentration [108]. FeNi/BEA (600) also promotes the formation of CH_4, presumable via reduction of CO as CH_4 concentration slightly increases while CO concentration slightly decreases. This may be due to insufficient presence of steam content during the reaction which resulted in reduction of CO with H_2 to produce CH_4 promoted by the presence of metallic Fe from over reduction of Fe_2O_3 [11, 108]. Indeed, Chaiprasert and Vitidsant [106] have studied the effect of steam during the gasification of biomass and found that increasing of steam feed resulted in higher H_2 formation, decrease in CO_2 and slight decrease in CH_4 because of water gas shift reaction and methane reforming.

Furthermore, addition of Ni to Fe/BEA (600) to from NiFe/BEA (600) resulted in reduction of H_2, CO, and CH_4, evolved. This trend is similar to FeNi/BEA (600) whereby the concentration of CO_2 increases indicating that NiFe/BEA (600) is less

reactive in steam gasification, thus promoting PKS to undergo oxidation of CO to produce more CO_2 [108]. It is probably that the presence of Cl as an impurity in NiFe/BEA (600) results in catalyst deactivation in the steam gasification process. According to McMinn *et al.* [110], chlorine poisons the water gas shift reaction by limiting the amount of OH groups on the support surface, thus lower the reaction activity.

Addition Fe to Ni/BEA (700) to form FeNi/BEA (700) in contrast, exhibited higher concentration of H_2. A slight decrease in CO concentration indicates that FeNi/BEA (700) promotes the water gas shift reaction even though slight decrease in concentration of CO_2 was observed. However, there is no significant difference in the concentration of CH_4 evolved. As shown in Eq. 4.7, CO and H_2O react in a 1:1 molar ratio in the water gas shift reaction to form CO_2 and H_2 [1, 11, 22 and 53].

$$CO + H_2O \leftrightarrow CO_2 + H_2 \qquad \text{[Eq. 4.7]}$$

As stated in the H_2-TPR analysis (section 4.1.4), the addition of Fe as the second metal and calcined at high temperature significantly improves the reducibility of NiO phase by reducing at low temperature. As a result, more active metals react with PKS to produce H_2 gas and facilitate the water gas shift reaction. Therefore, this indicates that FeNi/BEA (700) is active in steam gasification reaction; hence it is able to retard the PKS from undergoing combustion. The results are consistent with the work reported by Chaipraset and Vitidsant [32] whereby the presence of Fe as the second metal enhances the water gas shift reaction and amplified the H_2 production.

Addition of Ni to Fe/BEA (700) to form NiFe/BEA (700) also results in an increase in concentration of H_2 and reduction of CO_2 in the product gas. Incorporation of Ni as the second metal in this catalyst facilitate the reduction of Fe^{3+} to Fe^{2+} and enhance the steam methane reforming as reported in NiFe/BEA (500) whereby both H_2 and CO concentration increased. However, high concentration of CH_4 was observed may be due to NiFe/BEA (700) also promotes the formation of CH_4 through methanation. This possibly attributed to majority of Ni metals on the surface of the catalyst whereby Ni is the first component to be reduced

at 450 ºC as reported in H_2-TPR (section 4.1.4). Hence, this favours the methane steam reforming and methanation reaction on Ni surface [31] as opposed to water gas shift reaction on Fe surfaces [32].

The variations in the trends indicate that the concentration of H_2 gas for FeNi/BEA decrease in the order of calcination temperature: FeNi/BEA (700) > FeNi/BEA (500) > FeNi/BEA (600). This is because doping of Fe into Ni/BEA at different calcination temperatures resulted in higher surface area for FeNi/BEA (700) followed by FeNi/BEA (500) and FeNi/BEA (600) as observed in section 4.1.1.

The order of the H_2 formation for NiFe/BEA catalysts is NiFe/BEA (500) > NiFe/BEA (700) > NiFe/BEA (600), whereby the catalytic activity decreases with the increasing of calcination temperatures. This behaviour is expected since NiFe/BEA (500) shows higher reducibility as compared to NiFe/BEA (600) and NiFe/BEA (700). This can be explained by integration of Ni and Fe in the BEA structure as observed in TPR analysis (Section 4.1.4). It is notable that the BET surface area of NiFe/BEA catalysts is in order NiFe/BEA (600) > NiFe/BEA (500) > NiFe/BEA (700). Even though calcination at 600 ºC leads to a bigger surface area, NiFe/BEA (500) still shows a higher catalytic activity due to its reducibility at lower temperature. Hence, the second metal plays an important role and may act as a promoter to amplify the steam gasification reaction.

4.2.2.3 Effect of Preparation Method for Bimetallic Catalysts

The results so far show that there are distinct differences between FeNi/BEA and NiFe/BEA catalysts. It is suggested that the relative activities of the prepared catalysts is contributed by the catalyst preparation method since these catalysts were prepared via sequential impregnation method with different sequence of impregnating the Fe and Ni into the BEA support. The different concentrations of gas evolved from the steam gasification of PKS in the presence of these catalysts are attributed to the difference in the physicochemical properties of the catalysts. Therefore, it is of interest to study whether the catalytic activity of the bimetallic

catalysts will be different between those prepared via sequential impregnation and co-impregnation at different calcination temperatures.

Figure 4.17 (a) shows the product gas evolved from the steam gasification of PKS in the presence of FeNi/BEA (500), NiFe/BEA (500) and Fe-Ni/BEA (500) as catalysts. It can be seen that the methods used to prepare these catalysts whether via sequential impregnation method (FeNi/BEA (500) and NiFe/BEA (500)) or co-impregnation method (Fe-Ni/BEA (500)) do not have a significant effect on the distribution of product gas evolved from the reaction. These may be attributed to similar physicochemical properties possess by these catalysts as observed in XRD, FESEM and TPR analysis. However, preparation methods do have a significant effect on the concentrations of gases evolved from the steam gasification of PKS in the presence of bimetallic catalysts calcined at 600 and 700 ^{o}C.

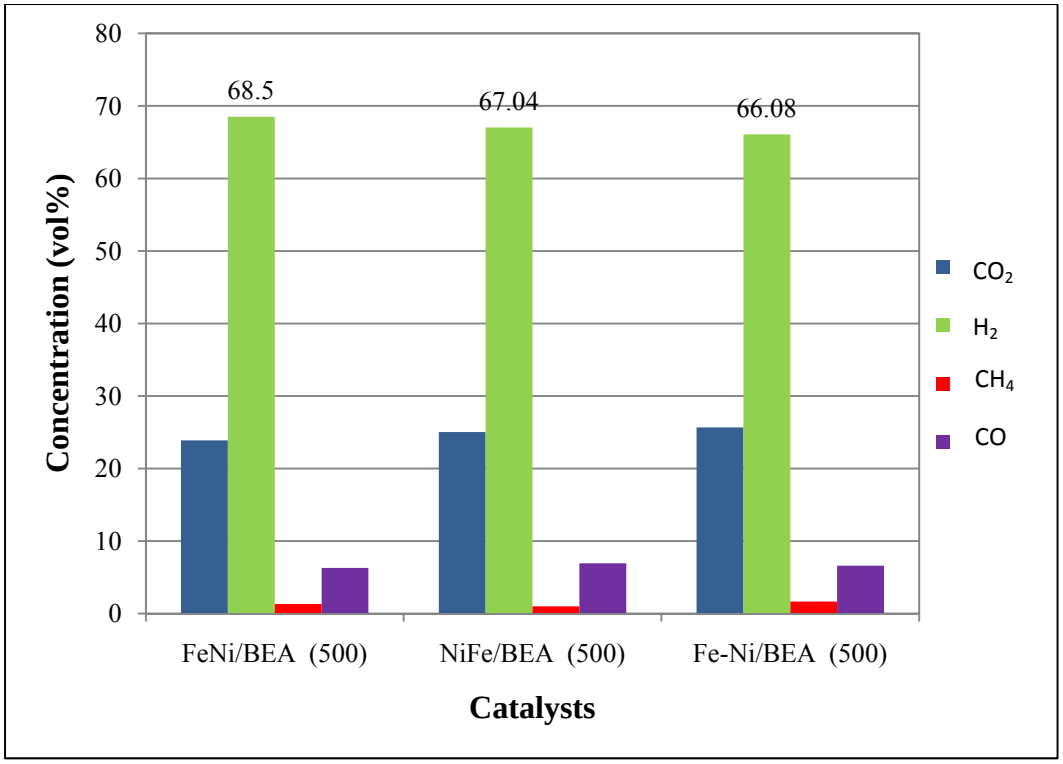

(a)

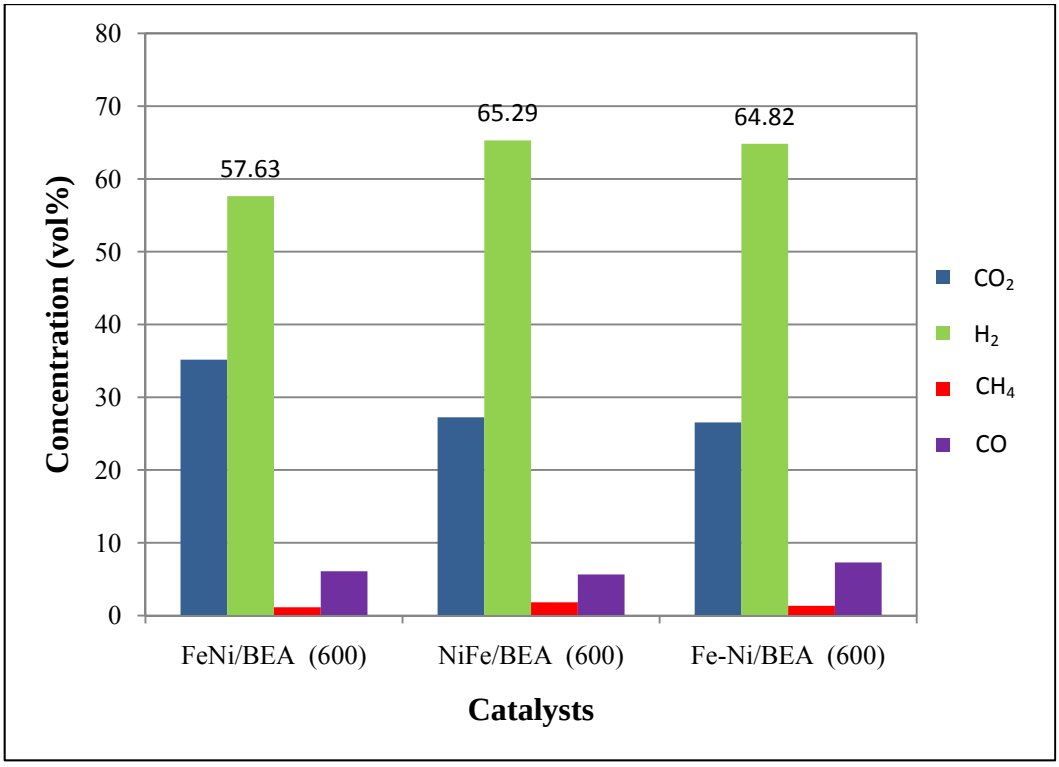

(b)

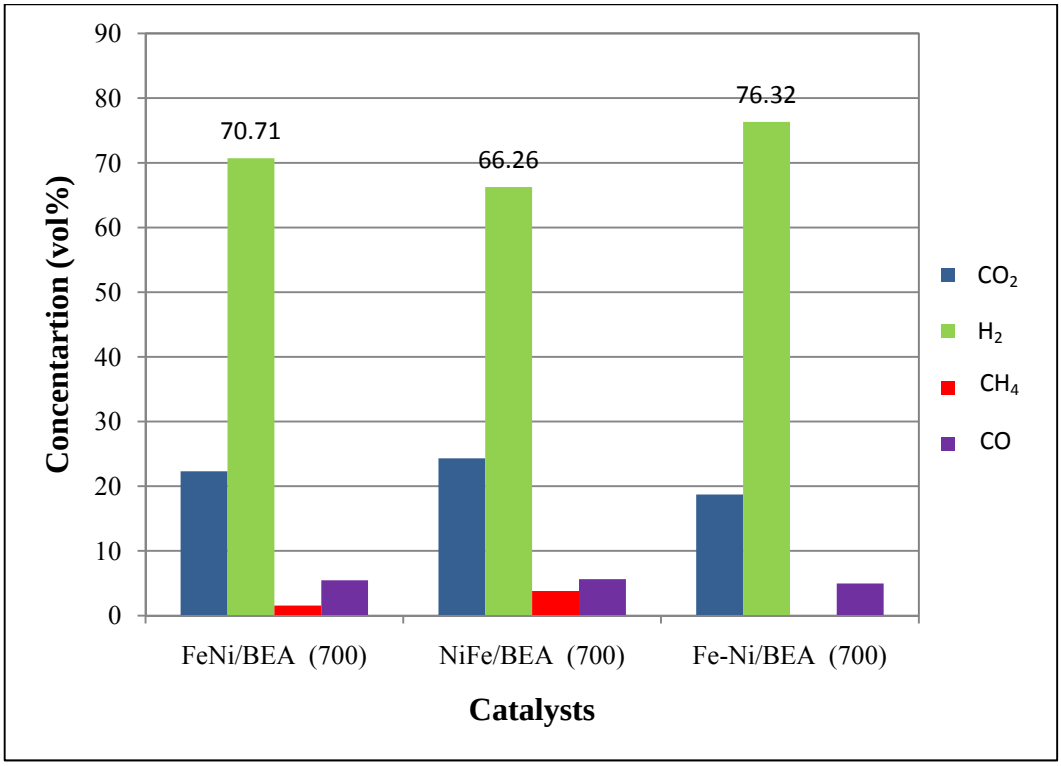

(c)

Figure 4.17 Effect of preparation method on the gaseous evolved from the steam gasification of PKS in the presence of bimetallic catalysts

FeNi/BEA (600) gives the lowest concentration of H_2 with the highest concentration of CO_2 while Fe-Ni/BEA (600) shows higher concentration of H_2 where the concentration is similar to those evolved when NiFe/BEA (600) was used as catalyst. However, the concentration of gaseous product are still lowered as compared to other bimetallic catalysts which promote PKS to undergo oxidation of CO to produce more CO_2 than H_2 [108]. These are presumably due to further reduction of Fe_2O_3 to metallic Fe which resulted in poor conversion of PKS to H_2 [108-109].

For catalysts calcined at 700 ^oC, Fe-Ni/BEA (700) shows the highest H_2 evolved as compared to FeNi/BEA (700), NiFe/BEA (700). This may be attributed to the presence of trevorite ($NiFe_2O_4$) phase within the catalyst system which facilitates the simultaneous reforming of methane formed on the surface of the catalyst, as observed by the absence of CH_4 evolved. High crystallization of $NiFe_2O_4$ increases the coverage of oxygen atoms during the reforming of methane where oxygen atoms on Fe species supplied to the Ni species to promote the reaction between carbonaceous on $NiFe_2O_4$ [95, 109-110]. Therefore, $NiFe_2O_4$ improved the catalyst to convert CH_4 into considerable amount of CO and H_2. The lower concentrations of CO_2 evolved also suggest that the $NiFe_2O_4$ phase may have promoted the water gas shift reaction to occur on the surface of catalyst and inhibited the PKS from undergoing combustion process. Therefore, these results are in accordance with Miki *et al*. [94] where the formation of mixed oxide between Fe and Ni are necessary for the formation of active sites

Unique textural characteristics of Fe-Ni/BEA (700) may have contributed to the highest H_2 production whereby Fe-Ni/BEA (700) has the highest pore volume (0.993 cm^3g^{-1}), largest pore diameter (10.43 nm), largest crystallite size and the crystal structure emerged as a trevorite ($NiFe_2O_4$). In addition, higher in pore volume allows maximum volume of PKS and gas molecules penetrating at highest pressure applied [80]. Larger pore diameter benefits for larger molecule reaction [87] while larger crystallite size provides a bigger active surface and thus, allows the PKS to penetrate the active sites of the catalyst and promote the reaction. The behaviour of the Fe-Ni/BEA (700) may also be related to a bigger reduction peak at 400-800 ºC in H_2-

TPR profile as compared to other catalysts whereby this peak is attributed to reduction of $NiFe_2O_4$. Bigger reduction peak means high H_2 consumption where it has more $NiFe_2O_4$ available within the catalyst system. Hence, the catalyst becomes more active for steam gasification due to availability of more active sites for the reaction to take place [95].

As discussed previously in section 4.2.2.2, different sequence of Fe and Ni as the second metal in bimetallic catalyst are active for the steam gasification of PKS when the precursors were calcined at a suitable calcination temperature. This is because incorporation of Fe as the second metal in the bimetallic catalyst and calcined at 700 ºC increases the reducibility of NiO phase and enhances the water gas shift reaction. While addition of Ni as the second metal facilitates the reduction of Fe_2O_3 phase and exhibits steam methane reforming. However, co-impregnation method and calcination at high temperature caused the stabilization of Fe^{3+} and Ni^{2+} ions in the BEA lattice results the reducibility for both Fe and Ni phase were increased by the formation of $NiFe_2O_4$. Fe-Ni/BEA (700) is able to combine the advantage of both Fe and Ni in the catalyst which facilitates the subsequent steam reforming of hydrocarbon fractions and water gas shift reaction.

The reason for this phenomenon is presumably due to different approach used to impregnate the metals with support which has give a significant effect to the structure of the catalysts. As observed from FESEM analysis (Section 4.1.3), a majority of the second metals in sequential impregnation bimetallic catalysts were observed on the catalyst surface rather than in the catalyst lattice due to competition during impregnation with the first metal. However, in co-impregnation bimetallic catalyst, both Fe and Ni metals interacted with each other upon integration into the BEA lattice and promote formation of mixed metal oxide which is necessary for the reaction.

The results also show similar trends to those observed by Chaiprasert and Vitidsant [32] and Tomishige *et al.* [58], where co-impregnated bimetallic catalyst has strong interaction between metals and support which, results the catalyst has better physicochemical properties of the catalyst and provides high catalyst activity in the gasification process.

It should be highlighted that among the catalysts developed in this work, the Fe-Ni/BEA (700) gives the highest composition of H_2 gas evolved with 76.32 vol% H_2, 18.72 vol% CO_2, 4.96 vol% CO and 0 vol% CH_4. These are comparable to the outlet gas composition from methane steam reforming reaction reported by Harrison [111] with 76 vol% H_2, 17 vol% CO_2, 3 vol% CO and 4 vol% CH_4. Therefore, the gas produced by the steam gasification of PKS in the presence of Fe-Ni/BEA (700) as a catalyst has a potential to replace commercial methane reforming for H_2 production.

CHAPTER FIVE

CONCLUSION AND RECOMMENDATIONS

5.1 Conclusion

Zeolite Beta (BEA) supported catalysts have been successfully developed through incipient wetness impregnation method. Catalyst preparation parameter in terms of monometallic, bimetallic, impregnation method and calcination temperatures significantly affect the textural properties, crystallite size, morphology and reducibility of metal present on the catalyst surface as well as the catalysts performance in the steam gasification of PKS.

BET analysis shows that co-impregnated catalysts posses lower surface area, higher pore volume and larger pore diameter as compared to other prepared catalysts. A presence of NiO and α-Fe_2O_3 phases in the monometallic and bimetallic catalysts affect the diffraction peak of BEA which indicate that the interaction between Fe and Ni with Al_2O_3 or SiO_2 in BEA. Calcination temperature and impregnation method also contribute to the crystallization of the prepared catalysts where high crystallization of Fe and Ni was observed in Fe-Ni/BEA (700) catalyst with the formation of NiO and $NiFe_2O_4$ phase. Furthermore, reduction of bimetallic catalysts shows the combination reduction of Fe and Ni monometallic phase where the reduction attributed to reduction of NiO and Fe_2O_3 which has weak interaction with support and followed by those with strong interaction with support.

From the screening process, the optimum temperature for steam gasification of PKS is 700 ºC. This is due to maximum of H_2 evolvement was achieved at 700 ºC with no H_2S detected. Moreover, the differences in the physicochemical properties of the catalysts affect the catalytic performance during the steam gasification of PKS whereby it exhibits the PKS to undergo either more steam reforming for higher H_2

evolution or it facilitates the oxidation of CO to produce more CO_2. In terms of monometallic, the highest H_2 concentration was observed from the steam gasification of PKS in the presence of Ni/BEA (500) and Fe/BEA (600) catalysts. This is because Ni/BEA (500) catalyst has high reducibility and surface area while Fe/BEA (600) has larger pore diameter. Nevertheless, both Ni/BEA and Fe/BEA catalysts promote PKS to undergo combustion to form CO_2 as the calcination temperature was increased to 700 ºC.

Different sequence of Fe and Ni as the second metal in bimetallic catalysts are active for the steam gasification of PKS when the precursors were calcined at a suitable calcination temperature. This is because incorporation of Fe as the second metal in the bimetallic catalyst and calcined at 700 ºC enhances the water gas shift reaction while addition of Ni as the second metal exhibits steam methane reforming. However, co-impregnation method and calcination at high temperature caused the stabilization of Fe^{3+} and Ni^{2+} ions in the BEA lattice enabled Fe-Ni/BEA (700) to combine the advantage of both Fe and Ni in the catalyst which facilitates the subsequent steam methane reforming and water gas shift reaction.

Among the prepared catalysts, Fe-Ni/BEA (700) is the best catalyst as it shows the highest composition of H_2 gas evolved with 76.32 vol% H_2, 18.72 vol% CO_2, 4.96 vol% CO and the absence of CH_4. The performance of this catalyst may be attributed to the presence of $NiFe_2O_4$ phase within the catalyst system which facilitates the subsequent steam reforming of hydrocarbon fractions and water gas shift reaction. High crystallization of $NiFe_2O_4$ increases the coverage of oxygen atoms during the reaction where formation of $NiFe_2O_4$ promotes Fe_2O_3 as an oxygen carrier for NiO. The outlet gas composition shows that the steam gasification of PKS in the presence of Fe-Ni/BEA (700) has a potential to replace the commercial methane reforming for H_2 production

Therefore, it can be concluded that various parameters in catalyst preparation resulted in deviation in the catalyst properties and interaction between the active metals with support as well as the catalytic activity.

5.2 Recommendations

H_2 was successfully produced from steam gasification of PKS in the presence of BEA supported Fe and Ni catalysts. Through the evaluation of the catalytic activity on gas composition, it was indicated that zeolite beta (BEA) supported bimetallic Fe-Ni catalyst prepared by co-impregnation method and calcined at 700° C is the best catalyst, which gives the highest production of H_2.

The catalytic gasification process is an attractive technological alternative to deal with tar and to produce a high yield of H_2. However, due to equipment constrain, some parameters of the catalytic activity in the steam gasification of PKS could not be investigated. Therefore, it will be more significant if this study can be extended by studying the efficiency of the prepared catalysts for tar removal and investigate the effect of operating condition such as catalyst/biomass ratio, steam/biomass ratio on the composition of gas produced from the steam gasification of PKS. Types of reactor are also one of the factors contributing to the activity of the catalysts. Therefore, the prepared catalysts can also be tested using fluidised-bed instead of fixed-bed reactor. This is because fluidised-bed steam gasification could maximise the yield of H_2 in gaseous product. Fluidised-bed can promote the heat transfer and make the reactor temperature homogeneous as well as being efficient for tar and char reduction.

Moreover, it is also suggested to evaluate the resistance of the catalyst to carbon deposition which can affect the catalyst lifetime due to deactivation. Indeed, reusing or regenerating of catalyst could make the process economical thus, reduce the cost of production. In terms of catalyst preparation, it is proposed to use different metal salts such as nitrate in order to compare the textural properties of the prepared catalysts. Defining suitable Ni/Fe ratio in the crystalline structure for a better and prolonged catalytic activity is also recommended. Instead of BET, XRD, FESEM-EDX and TPR characterization, it is also crucial to conduct Temperature-Programmed Desorption Ammonia (TPD-NH_3) for characterizing the quantity and strength of the acid sites on oxide surfaces of a catalyst. Acidity measurement provides the information about the cracking capability of the catalysts.

Hence, with sufficient information, findings and recommendations from this study can be used as a future reference for the catalyst development especially regarding biomass gasification application in order to produce high yield of hydrogen gas.

REFERENCES

[1] M. A. A. Mohammed, A. Salmiaton, W. A. K. G. Wan Azlina, M. S. Mohammad Amran, A. Fakhrul-Razi and Y. H. Taufiq-Yap, "Hydrogen rich gas from oil palm biomass as a potential source of renewable energy in Malaysia," *Renewable Sustainable Energy Rev.*, vol. 15, pp. 1258-1270, 2011.

[2] A. Midilli and I. Dincer, "Hydrogen as a renewable and sustainable solution in reducing global fossil fuel consumption," *Int. J. Hydrogen Energy*, vol. 33, pp. 4209-4222, 2008.

[3] R. A. Begum, R. D. Z. R. Z. Abidin and J. J. Pereira, "initiatives and market mechanisms for climate change actions in Malaysia," *J. Environ. Sci. Technol.*, vol. 4, pp. 31-40, 2011.

[4] P. Westermann, B. Jargensen, L. Lange, B. K. Ahring, C. H. Christensen, "Maximizing renewable energy hydrogen production from biomass in a bio/catalytic refinery," *Int. J. Hydrogen Energy*, vol. 32, pp. 4135-4141, 2007.

[5] P. McKendry, "Energy production from biomass (part 1): Overview of biomass," *Bioresource Technol.*, vol. 83, pp. 37-46, 2002.

[6] A. Cadenas and S. Cabezudo, " Biofuels as sustainable technologies: Perspectives for less developed countries," *Technol. Forecasting Soc. Change*, vol. 58. Pp. 83-103, 1998.

[7] T. L. Kelly-Yong, K. T. Lee, A. R. Mohamed and S. Bhatia, "Potential of hydrogen from oil palm biomass as a source of renewable energy worldwide", *Energy policy*, vol. 35. pp. 5692-5701, 2007.

[8] R. Zhang, Y. Wang and R. C. Brown, "Steam reforming of tar compounds over Ni/olivine catalysts doped with CeO_2," *Energy Conv & Manage..*, vol. 48, pp. 68-77, 2007.

[9] A. Demirbas, "Progress and recent trends in biofuels," *Progress in Energy Combustion Sci.*, vol. 33, pp. 1-18, 2007.

[10] T. Nordgreen, T. Liliedahl and K. Sjostrom. Metallic iron as a tar breakdown catalyst related to atmospheric, fluidised bed gasification of biomass. *Fuel*. 85 (2006) 689-694.

[11] P. McKendry, "Energy production from biomass (part 3): gasification technologies," *Bioresource Technol.*, vol. 83, pp. 55-63, 2002.

[12] S. J. Juutilainen, P. A. Simell and A. O. I. Krause, "Zirconia: selective oxidation catalyst for removal of tar and ammonia from biomass gasification gas," *Appl. Catal. B,* vol. 62, pp. 86-92, 2006.

[13] M. Asadullah, T. Miyazawa, S. I. Ito, K. Kunimori and K. Tomishige, "Demonstration of real biomass gasification drastically promoted by effective catalyst. *Appl. Catal. A,* vol. 246 pp. 103-116, 2003.

[14] F. H. Sobrino, C. R. Monray and J. L. H. Perez, "Critical analysis on hydrogen as an alternative to fossil fuels and biofuels for vehicle in Europe," *Renewable Sustainable Energy Rev.*, vol. 14, pp. 772-780, 2010.

[15] T. Kimura, T. Miyazawa, J. Nishikawa, S. Kado, K. Okumura, T. Miyao, S. Naito, K. Kunimori and K. Tomishige, "Development of Ni catalyst for tar removal by steam gasification of biomass. *Appl. Catal. B,* vol. 68, pp. 160-170, 2006.

[16] S. H. Shuit, K. T. Tan, K. T. Lee, A. H. Kamaruddin, "Oil palm biomass as a sustainable energy source: A Malaysian case study," *Energy*, vol. 34, pp. 1225-1235, 2005.

[17] C. Y. May, N. A. Bakar, H. Lau, Y. Hawari and M. B. Wahid. (2009, Sept.7). National Biofuel Policy, Deployment and Plans. Presented at 3rd Annual MoEN-IEA Joint Forum "Sustainable Development of Biofuels" [Online]. Available: http://www.iea.org/work/2009/bangkok/1_3_Abu_Bakar.pdf.

[18] N. Wambeck, Oil Palm Process Synopsis, Vol 1, 1st ed. June, 1999.

[19] M. Momirlan, T. N. Veziroglu, "Current status of hydrogen energy," *Renewable Sustainable Energy Rev.*, vol. 6, pp. 141-179, 2002.

[20] B. M. Besancon, V. Hasanov, R. Imbault-Lastapis, R. Benesch, M. Barrio, M. J. Molnvik, " Hydrogen quality from decarbonized fossil fuels to fuel cells," *Int. J. Hydrogen Energy*, vol. 34, pp. 2350-2360, 2009.

[21] Int. Energy Agency. (2006). Hydrogen production and storage: R & D priorities and gaps. [Online]. Available at: http://www.iea.org/papers/2006/hydrogen.pdf.

[22] A. Tanksale, J. N. Beltramini, M. L. GaoQing, "A review of catalytic hydrogen production processes from biomass," *Renewable Sustainable Energy Rev.*, vol. 14. Pp. 166-182, 2010.

[23] A. Demirbas, "Biofuels sources, biofuel policy, biofuel economy and global projections," *Energy Convers. Manage.*, vol. 49, pp. 2106-2116, 2008.

[24] M. A. Uddin, H. Tsuda and E. Sasaoka, "Catalytic decomposition of biomass tars with iron oxide catalyst," *Fuel*, vol. 87 pp. 451-459, 2008.

[25] D. Sutton, B. Kelleher and J. R. H. Ross, "Review of literature on catalyst for biomass gasification," *Fuel Process. Technol.* vol. 73 pp. 155-173, 2001.

[26] G. Hu, S. Xu, S. Li, C. Xiao and S. Liu, "Steam gasification of apricot stones with olivine and dolomite as downstream catalysts," *Fuel Process Technol.*, vol. 87**,** pp. 375-382, 2006.

[27] C. H. Bartholomew, "Mechanisms of catalyst deactivation," *Appl. Catal. A*, vol. 212, pp. 17-60, 2001.

[28] K. Nakamura, T. Miyazawa, T. Sakurai, T. Miyao, S. Naito, N. Begum, K. Kunimori and K. Tomishige, "Promoting effect of MgO addition to $Pt/Ni/CeO/Al_2O_3$ in the steam gasification of biomass" *Appl. Catal. B*, vol. 86, pp. 36-44, 2009.

[29] J. Wang, M. Jiang, Y. Yao, Y. Zhang and J. Cao, "Steam gasification of coal char catalyzed by K_2CO_3 for enhanced production of hydrogen without formation of methane," *Fuel*, vol. 88, pp. 1572-1579, 2009.

[30] K. Sato and K. Fujimoto. Development of New Nickel based Catalyst for Tar Reforming with Superior Resistance to Sulfur Poisoning and Coking in Biomass Gasification. *Catal. Commun.* 8 (2007) 1697-1701.

[31] D. Swierczynksi, S. Libs, C. Courson and A. Kiennemann, "Steam reforming of tar from biomass gasification process over Ni/olivine catalyst using toluene as a model compound," *Appl. Catal. B*, vol. 74, pp. 211-222, 2007.

[32] P. Chaiprasert and T. Vitidsant, "Effect of promoters on biomass gasification using nickel/dolomite catalyst," *Korean J. Chem. Eng*., vol. 26, pp. 545-1549, 2009.

[33] S. Rapagna, H. Provendier, C. Petit, A. Kiennemann and P. U. Foscolo, "Development of catalyst suitable for hydrogen or syn-gas production from biomass gasification," *Biomass Bioenergy*, vol. 22, pp. 377-388, 2002.

[34] H. M. Swaan, V. C. H. Kroll, G. A. Martin and C. Mirodatos, "Deactivation of supported nickel catalysts during the reforming of methane by carbon dioxide," *Catal. Today*, vol. 21, pp. 571-578, 1994.

[35] B. C. Gates, "Catalytic chemistry," USA: John Wiley & Sons, Inc, 1991.

[36] M. H. Jordao, V. Simoes and D. Cardoso, "Zeolite supported Pt-Ni catalysts in n-hexane isomerisation, *Appl. Catal. A*, vol. 319, pp. 1-6, 2007.

[37] M. H. Jordao and D. Cardoso, "14-P-36-Characterization of Ni, Pt zeolite catalysts by TEM and EDX," *Stud. in Surface Sci. Catal.*, vol. 135, pp. 357, 2001.

[38] Energy Inform. Admin. (2011, July). Monthly energy review. [Online]. Available at: http://www.eia.gov/totalenergy/data/monthly/#summary

[39] F. Sulaiman, N. Abdullah, H. Gerhauzer and A. Shariff, "A Perspective of oil palm and its wastes," *J. of Phys. Sci.*, vol. 21, pp. 67-77, 2010.

[40] M. Z. Jaafar, W. H. Kheng and N. Kamaruddin, "Greener energy solutions for a suitable future: issues and challenges for Malaysia. *Energy Policy*, vol. 31, pp. 1061-1072, 2003.

[41] M. A. Fazal, A. S. M. A. Haseeb and H. H. Masjuki, "Biodiesel feasibility study: An evaluation of material compatibility; performance; emission and engine durability," *Renewable Sustainable Energy Rev.*, vol. 15, pp. 1314-1324, 2011.

[42] I.M. Atadashi, M.K. Aroua, A. A. Aziz, "High quality biodiesel and its diesel engine application: A review," *Renewable Sustainable Energy Rev.*, vol. 14, pp. 1999-2008, 2010.

[43] T. L. Brown, H. E. LeMay and B. E. Bursten, "Chemistry the central science," 10th ed. USA: Prentice Hall, 2006.

[44] H. Yang, R. Yan, H. Chen, D. H. Lee and C. Zheng, "Characteristics of hemicelluloses, cellulose and lignin pyrolysis," *Fuel*, vol. 86, pp. 1781-1788, 2007.

[45] G. Singh, L. K. Huan, T. L. Kow, D. L., "Oil palm and the environment: A Malaysian perspectives," Malaysia Oil Palm Growers Council, pp. 41-53.

[46] A. B. Nasrin, A. N. Ma, Y. M. Choo, S. Mohamad, A. Azali and Z. Zainal, "Oil palm biomass as potential substitution raw materials for commercial biomass briquettes production," *American J. Appl. Sci.*, vol. 5, pp. 179-183, 2008.

[47] P. McKendry, Energy production from biomass (part 2): conversion technologies," *Bioresource Technol.*, vol. 83, pp. 47-54, 2002.

[48] A. K. Rajvanshi, "Biomass Gasification," in *Alternative Energy in Algriculture*, vol. 2, D. Y. Goswami, Ed., India: CRC Press, 1986, pp. 83-102.

[49] M. Ni, D. Y. C. Leung, M. K. H. Leung and K. Sumanthy, "An overview of hydrogen production from biomass," *Fuel Process. Technol.*, vol. 87, pp. 461-472, 2006.

[50] S. Rapagna, N. Jand, A. Kiennemann and P. U. Foscolo, "Steam-gasification of biomass in a fluidised bed of olivine particles," *Biomass Bioenergy*, vol. 19, pp. 187-197, 2000.

[51] L. Wang, C. L. Weller D. D. Jones and M. A. Hanna, "Contemporary issues in thermal gasification of biomass and its application to electricity and fuel production," *Biomass Bioenergy*, vol. 32, pp. 573-581, 2008.

[52] A. Effendi, Z. G. Zhang, K. Hellgardt, K. Honda and T. Yoshida, "Steam reforming of a clean model biogas over Ni/Al2O3 in fluidized- and fixed-bed reactors," *Catal.Today*, vol. 77, pp. 181-189, 2002.

[53] D. Dayton, "A review of the literature on catalytic biomass tar destruction," Nat. Renewable Energy Lab. Golden, Colorado. Rep. NREL/TP-510-32815, 2002.

[54] C. N. Satterfield, "Heterogeneous catalysis in industrial practice," 2nd ed. Singapore: McGraw Hill, Inc, 1991.

[55] L. Devi, K. J. Ptasinski and F. J. J. G. Janssen, "Pretreated olivine as tar removal catalyst for biomass gasifiers: investigation using naphthalene as model biomass tar," *Fuel Process. Technol.*, vol. 86 pp. 707-730, 2005.

[56] R. Martinez, E. Romero, L. Garcia and R. Bilbao, "The effect of lanthanum on Ni-Al catalyst for catalytic steam gasification of pine sawdust," *Fuel Process. Technol.*, vol. 85, pp. 201-214, 2003.

[57] C. Courson, L. Udron, D. Swierczynski, C. Petit and A. Kiennemann, "Hydrogen production from biomass gasification on nickel catalysts test for dry reforming of methane," *Catal. Today*, vol. 76, pp. 75-86, 2002.

[58] K. Tomishige, T. Kimura, J. Nishikawa, T. Miyazawa and K. Kunimori, "Promoting effect of the interaction between Ni and CeO2 on steam gasification of biomass," *Catal. Commun.*, vol. 8, pp. 1074-1079, 2007.

[59] J. Nishikawa, T. Miyazawa, K. Nakamura, M. Asadullah, K. Kunimori and K. Tomishige, "Promoting effect of Pt addition to $Ni/CeO_2/Al_2O_3$ catalyst for steam gasification of biomass," *Catal. Commun.*, vol. 9, pp. 1950201, 2008.

[60] Y. Matsumura and T. Nakamori, "Steam reforming of methane over nickel catalysts at low reaction temperature," *Appl. Catal. A*, vol. 258, pp. 107-114, 2004.

[61] T. Furusawa and A. Tsutsumi, "Comparison of Co/MgO and Ni/MgO catalysts for the steam reforming of naphthalene as a model compound of tar derived from biomass gasification," *Appl Catal. A*, vol. 278, pp. 207-212, 2005.

[62] T. Furusawa, T. Sato, M. Saito, Y. Ishiyama, M. Sato, N. Itoh and N. Suzuki, "The evaluation of the stability of Ni/MgO catalysts for the gasification of lignin in supercritical water," *Appl Catal. A*, vo. 327, pp. 300-310, 2007.

[63] Y. Ishida, K. Kumabe, K. Hata, K. Tanifuji, T. Hasegawa, K. Kitagawa, N. Isu, Y. Funahashi and T. Asai, "Selective hydrogen generation from real biomass through hydrothermal reaction at relatively low temperature," *Biomass Bioenergy*, vol. 33, pp. 8-13, 2009.

[64] K. Sahner, G. Hagen, D. Schonauer, S. Reib and R. Moos, "Zeolites-versatiles materials for gas sensors," *Solid State Ionics*, vol. 179, pp. 2416-2423, 2008.

[65] J. B. Higgins, R. B. LaPierre, J. L. Schlenker, A. C. Rohrman, J. D. Wood, G. T. Kerr and W. J. Rohrbaugh, "The framework topology of zeolite beta," *Zeolites*, vol. 8, pp. 446-452, 1988.

[66] C. A. Rios, C. D. Williams and M. A. Fullen, M.A. "Nucleation and growth history of zeolite LTA synthesized from kaolinite by two different methods," *Appl. Clay Sci*., vol. 42, pp. 446-454, 2009.

[67] A. Aho, N. Kumar, K. Eranen, T. Salmi, M. Hupa and D. Y. Murzin, "Catalytic pyrolysis of biomass in a fluidized bed reactor: influence of the acidity of H-beta zeolite," *IChemE*, vol. 85, pp. 473-480, 2007.

[68] M. M. Yung, W. S. Jablonski and K. A. Magrini-Bair, "Review of catalytic conditioning of biomass-derived syngas," *Energ Fuels*, vol. 23, pp. 1874-1887, 2009.

[69] S. Abdullah and S. Yusup, "Method for screening of Malaysia biomass based on aggregated matrix for hydrogen production through gasification," *J. Appl. Sci.*, vol. 10, pp. 3301-3306, 2010.

[70] K. Engelen, Y. Zhang, D. J. Draelants and G. V. Baron, "A novel catalytic filter for tar removal from biomass gasification gas: improvement of the catalytic activity in presence of H_2S," *Chem. Eng. Sci.*, vol. 58, pp. 665-670, 2003.

[71] K. Tomishige, T. Miyazawa, T. Kimura, K. Kunimori, N. Koizumi, M and Yamada, "Resistance to sulfur poisoning of hot gas cleaning catalysts for the removal of tar from the pyrolysis of cedar wood," *Appl. Catal. B.*, vol. 60, pp. 299-307, 2005.

[72] S. Albertazzi, F. Basile, J. Brandin, J. Einvall, G. Fornasari, C. Hulteberg, M. Sanati, F. Trifiro, A. Vaccari, "Effect of fly ash and H_2S on a Ni-based catalyst for the upgrading of a biomass-generated gas" *Biomass Bioenergy*, vol. 32, pp. 345-353, 2008.

[73] J. Hepola and P. Simell, "Sulphur poisoning of nickel-based hot gas cleaning catalysts in synthetic gasification gas, I. Effect of different process parameters," *Appl. Catal. B*, vol. 14, pp. 287-303, 1997.

[74] J. Barbier, "Effect of poisons on the activity and selectivity of metallic catalysts," in *Deactivation and poisoning of catalysts*, vol. 20, New York: Marcel Dekker, Inc, 1985, ch. 3, pp. 110-147.

[75] S. M. Augustine, G. N. Alameddin, W. M. H. Sachtler, "The effect of Re, S, and Cl on the deactivation of $Pt/\gamma\text{-}Al_2O_3$ reforming catalysts," *J. Catal.*, vol. 115, pp. 217-232, 1989.

[76] S. E. Dann, "Reactions and characterization of solids," 1st Ed. New York: John Wiley & Sons, 2002.

[77] V. Ramaswamy, "Structural characterization of catalysts by x-ray analysis," in Catalysis Priciples and Applications, B. Viswanathan, S. Sivasanker and A. V. Ramaswamy, India: Narosa Publishing House, 2002, pp. 92-115.

[78] H. Yao and K. Kimura. (2007). Field emission scanning electron microscopy for structural characterization of 3D gold nanoparticle superlattices. *Modern Research and Educational Topics in Microscopy.* [Online]. Available: http://www.formatex.org/microscopy3/pdf/pp568-575.pdf

[79] S. Subramanian, "Temperature-progrannmed reduction of platinum group metals catalysts: recent trends in characterization techniques," *Platinum Metals Rev.*, vol. 36, pp. 98-103, 1992.

[80] M. Asadullah, T. Miyazawa, S. I. Ito, K. Kunimori, S. Koyama and K. Tomishige, "A comparison of $Rh/CeO_2/SiO_2$ catalysts with steam reforming catalysts, dolomite and inert materials as bed materials in low throughput fluidized bed gasification systems," Biomass Bioenergy, vol. 26, pp. 269 – 279, 2004.

[81] S. Luo, B. Xiao, Z. Hu, S. Liu, X. Guo and M. He, "Hydrogen-rich gas from catalytic steam gasification of biomass in a fixed bed reactor: Influence of temperature and steam on gasification performance," *Int. J. Hydrogen Energy*, vol. 34 pp. 2191-2194, 2009.

[82] .F. Gonzalez, S. Roman, D. Bragado, M. Calderon, "Investigation on the reactions influencing biomass air and air/steam gasification for hydrogen production," *Fuel Process. Technol.*, vol.89, pp. 764-772, 2008.

[83] P. A. Webb and C. Orr, "Analytical methods in fine particle technology," Norcros, USA: Micrometrics instrument Corp., 1997.

[84] S. H. Kang, and J. K. W. Bae. Fisher-Tropsch synthesis using zeolite-supported iron catalysts for the production of light hydrocarbons. *Catal Lett.*, vol. 125, pp. 264-270, 2008.

[85] D. Chen, Y. Yang, K. Zhang and J. Wang, "BETA zeolite made from mesoporous material and its hydrocracking performance. *Catal. Today*, vol. 116, pp. 2-5, 2006.

[86] S. J. Gregg and K. S. W. Sing, "Adsorption, surface area and porosity," 2^{nd} ed. London: Academic Press Inc., 1982,

[87] Y. Chen, P. Cui, G. Xiong and H. Xu, "Novel nickel-based catalyst for low temperature hydrogen production from methane steam reforming in membrane reformer," Asia-Pac. J. Chem. Eng., vol. 5, pp. 93-100, 2010.

[88] A. Hassan, S. Ahmed, M. A. Ali, H. Hamid and T. Inui, "A comparison between β- and USY-zeolite- bases hydrocracking catalysts," *Appl. Catal. A*, vol. 220, pp. 59-68, 2001.

[89] A. Ramli, A. R. A. Hamid, F. Manaf and S. M. Ibrahim, "Effect of vanadium and titanium substitution over an antimony- based mixed oxide catalysts for propane ammoxidation to acrylonitrile," *Malaysian J. Analytical Sci.*, vol. 11, pp. 166-172, 2007.

[90] J. M. Rynkowski, T. Paryjczak and M. Lenik, "On the nature of oxidic nickel phase in NiO/γ-Al_2O_3 catalysts," *Appl. Catal. A*, vol. 106, pp. 73-82, 1993.

[91] J. Zielinski, "Morphology of nickel/alumina catalysts," *J. Catal.*, vol. 76, pp. 157-163, 1982.

[92] P. Salagre, J. L. G. Fierro, F. Medina and J. E. Sueiras, "Characterization of nickel species on γ-alumina supported nickel samples," *J. Mol. Catal.* A, vol. 106, pp. 125-134, 1996.

[93] M. Mattos, V. M. Souza and M. Schmal. (2005). Supported nickel catalysts for steam reforming of methane. Presented at 2nd mercosur Congress on Chemical Engineering. [Online]. Available: http://www.enpromer2005.eq.ufrj.br/nukleo/pdfs/0141_enpromer_141.pdf

[94] J. Miki, M. Asanuma, Y. Tachibana and T. Shikada, "Vapor phase oxidation of benzoic acid to phenol over a novel catalyst system consisting of NiO and $NiFe_2O_4$," *J. Catal.*, vol. 151, pp. 323-329, 1995.

[95] L. Wang, B. Li, M. Koike, S. Koso, Y. Nakagawa and Y. Xu, "Catalytic performance and characterization of Fe-Ni catalysts for the steam reforming of tar from biomass pyrolysis to synthesis gas" *Appl. Catal. A*, vol. 392, pp. 248-255, 2011.

[96] H. Zhang and Y. Li, "Preparation and characterization of Beta/MCM-41 composite zeolite with a stepwise-distributed pore structure," *Power Technol.*, vol. 183, pp. 73-78, 2008.

[97] G. Ning, F. Wei, Q. Wen, G. Luo, Y. Wang and Y. Jin, "Improvement of Fe/MgO catalysts by calcination for the growth of single and doubled walled carbon nanotubes," *J. Phys. Chem. B.*, vol. 110, pp. 1201-1205, 2006.

[98] Z. X, Cheng, X. G. Zhao, J. Li and Q. M. Zhu, "Role of support in CO_2 reforming of CH_4 over Ni/Al_2O_4 catalyst," *Appl. Catal. A*, vol. 205, pp 31-36, 2001.

[99] P. A. Santiago. (2008). TPR analysis of Fe/Zsm-5 for the reaction of syngas to gasoline. [Online]. Available at: http://apps.aiche.org/proceedings/Abstract.aspx?PaperID=142686

[100] H. J. Wan, B. S. Wu, C. H. Zhang, H. W. Xiang, Y. W. Li, B. F. Xu and F. Yi, "Study of Fe-Al_2O_3 interaction over precipitated iron catalyst for fisher-tropsch synthesis," *Catal. Commun.*, vol. 8, pp. 1538-1545, 2007.

[101] A. F. H. Wielers, A. J. H. M. Kock, C. E. C. A. Hop and J. W. Geus, "The Reduction Behavior of Silica-Supported and Alumina-Supported Iron Catalysts: A mossbauer and Infrared Spectroscopic Study," *J. Catal.*, vol. 117, pp. 1-18, 1989.

[102] C. H. Zhang, B. T. Yang, B. T. Teng, T. Z. Li, H. Y. Zheng, H. W. Xiang and Y. W. Li, "Study of an iron manganese fisher-thropsh synthesis catalyst promoted with copper," *J. Catal*., vol. 237, pp. 405-415, 2006.

[103] P. Decyk, M. Trejda and M. Ziolek, "Iron containing mesoporous solids: preparation, characterization and surface properties," *C. R. Chimie*, vol. 8, pp. 635-654, 2005.

[104] M. Virginie, S. Libs, A. Courson and A. Kiennemann. (2008). Iron/olivine catalysts for tar reforming: comparison with nickel/olivine. [Online]. Available: http://gdricatal.univlille1.fr/GDRI%20FR/21-28.pdf

[105] P. Lv, Z. Yuan, C. Wu, L. Ma, Y. Chen and N. Tsubaki, "Bio-syngas production from biomass catalytic gasification," *Energy Convers. Manage.*, vo. 48, pp. 1132-1139, 2007.

[106] P. Chaipraset and Vitidsant, "Promotion of coconut shell gasification by steam reforming on nickel-dolomite," *J. Appl. Sci.*, vol. 6, pp. 332-336, 2009.

[107] K. Tomishige, M. Asadullah and K. Kunimori, "Syngas production by biomass gasification using $Rh/CeO_2/SiO_2$ catalysts and fluidised bed reactor," *Catal. Today*, vol. 89, pp. 389-403, 2004.

[108] M. P. Aznar, M. A. Caballero, J. Corella, G. Molina and J. M. Toledo, "Hydrogen production by biomass gasification with steam-O_2 mixtures

followed by a catalytic steam reformer and a CO-shift system," *Energy Fuels*, vol. 20, pp. 1305-1309, 2006.

[109] M. Ryden, E. Cleverstam, M. Johnsson, A. Lyngfelt and T. Mattisson, " Fe2O3 on Ce-, Ca-, or Mg-stabilized ZrO2 as oxygen carrier for chemical-looping combustion using NiO as additive," *AIChE J.*, vol. 56, pp. 2211-2220, 2010.

[110] T. E. McMinn, F. C. Moates and J. T. Richardson, "Catalytic steam reforming of chlorocarbons: catalyst deactivation," *Appl. Catal. A.* Vol. 8, pp. 93-105, 2001.

[109] M. Ryden, E. Cleverstam, A. Lyngfelt and T. Mattisson, "Waste products from the steel industry with NiO as additive as oxygen carrier for chemical-looping combustion," *Int. J. of Greenhouse Gas Control*, vol. 3, pp. 693-703, 2009.

[110] D. P. Harrison, "Sorption-enhanced hydrogen production: a review," Ind. Eng. Chem. Res., vol. 47, pp.6 486-6501, 2008.

APPENDIX A

RESULTS FROM DALIAN INSTITUE OF

CHEMICAL PHYSICS, CHINA

Test for Biomass Gasification to Hydrogen (Palm Kernel)

Hengyong Xu, Qingjie Ge,
Chenchen Qi, Wei Zhang, Bing Liu

Dalian Institute of Chemical Physics, CAS

2010. 10. 6

Gasification of Biomass (Palm Kernel)

Conditions: Steam/N_2, 0.3g Biomass, 0.1g catalyst, 1atm, Steam/Biomass = 4/1

	Steam/N_2 + Biomass (0.3g)				Steam/He + Biomass(0.3g) + Catalyst(0.1g)			
T / °C	H_2S(ppm)	CO*	CH_4	CO_2	H_2S(ppm)	CO	CH_4	CO_2
600	0	Not	210	709	0	458	100	2126
650	0	detect	93	1866	0	592	77	2429
700	0	ed!	162	3622	0	750	63	3161
750	0		252	5054	0	1020	0	4373
800	2.5		124	3726	0	1291	0	5388
850	4.5		107	6479	0	1362	0	5900
900	6.2		42	4572	0	781	0	4264

- With Catalyst, biomass gasification process could not found H_2S in the products while H_2S were found in the gases product above 800°C without catalyst.
- Low temperature, catalyst will cause more CO_2 production.
- During Catalytic process, methane produce less, especially above 750°C.

Catalysts have large influences on biomass gasification!

Catalyst samples catalytic performance

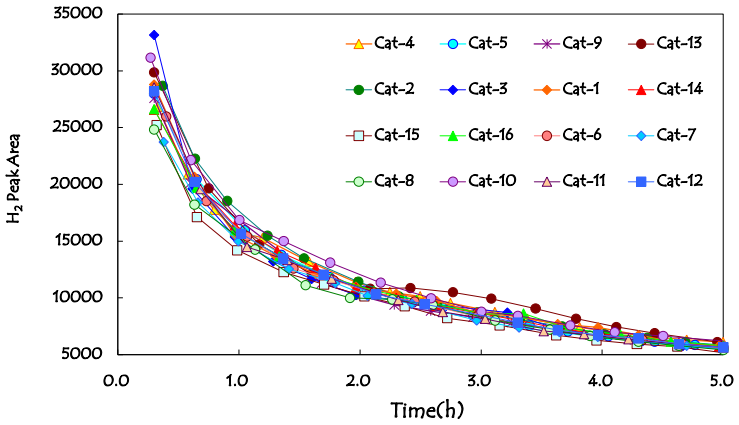

Reaction Conditions: 700°C, Steam/Ar=1/6(v/v), 0.9g Biomass, 0.3g catalyst, 1atm, Steam/Biomass = 4/1(w/w)

Catalyst No.3 and No. 10 exhibit a better hydrogen production ability.

Hydrogen production ability order: Cat-3 (33156) > Cat-10 (31163) > cat-1 (28785) > cat-11 (28535) > cat-12(28214) > cat-5(27994) > cat-4 (26823) ~cat-16(26628) ~ cat-14 (26579) > cat-6(25940) > cat-15 (25228) > cat-8 (24833) > cat-2 (22258) > Cat-9 (20132) > cat-13 (19643) > Cat-7 (16962)

Outlet Gas composition over different composition (1)

Conditions: 700°C, Steam/Ar=1/6(vol.), 0.9g Biomass, 0.3 g catalyst, 1atm, Steam/Biomass = 4/1(wt)

Catalyst	Outlet gas composition*(%)			
	H_2	CO	CH_4	CO_2
Biomass only	55.0	4.6	1.5	26.7
Cat-1	66.0	6.2	2.1	22.4
Cat-2	69.2	7.6	1.1	20.6
Cat-3	63.0	5.3	0.8	28.8
Cat-4	67.4	6.2	1.3	23.5
Cat-5	66.7	6.9	1.0	24.9
Cat-6	64.1	7.0	0	25.3
Cat-7	68.9	6.5	2.4	19.0
Cat-8	55.9	5.9	1.1	34.1
Cat-9	64.7	5.6	1.8	27.0
Cat-10	61.9	6.1	1.6	27.8

*: gas composition after water removal.

Outlet Gas composition over different composition (2)

Conditions: 700°C, Steam/Ar=1/6(vol.), 0.9g Bi1omass, 0.3 g catalyst, 1atm, Steam/Biomass = 4/1(wt)

Catalyst	Outlet gas composition*(%)			
	H_2	CO	CH_4	CO_2
Cat-11	60.3	4.3	0	33.1
Cat-12	68.8	5.3	1.5	21.7
Cat-13	64.6	5.5	3.7	23.7
Cat-14	64.1	6.4	1.6	24.9
Cat-15	63.0	7.1	1.3	25.8
Cat-16	73.8	4.8	0	18.1

*: gas composition after water removal.

Hydrogen content in dry-based outlet gases (%): Cat-16 (73.8) > Cat-2 (69.2) > cat-7 (68.9) ~ cat-12 (68.8) > cat-4 (67.4) > cat-5(66.7) > cat-1 (66.0) > cat-9(64.7) ~ cat-13 (64.6) > cat-6(64.1)~cat-14 (64.1) > cat-15 (63.0) > cat-3 (63.0) > cat-10 (61.9) > Cat-11 (60.3) > Cat-8 (55.9) ~ Biomass only (55.0)

Combined the hydrgen peak area with the hydrogen content, it could be known that cat-4, cat-5, cat-12, and cat-16 should be more suitable for biomass to hydrogen than other catalysts.

APPENDIX B

LIST OF PUBLICATIONS

1. S. E. E. Misi, A. Ramli, F.H. Rahman, "Characterization of the structure feature of bimetallic Fe-Ni catalysts", *Journal of Applied Science*, vol. 11, pp.1297-1302, 2011.

2. Z. Khan, S. Yusup, M. Melati A., A. Ramli, M. T. Arpin., S. S. Abdullah., M. F. Mohamad, S. E. E. Misi and A. Inayat 'Effect of Steam and Catalyst on Palm Oil Wastes Thermal Decomposition for Hydrogen Production' *Research journal of Chemistry and Environment*, Vol 15 (2), pp.466-472, 2011.

3. S. E. E. Misi, A. Ramli, S. Yusup, "Preparation and characterization of zeolite supported monometallic and bimetallic catalysts," accepted in Journal of Industrial Technology, vol. 19(2), 2010.

4. A. Ramli, S. E. E. Misi, M. F. Mohamad, S. Yusup, "Performance of zeolite beta supported Fe and Ni catalysts for steam gasification of palm kernel shell to hydrogen," accepted for publication in Catalysis Today Journal (special issues for CatBior 2011).